ECMWF COPERNICUS REPORT

Copernicus Atmosphere Monitoring Service

Observation characterization and validation methods document

Issued by: KNMI

Date: 1 July 2021

Ref: CAMS84_2018SC2_D6.1.1-2020_observations_v6

IMPLEMENTED BY ECMWF

Observation characterisation and validation methods document

AUTHORS:
S. Basart (BSC), A. Benedictow (MetNo), Y. Bennouna (CNRS-LA),
A.-M. Blechschmidt (IUP-UB), S. Chabrillat (BIRA-IASB), E. Cuevas (AEMET),
Q. Errera (BIRA-IASB), H. Flentje (DWD), K. M. Hansen (AU), J. Kapsomenakis (AA),
B. Langerock (BIRA-IASB), M. Ramonet (CEA-LSCE), A. Richter (IUP-UB),
M. Schulz (MetNo), N. Sudarchikova (MPG), A. Wagner (DWD),
T. Warneke (UBC), C. Zerefos (AA)

EDITOR:
H. J. Eskes (KNMI)

REPORT OF THE COPERNICUS ATMOSPHERE MONITORING SERVICE, VALIDATION SUBPROJECT (CAMS-84).

CITATION:
Eskes, H.J., S. Basart, A. Benedictow, Y. Bennouna, A.-M. Blechschmidt, S. Chabrillat, E. Cuevas, Q. Errera, H. Flentje, K. M. Hansen, J. Kapsomenakis, B. Langerock, M. Ramonet, A. Richter, M. Schulz, N. Sudarchikova, A. Wagner, T. Warneke, C. Zerefos, Observation characterisation and validation methods document, Copernicus Atmosphere Monitoring Service (CAMS) report, CAMS84_2018SC2_D6.1.1-2021_observations_v6.pdf, July 2021, doi:10.24380/3b4e-xb93.

STATUS:
Version 6

DATE:
July 2021

REF:
CAMS84_2018SC2_D6.1.1-2021_observations_v6

Executive Summary

The Copernicus Atmosphere Monitoring Service (http://atmosphere.copernicus.eu, CAMS) is a component of the European Earth Observation program Copernicus. CAMS is providing operational forecasts, analyses and reanalyses on the global and European scale of the composition of the atmosphere (reactive gases, greenhouse gases, aerosols).

CAMS-84 is a sub-project of CAMS, dealing with the validation of the service products. CAMS-84 provides 3-monthly updates of validation reports for the global and regional services. The validation is based on a large number of observations and measurement techniques, including surface in-situ, surface remote sensing, observations by airplanes, balloon sounding, observations from ships and satellite observations. The three-monthly cycle of the validation reports adds constraints on the timely availability of the observations, with a deadline roughly one month after sensing.

This document serves as a reference for the validation reports, in order to provide the traceability for the independent observations used in the validation work. The two main aspects discussed are:

1. A description of the observations used, including the list of contributing stations, observation networks, measurement techniques, QA procedures, and error estimates.
2. A description of the methods to compare these observations with the CAMS modelling and assimilation products.

The focus of this document is on the evaluation of the CAMS real-time global service for reactive trace gases, aerosols, and greenhouse gases. Observations used for the reanalysis will be distinguished from observations used for the quarterly reports but are not discussed in this version 6 of the document.

Version 1 of this document was published on the CAMS website in April 2016, version 2 in October 2017, version 3 in November 2018, version 4 in December 2019, and version 5 in January 2021.

Table of Contents

1 Introduction

In the sections of this document the individual datasets used for the validation will be discussed one by one. The sections will provide information on the datasets and the way these observations are processed and used for the validation of the CAMS services. A list of relevant references is provided, as well as acknowledgments for the data providers.

Table 1.1 (see also Eskes et al., 2015) provides an overview of the trace gas species and aerosol quantities relevant for the real-time global atmospheric composition service. Shown are the data sets assimilated (second column) and the data sets used for validation (third column). Green colour indicates that substantial data are available to either constrain the species in the analysis, or substantial data are available to assess the quality of the analysis. Yellow colour indicates that measurements are available, but that the impact on the analysis is not very strong or indirect (second column), or that only certain aspects are validated (third column).

We note that in some cases we investigate the comparisons with satellite data which is also used in the assimilation. This holds in particular for IASI and MOPITT CO and GOME-2 NO_2. Often different retrieval versions or retrieval approaches are considered. Even though this is strictly speaking not an independent validation of the CAMS results, it provides additional information on the efficiency of the assimilation (e.g., for NO_2 the short lifetime causes the analysis to quickly relax back to the model forecast equilibrium), on biases in the control run, on the intrinsic uncertainty related to different retrieval approaches, and on the differences between different instruments (e.g., IASI and MOPITT). Furthermore, the global view of the satellites provides the horizontal coverage needed to study the evolution of pollution events, such as the transport and intensity of pollution plumes coming from major fire events. Station or aircraft data will be independent, may be of higher quality but do not provide this coverage.

The description of the observations covers the following aspects:

1. Introduction to the instruments & observation network providing the data.
2. List of stations, if applicable.
3. List of measurements (species, aerosol properties).
4. Specification of the instruments.
5. Specification of the QA/QC procedures and processing.
6. Error estimates for the observations.
7. Analysis of the location of individual stations, representativity errors, possibly selection criteria to discard stations.
8. An appropriate list of references.
9. Acknowledgements

The description of the validation methodology covers the following aspects:

1. Units of quantity, list the unit conversion operations.
2. Specification of averaging over regions, time.
3. Description how observations and models are compared, including e.g., averaging kernels and re-gridding.

Table 1.1. Observations used in the assimilation and validation activities of CAMS, ordered by species.

Species, vertical range	Assimilation	Validation
Aerosol, optical properties	MODIS Aqua/Terra AOD, PMAp AOD	AOD, Ångström: AERONET, GAW, Skynet, MISR, OMI, lidar, ceilometer
Aerosol mass (PM10, PM2.5)	MODIS Aqua/Terra	European AirBase stations
O_3, stratosphere	MLS, GOME-2, OMI, SBUV-2, OMPS, TROPOMI	Sonde, lidar, MWR, FTIR, OMPS, ACE-FTS, SAGE3-ISS and BASCOE analyses
O_3, UT/LS	MLS	IAGOS, ozone sonde
O_3, free troposphere	Indirectly constrained by limb and nadir sounders	IAGOS, ozone sonde, IASI
O_3, PBL / surface		Surface ozone: WMO/GAW, NOAA/ESRL-GMD, AIRBASE
CO, UT/LS	IASI, MOPITT	IAGOS, TROPOMI, NDACC FTIR
CO, free troposphere	IASI, MOPITT	IAGOS, MOPITT, IASI, NDACC FTIR
CO, column	IASI, MOPITT	TCCON
CO, PBL / surface	IASI, MOPITT	Surface CO: WMO/GAW, NOAA/ESRL
NO_2, troposphere	OMI, GOME-2, partially constrained due to short lifetime	TROPOMI, GOME-2, SCIAMACHY, MAX-DOAS
HCHO		TROPOMI, GOME-2, SCIAMACHY, MAX-DOAS
SO_2	GOME-2, TROPOMI (Volcanic eruptions)	
Stratosphere, other than O_3		NO_2 column only: SCIAMACHY, GOME-2, TROPOMI
CO_2, surface, PBL		ICOS
CO_2, column	GOSAT	TCCON
CH_4, surface, PBL		ICOS
CH_4, column	GOSAT, IASI	TCCON, NDACC FTIR

4. Use of error bars & uncertainty propagation (how are individual observation errors translated to comparison errors).
5. A-posteriori discarding of some stations (if applicable) or checks on outliers.

2 Ozonesonde observations

Ozonesondes are small, lightweight balloon borne instruments, developed for measuring the vertical distribution of atmospheric ozone up to an altitude of about 30-35 km and interfaced to a standard meteorological radiosonde for data transmission to the ground station (e.g. Smit, 2002). There are different sonde types in use, the most common ones are i.e. Brewer-Mast (Brewer and Milford, 1960), electrochemical concentration cell (ECC) (Komhyr 1969), and the carbon iodine cell (Kobayashi and Toyama, 1966), each having its one specific design but all the sensors utilize the principle of the fast reaction of ozone and iodide within an electrochemical cell (Smit, 2002).

Ozonesonde measurements are regularly downloaded from the Norwegian Institute for Air Research (NILU), the World Ozone and Ultraviolet Radiation Data Centre (WOUDC), the Network for the Detection of Atmospheric Composition Change (NDACC) and the Southern Hemisphere ADditional OZonesondes (SHADOZ) databases.

The NILU database is a near-real-time service to collect ozonesonde data of registered stations (mostly located in Europe) within a few minutes after a complete sounding. These files are then read and checked for errors (Smit 2013).

The WOUDC database follows the objectives of the GAW quality assurance system, which ensures that the data deposited in the database are consistent, meet GAW quality objectives and contain a comprehensive description of methodology (Smit 2013). The system involves quality assurance, science activity and calibration centres that ensure the quality of observations through adherence to measurement guidelines established by the Scientific Advisory Groups and through calibrations that are traceable to World Calibration Standards.

The SHADOZ and NDACC ozonesonde stations, which largely overlap with the GAW network, follow the same quality assurance routines as in GAW (Staehelin 2008, Smit 2013).

The gross of soundings is performed with ECC sondes, except at Hohenpeissenberg in Germany (Brewer Mast) and at Japanese stations (carbon iodine sensor). The sondes have a precision of 3-5% (~10% in the troposphere for Brewer Mast) and an accuracy of 5-10% for the free troposphere and the stratosphere. Larger accuracies (up to 18%) may occur in altitudes above 28 km. For further detail see J. T. Deshler et al. (2008) and H.G.J. Smit et al (2007, 2013).

Please note that recent scientific findings (https://tropo.gsfc.nasa.gov/shadoz/Archive.html, Thompson et al., 2017; Witte et al., 2017; Stauffer, et al. 2020) show a drop-off in Total Ozone at various global ozone stations in comparison with satellite instruments. It amounts between 5-10% for stratospheric ozone. Stauffer et al. (2020) documents that this drop-off is detected at 1/3 of the global ozonesonde stations. Changes in the ECC ozone instrument are associated with the drop-off, but no single factor has been identified as cause yet. Analysis and tests by the ozonesonde community are ongoing and will be documented in a future publication.

In our validation routines, extra format checks ensure that in case the measurement is of non-standard format, the file is rejected.

For the validation, the sonde profiles are compared to the model data closest in time. The gridded model data are linearly interpolated to the latitude and longitude of the stations' location and converted into partial pressure. In the vertical, the ozone sonde data are resampled at the altitude closest to the model level. The horizontal drift during ascend of the sonde is considered negligible in comparison with the global model resolution. For all individual launches the differences between observation and model are calculated and aggregated to monthly means for each station and region (Arctic, Antarctica, Northern midlatitudes, Southern midlatitudes, Tropics) over specific altitude ranges, namely free troposphere and stratosphere. Here, the free troposphere is defined as the

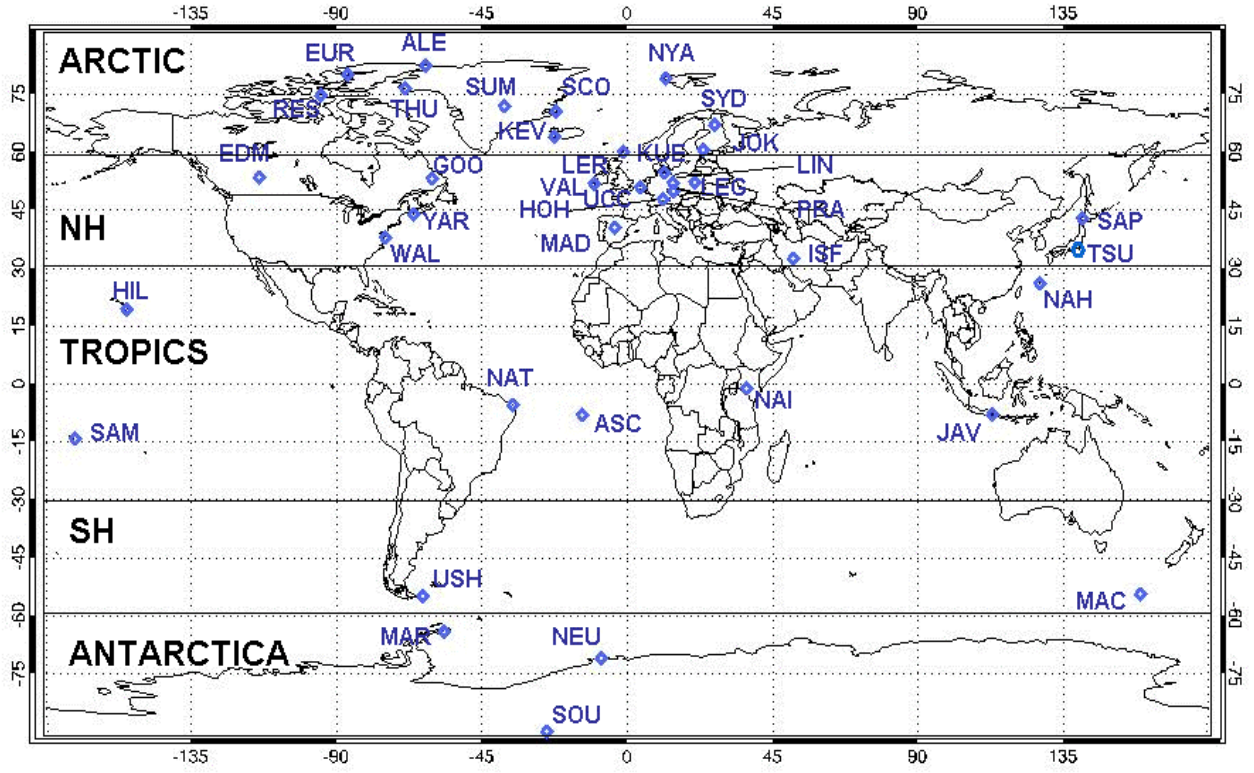

Figure 2.1: Location of the ozone sounding stations and their attribution to the different stratospheric regions

altitude region between 750 and 200 hPa in the tropics and between 750 and 300 hPa elsewhere. The stratosphere is defined as the altitude region between 60 and 10 hPa in the tropics and between 90 and 10 hPa elsewhere.

Profile plots for each month display mean model profiles in comparison with mean monthly sonde profiles for each region. The standard deviation between the individual launches is displayed in the plots. For some regions (e.g. Southern midlatitudes) only few stations and measurements are available and especially towards the end of the validation period the observations get sparse and the results are thus less representative.

3 Surface observations

3.1 GAW ozone and carbon monoxide

The Global Atmosphere Watch (GAW) programme of the World Meteorological Organisation (WMO) has been established to provide reliable long-term observations of the chemical composition and physical properties of the atmosphere, which are relevant for understanding long-term atmospheric chemistry trends and climate change (WMO, 2013). Within GAW, the focus is set on observations that are regionally representative and should be free from influence of significant local pollution sources and thus suited for the validation of global chemistry climate models (WMO, 2007).

The recommended routine measurement technique for O_3 is UV absorption (see GAW report No 209, WMO 2013) and for CO, the analytical measurement techniques are NDIR, GC/HgO, GC/FID, VURF or QCL, (see GAW report No 192, 2010). For NRT data, no intensive data quality control has to be performed by the providers except the standard checks of the measuring equipment according to the Standard Operating Procedures (SOPs) or Measurements Guidelines (MGs) for the respective gases. For NRT O_3 and CO GAW data, an uncertainty of 15% is acceptable: for surface ozone ±5ppb and for CO ±10ppb.

The current Near-Real-Time (NRT) validation relies on 15 GAW stations delivering O_3 and 11 stations delivering CO surface mixing ratios (Fig. 3.1). Eight stations (Hohenpeissenberg, Jungfraujoch, Sonnblick, Zugspitze, Lampedusa, Capo Granitola, Col Margherita and Monte Cimone) are located in Europe. All of them, except Lampedusa, are mountain stations. Col Margherita is operated by the Institute for the Dynamics of Environmental Processes (CNR-IDP) in Italy measuring ozone according to WMO/GAW guidelines.

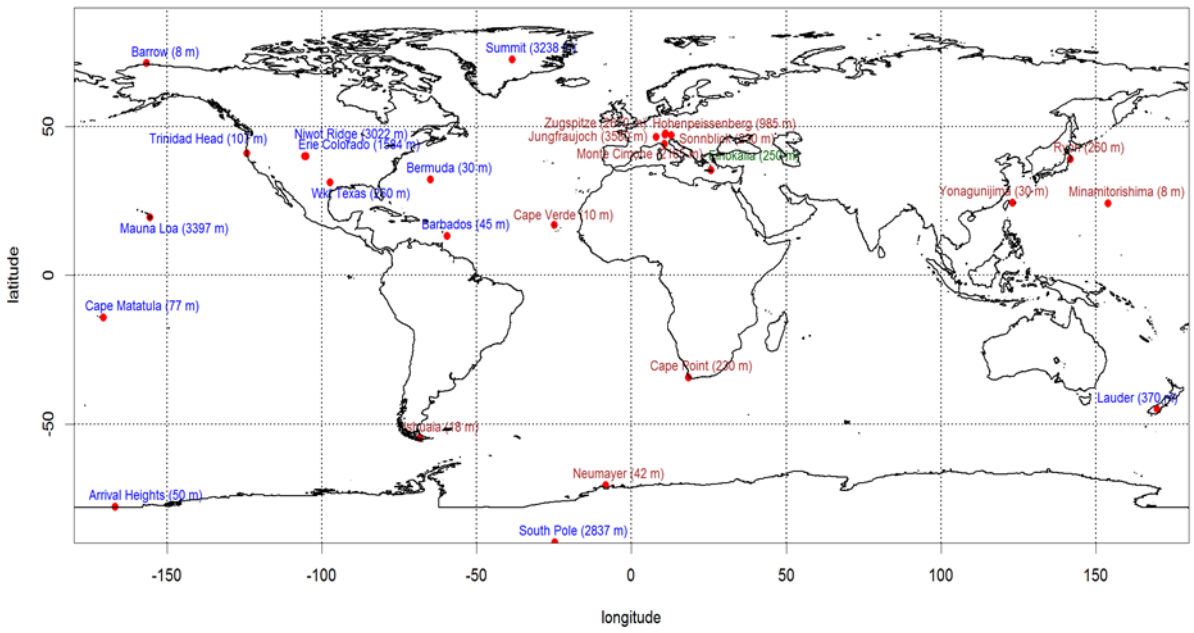

Figure 3.1: Map of the GAW (brown), ESRL (blue) and EMEP (green) validation stations.

Table 3.1. List of GAW and ozone sonde stations used for the validation.

Station/location	lat [°]	lon [°]	Altitude [m]	Instruments/species measured	type/network
Capo Granitola	37.6667	12.65	5	O3	GAW
Cape Point	-34.35	18.48	230	O3, CO surface	GAW
Cape Verde	16.85	-24.87	10	O3, CO surface	GAW
Col Margherita	46.3668	11.7919	2550	O3	CNR-IDPA
Hohenpeissenberg	47.8	11.02	985	O3, CO surface	GAW
Jungfraujoch	46.55	7.99	3580	O3, CO surface	GAW
Lampedusa	35.5182	12.6305	45	O3	GAW
Minamitorishima	24.29	153.98	8	O3, CO surface	GAW
Monte Cimone	44.18	10.7	2165	O3, CO surface	GAW
Neumayer	-70.65	-8.25	42	O3	GAW
Ryori	39.03	141.82	260	O3, CO surface	GAW
Sonnblick	47.05	12.96	3105	O3, CO surface	GAW
Ushuaia	-54.85	-68.32	18	O3, CO surface	GAW
Yonagunijima	24.47	123.02	30	O3, CO surface	GAW
Zugspitze	47.4	10.9	2670	O3, CO surface	GAW
Alert	82.4	-62.3	66	O3, free troposphere	sonde/NILU
Debilt	52.1	5.18	2	O3, free troposphere	sonde/NILU
Edmonton	53.5	-114	766	O3, free troposphere	sonde/NILU
Eureka	80	-86.5	10	O3, free troposphere	sonde/NILU
Goose Bay	53.2	-60.5	36	O3, free troposphere	sonde/NILU
Hohenpeissenberg	47.8	11	976	O3, free troposphere	sonde/NILU
Jokioinen	60.81	23.5	103	O3, free troposphere	sonde/NILU
Legionow	52.4	20.9	96	O3, free troposphere	sonde/NILU
Lerwick	60.14	-1.19	82	O3, free troposphere	sonde/NILU
Ny Alesund	79	12	17	O3, free troposphere	sonde/NILU
Prag	50	14.4	304	O3, free troposphere	sonde/NILU
Resolute	74.72	-94.98	200	O3, free troposphere	sonde/NILU
Scoresbysund	70.5	-22	76	O3, free troposphere	sonde/NILU
Sodankyla	67	27	179	O3, free troposphere	sonde/NILU
Uccle	50.8	4.36	100	O3, free troposphere	sonde/NILU
Hilo	19.43	-155.4	11	O3, free troposphere	sonde/SHADOZ
Java (Watukosek)	-8	113	50	O3, free troposphere	sonde/SHADOZ
Nairobi	-1	37	1795	O3, free troposphere	sonde/SHADOZ
Natal	-5.49	-35.26	14	O3, free troposphere	sonde/SHADOZ
Reunion	-21.06	55.48	24	O3, free troposphere	sonde/SHADOZ

Samoa (Cape Matatula)	-14	-171	77	O3, free troposphere	sonde/SHADOZ
Macquarie Island	-54.5	158.9	7	O3, free troposphere	sonde/WOUDC
Madrid	40.5	-3.8	631	O3, free troposphere	sonde/WOUDC
Marambio	-64.23	-56.62	198	O3, free troposphere	sonde/WOUDC
Naha	26.2	127.7	28	O3, free troposphere	sonde/WOUDC
Sapporo	43	141	26	O3, free troposphere	sonde/WOUDC
Tsukuba	36.06	140.13	31	O3, free troposphere	sonde/WOUDC
Ushuaia	-54.85	-63.32	17	O3, free troposphere	sonde/WOUDC
Valentia	51.9	-10.3	14	O3, free troposphere	sonde/WOUDC

Three stations (Ryori, Minamitorishima and Yonaguijima) are located in Japan: Ryori is situated on the pacific coast; the other two stations are island stations. Cape Verde is a coastal station. There are three stations located in the Southern Hemisphere: Ushuaia, placed on a remote sub-Antarctic marine coast, Cape Point at the southern end of the Cape Peninsula on top of a cliff 230 m above sea level, exposed to the sea, and Neumayer in Antarctica. The three Japanese stations are classified as regional stations, all others are global stations. A detailed description of the stations and the specific requirements for classification are given at: http://gaw.empa.ch/gawsis/default.asp and http://gaw.empa.ch/gawsis/requirements.html.

For the validation, 6-hourly values (0:00, 6:00, 12:00, 18:00 UTC) of the analysis mode are extracted from the model and are matched with hourly observational GAW station data. Model mixing ratios at the stations' locations are linearly interpolated from the model data in the horizontal. In the vertical, modelled gas mixing ratios are extracted at the model level, which is closest to the GAW stations' altitude. Validation scores (MNMB, correlation) are calculated for each station on a quarterly basis (DJF, MAM, JJA, SON). Time series plots show the model runs in comparison with the observations.

3.2 ESRL Global Monitoring Division and EMEP surface ozone observations

Simulated Near-Real-Time (NRT) ozone mixing ratios were validated against observations provided by the ESRL Global Monitoring Division (http://www.esrl.noaa.gov/gmd/; Oltmans et al.,1994; McClure-Begley et al.,2014). The vast majority of measurements used for the validation were made using ozone monitors that use the absorption of ultraviolet (UV) radiation at 254 nm as the principle of measurement (see GAW report No 209, WMO 2013). Most of the measurements are tied to a network standard maintained by CMDL which is in turn linked by inter-comparison with the standard ozone photometer maintained by the U.S. National Institute of Standards and Technology (For more information regarding instrument specifications and limits: http://www.thermoscientific.com/content/tfs/en/product/model-49-i-i-i-ozone-analyzer.html)

Thirteen ground-based stations, namely 1. Arrival Heights, Antarctica, New Zealand (ARH), 2. Tudor Hill, Bermuda, United Kingdom (BER), 3. Barrow, Alaska, United States (BRW), 4. Eureka, Canada (EUK), 5. Lauder, New Zealand (LDR), 6. Mauna Loa, Hawaii, United States (MLO), 7. Niwot Ridge, Colorado, United States (NWR), 8. Ragged Point, Barbados (BAR), 9. South Pole, Antarctica (SPO) 10. Summit, Greenland, (SUM), 11. Table Mountain, Colorado, United States (TBL), 12. Trinidad Head,

California, United States (THD) and 13. Tiksi, Russia (TIK) were included in the validation scheme. In the validation process additional data from one EMEP station in the Mediterranean, namely 14. Finokalia (FK) are used. The majority of these sites are generally free from local sources of contamination. At two of the sites-Barrow and Bermuda, the locally contaminated measurements can be screened using the local wind direction. Note that at Mauna Loa, the strong mountain wind circulation separates the measurements into upslope and downslope conditions. During the daytime, upslope regime boundary layer air is mixed with the free tropospheric air, while during night-time downslope flow, free tropospheric air is sampled (Oltmans and Komhyr, 1986).

The uncertainty required for NRT surface data delivery is less than ± 5 nmol/mol for hourly values of unvalidated data. Detailed information on the ESRL O_3 measurements can be found in Oltmans et al, 1994. Data QA/QC: The quality of data is a joint effort by the program managers and the station technicians.

Table 3.2: Coordinates of stations and number of observations (3-hourly) used in the present validation analysis.

Station	Latitude	Longitude	Altitude (m)	Country	Latitudinal Zone
Summit (SUM)	72.57°N	38.38°W	3266	Greenland	Arctic
Tiksi (TIK)	71.58°N	128.92°E	8	Siberia, Russia	Arctic
Barrow (BRW)	71.32°N	156.61°W	8	Alaska, United States	Arctic
Trinidad Head (THD)	41.05°N	124.15°W	107	California, United States	USA; NH mid-latitudes
Table Mountain (TBL)	40.12°N	105.24°W	1689	Colorado United States	USA; NH mid-latitudes
Niwot Ridge (NWR)	40.04°N	105.54°W	3022	Colorado United States	USA; NH mid-latitudes
Finokalia (FK)	35.32°N	25.67°E	250	Greece	Mediterranean; NH mid-latitudes
Bermuda (BER)	32.27°N	64.88°W	30	United Kingdom	Tropics
Mauna Loa (MLO)	19.54°N	155.58°W	3397	Hawaii, United States	Tropics
Ragged Point (BAR)	13.17°N	59.46°W	45	Barbados	Tropics
Lauder (LDR)	45.04°S	169.68°E	370	New Zealand	SH mid-latitudes
Arrival Heights (ARH)	77.80°S	166.78°W	50	New Zealand, Antarctica	Antarctica
South Pole (SPO)	90.00°S	24.80°W	2837	Antarctica	Antarctica

For the validation, 3-hourly model values have been interpolated linearly in the horizontal at the stations' location (see Table 3.1, 3.2 and Fig. 3.1). In the vertical, simulated ozone concentrations have been extracted at the model level that matches the real altitude of the stations, which is equivalent to matching the mean pressure of model level and station. Validation scores (MNMB, r) are calculated for each station on a quarterly basis (DJF, MAM, JJA, SON). Time series plots show the model runs in comparison with the observations.

3.3 Ozone, NO2 and PM2.5/PM10 from the Chinese air-quality monitoring network

More than 1,500 in situ stations covering all major cities in China are operated by the China National Environmental Monitoring Center. They provide hourly observations of the pollutants PM10, PM2.5, O_3, NO_2, SO_2, and CO (Bai et al., 2020; Gou et al., 2017; Li et al., 2017; Liu et al., 2018). NO_2 is measured by a chemiluminescence technique (Zhang & Cao, 2015).

Unfortunately, historic data is not publicly available, but the real-time data can be accessed via websites of third parties (such as http://www.pm25.in and http://www.aqicn.org). Here we made use of the automated data download which was set up in the context of the MARCOPOLO and PANDA EU projects, http://www.marcopolo-panda.eu. Hourly data is available for individual stations, but also as city-mean averages of station values for megacities in China.

For the CAMS validation we have used averages of the various in situ PM, O_3 and NO_2 observations in a city to a single value per hour for each of 36 selected major cities. For comparison with the CAMS o-suite, we interpolated the model fields to the city centres.

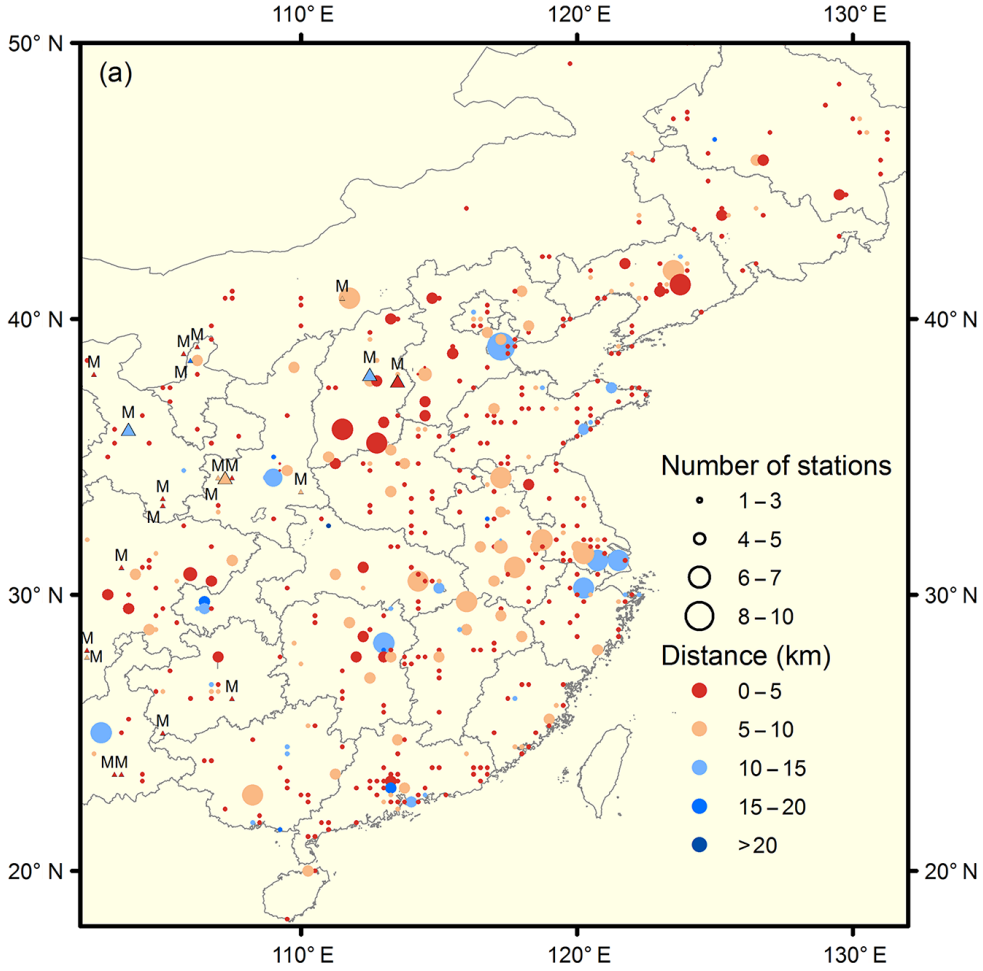

Figure 3.3. (Reproduced from Liu et al, 2018) Spatial distribution of in situ measurements. Measurements are allocated to 0.25 degree grid cells based on their geolocations. The magnitude of the size of symbols denotes the number of stations located in the same grid cell. The colour of the symbols denotes the average distance between stations located in the same grid cell. Triangles and "M" denote sites located in mountainous areas.

3.4 PM10, PM25, Ozone and NO2 from North America

Air quality surface data are acquired from the Airnow partnership (https://www.airnow.gov/) and Environment Canada for North America. This comprises data from a large number of surface observations performing routine air quality measurements (ozone: ca 790 sites; NO2: ca 160 sites, PM10: ca 170 sites, PM25: ca 660 sites. The data coverage can be seen on the pilot CAMS surface evaluation page (https://policy.atmosphere.copernicus.eu/aeroval.php#) by selecting the parameters and the AirNow network. As example, a map with mean ozone levels at the sites in North America in DJF 2020/2021 is shown in Figure 3.4:

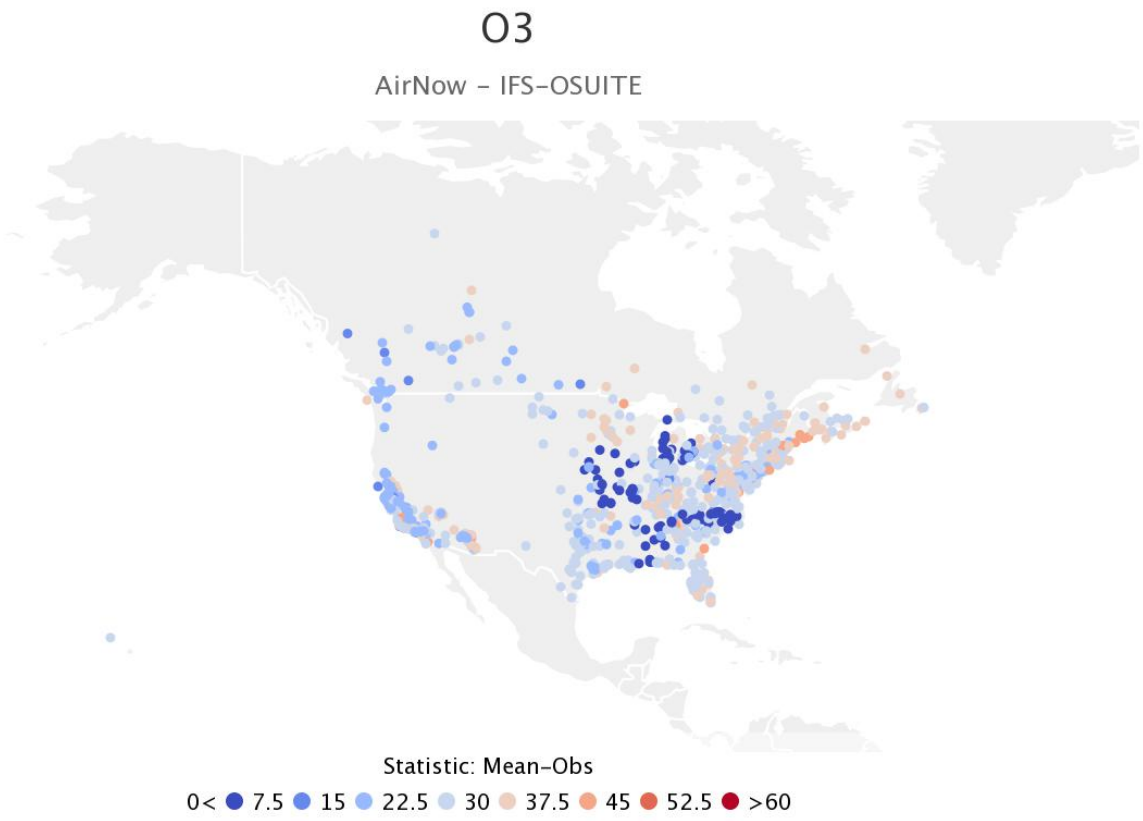

Figure 3.4 Location of active ozone measurements in North America in the period DJF 2020/2021. The color represents the mean ozone concentration in ppb, see legend below map.

Within the AirNow network measurements are collected by state, local or tribal monitoring agencies using federal reference or equivalent monitoring methods approved by EPA. Although preliminary data quality assessments are performed, the data in AirNow are not subjected to the full validation used to officially submit and certify data in EPA's regulatory database - the Air Quality System (AQS). AQS data are used for regulatory purposes, such as determining the attainment of the National Ambient Air Quality Standards (NAAQS), while AirNow data are used only to report the AQI to the public.

The National Air Pollution Surveillance (NAPS) program by Environment Canada is the main source of ambient air quality data in Canada. The NAPS program, which began in 1969, is now comprised of nearly 260 stations in 150 rural and urban communities reporting to the Canada-Wide Air Quality Database (CWAQD). Managed by Environment and Climate Change Canada (ECCC) in collaboration with provincial, territorial, and regional government networks, the NAPS program forms an integral component of various diverse initiatives, including the Air Quality Health Index (AQHI), Canadian Environmental Sustainability Indicators (CESI), and the US-Canada Air Quality Agreement.

4 IASOA surface observations in the Arctic

Simulated Near-Real-Time (NRT) ozone mixing ratios are validated against observations provided by the IASOA network (http://www.esrl.noaa.gov/psd/iasoa/).

Table 4.1: Coordinates of stations and list of species used in the present validation analysis.

Station	Latitude	Longitude	Altitude (m)	Country	Species
Villum Research station, Station Nord (VRS)	81° 36'5.26" N	16 ° 39'43.31" W	24	Greenland	O_3
Alert	82° 29'31.2'' N	62° 30'28.8'' W	186	Nunavut, Canada	O_3
Tiksi	71° 35'45.6'' N	128° 53'20.4'' E	249	Russia	O_3
Zeppelin Mountain	78° 54'29'' N	11° 52'53'' E	475	Svalbard	O_3

Villum Research Station, Station Nord, Greenland

Half-hour values of Ozone are measured with an UV absorption monitor, API, with a detection limit of 1 ppbv and an uncertainty of 3% for concentrations above 10 ppbv and 6% for concentrations below 10 ppbv (all uncertainties are at a 95% confidence interval). From December 2015 two monitors are measuring in parallel.

Ozone measurements in Denmark are performed under EN 17025 accreditation. It is not possible to follow the standards at the Villum Research Station due to the long distance from civilization and difficult logistics. However, the measurements are made as close as possible to the accreditation and the fewer visits possible is compensated by using 2 instruments for ozone monitoring (Skov et al. 2004, Heidam et al. 2004 and Skov et al. 2019 read for submission; Yang et al. 2019; ready for submission). The data are validated within a six months period after the data acquisition. The measurement site is located 2 km away from the military station, Station Nord, and thus local influence on ozone concentrations is at a minimum.

Measurements are aggregated to 3-hour averages to match the temporal resolution of the model. Model values have been interpolated linearly in the horizontal at the location of the stations. In the vertical, simulated ozone concentrations have been extracted at the model level that matches the real altitude of the station (surface). The average value is used for model validation when both monitors are operational. Error bars and uncertainties on the measurements are not applied in the analyses.

Zeppelin Mountain, Svalbard

Ozone is measured using an API 400A instrument. The data are reported as 1-hour averages with an uncertainty of 9% above 60 ppb, and 5.4 ppb below 60 ppb, (95% conf. interval) and a detection limit of 1 ppb. The QA/QC procedures consists of daily zero/span checks (internal), daily data check,

3 monthly visit, yearly linearity test. The measurement method is accredited according to ISO 17025.

Measurements are aggregated to 3-hour averages to match the temporal resolution of the model. Model values have been interpolated linearly in the horizontal at the location of the stations. In the vertical, simulated ozone concentrations have been extracted at the model level that matches the real altitude of the station (level 57 for the 60 layer version and level 131 for the 137 layer version). The average value is used for model validation when both monitors are operational. Error bars and uncertainties on the measurements are not applied in the analyses.

Alert, Nunavut, Canada

Hourly average surface ozone mixing ratios in parts per billion by volume (ppbv) are measured at Alert, Nunavut, Canada by the Canadian Air and Precipitation Monitoring Network (CAPMoN) of Environment and Climate Change Canada by UV absorption monitors. Each mixing ratio value is accompanied by a data validity flag and the detection limit of the measurement. The hourly averaged values are derived from the original sampling period of one-minute averages. The measurements have been referenced and adjusted to a NIST primary ozone photometer. Mixing ratios are reported to one decimal place, the detection limit is 1 ppbv, and all less than the detection limit mixing ratios are flagged as V1 and reported as measured by the instrument (i.e., not censored at the detection limit). Uncertainty of hourly average concentrations = ± 0.6 ppb (± 0.8 ppb in warm season; ± 0.5 ppb in cold season); daily and monthly average concentrations = ± 0.6 ppb; annual average concentrations = ± 0.5 ppb. The uncertainty is based on simultaneous field measurements of two collocated instruments both adjusted to National Institute of Standards and Technology Standard Reference Photometer (NIST/SRP) #16. The uncertainty was calculated as the standard deviation of differences from the true value assumed equal to the mean of the two instruments.

Measurements are aggregated to 3-hour averages to match the temporal resolution of the model. Model values have been interpolated linearly in the horizontal at the location of the stations. In the vertical, simulated ozone concentrations have been extracted at the lowest model layer (the height of the model surface at the station is 194m, while the real height is 186m). Error bars and uncertainties on the measurements are not applied in the analyses.

Tiksi, Russia

The quality of data is a joint effort by the program managers and the station technicians. Raw data is considered to be any original information as reported by the instrument and acquired by NOAA GMD data collection systems. No calibration coefficients are applied, and no data is removed from the record.

Quality controlled and processed data have undergone the adjustments of calibration coefficients and instrumental checks: A linear equation is applied to all data. The slope and zero values are calculated from a routine National Institute of Standards and Technology (NIST) Traceable calibration (Thermo 49i). In addition, monthly level span checks are performed at the station to ensure instrument stability and accurate instrument calibration. The instrumental is checked for flow through, lamp settings, and temperature and pressure corrections. Routine level checks ensure that the instrument calibration has not drifted

The data are processed to apply calibration factors and average minute data into one-hour average values. Outliers are removed, but only if they are extreme outliers exceeding 2 standard deviations from 5% or 95% seasonal values and cannot be explained. Data PI may also remove data that is of questionable quality with documentation as to the reason the data was removed. Example: Unexpected spike in otherwise very clean environment which was caused by people driving by inlet line during the sample time. Data is removed if there are instrumental errors or contamination to the system (ex. Water contamination through inlet line).

Measurements are aggregated to 3-hour averages to match the temporal resolution of the model. Model values have been interpolated linearly in the horizontal at the location of the stations. In the vertical, simulated ozone concentrations have been extracted at the model level that matches the real altitude of the station (level 56). Error bars and uncertainties on the measurements are not applied in the analyses.

5 Airbase surface observations for the Mediterranean and Europe

For ground-level concentrations, we use observations from the European Air quality database (AirBase; http://acm.eionet.europa.eu/databases/airbase/) which is the public air quality database system of the European Environmental Agency (EEA; http://www.eea.europa.eu/). AirBase contains air quality monitoring data and information from the European Environment Information and Observation Network (EIONET) submitted by the participating countries throughout Europe. The air quality database consists of multi-annual time series of air quality measurement data and their statistics for a representative selection of stations and for a number of pollutants. It also contains meta-information on the involved monitoring networks, their stations and their measurements.

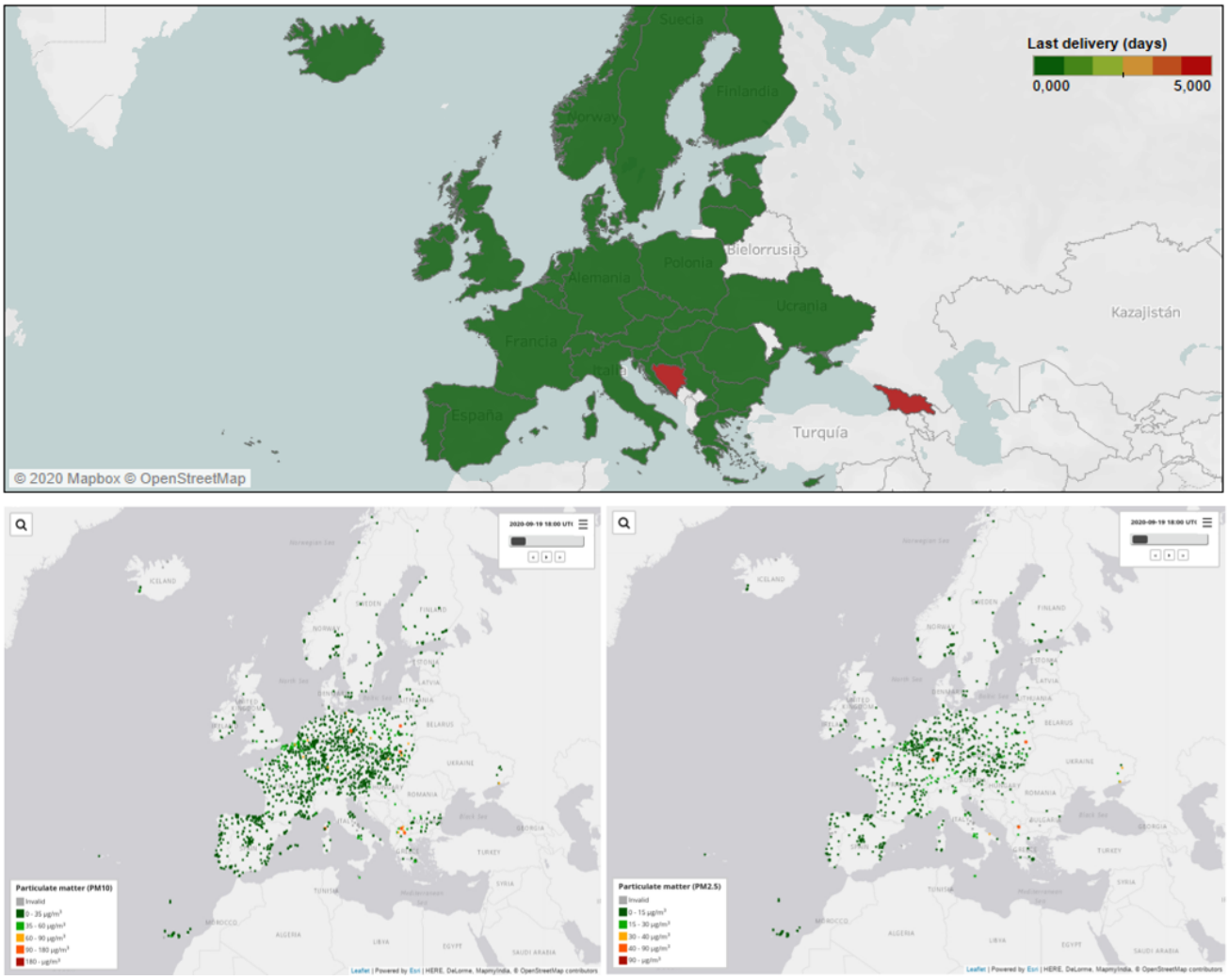

Figure 5.1. UTD report on data most recent delivery (all pollutants) (date of connection 29 September 2020). Top panel: Snapshot of the UTD report on data most recent delivery (all pollutants) for 29 September 2020, per country. Only 'hourly' data is included in this graph. Bottom panels: Up-to-date air quality data for PM10 and PM2.5 for 19 September 2020.

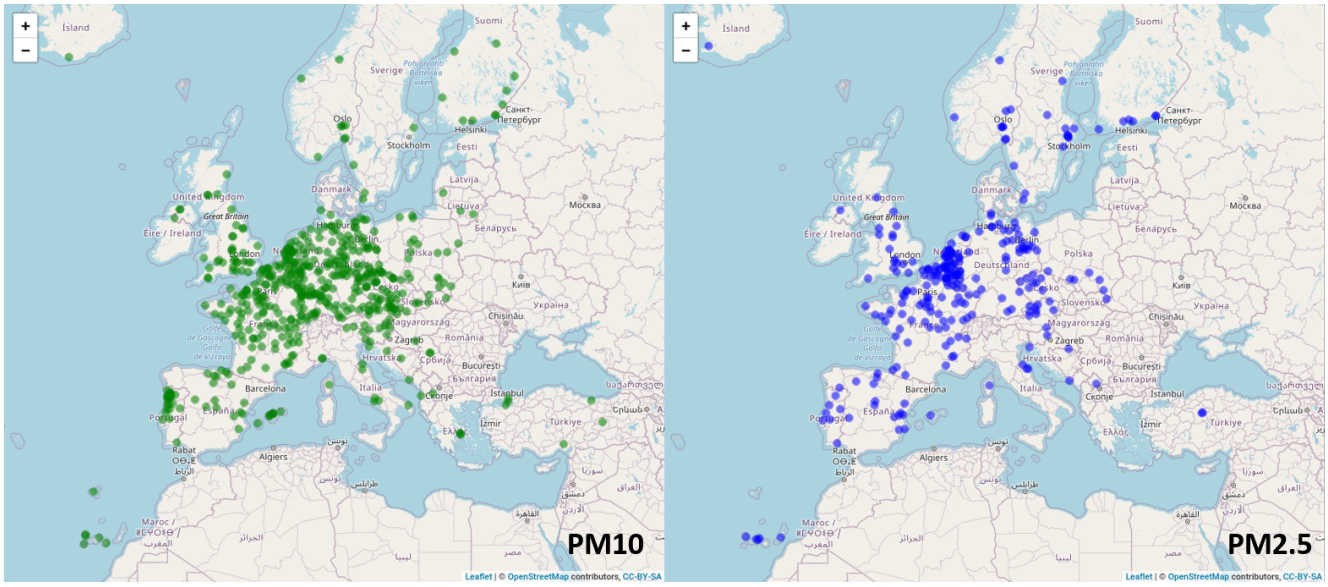

Figure 5.2. Joly-Peuch background regional sites (i.e., categories 1 to 5) in total 665 stations in Airbase for 2019. Left panel: PM10 stations (in total 545 stations) and right panel PM2.5 stations (in total 270 stations).

For the aerosol NRT evaluation, the data catalogue included the LIVE Air Quality Data service (http://discomap.eea.europa.eu/map/fme/AirQualityUTDExport.htm), which is the up-to-date (UTD) air quality data provided by EEA, is used, including PM10 and PM2.5 data. The download service provides access to UTD air quality data reported to EEA on hourly basis from EEA member countries. Depending on the member country a delay of some hours is expected from the measurement is taken until it is available in the download service. The delay is normally between 1 and 6 hours but it can take longer depending on the infrastructure setup in the specific country. The UTD dataflow is voluntary and the list currently counts 30 countries around Europe. The current status on data delivery (Fig. 5.1), reporting which countries are delivering data and what they deliver, may be found here:
https://tableau.discomap.eea.europa.eu/#/site/Aironline/views/Airquality_E2a_monitoring/DashboardE2a?:iid=10

The data offered via this service is provided as delivered by the member countries to EEA. EEA are not responsible for the quality or the correctness of the data.

Particularly, for PM10 and PM2.5 validation, those stations considered as background rural in the Joly-Peuch (Joly and Peuch, 2012) and EEA classification are considered in the aerosol validation. This classification method considers that on each site to be categorized, eight indicators are defined to characterize each pollutant time series (O_3, NO_2, NO, SO_2, or PM10) of the European AirBase network. A Linear Discriminant Analysis (Fisher, 1936) is used to best discriminate the rural and urban sites. After projection on the Fisher axis, ten classes are finally determined based on fixed thresholds, for each pollutant. Within this classification, background regional sites group falls into classes 1-5. As a result, a total of 665 EEA stations (see Figure 5.2) are considered in this comparison.

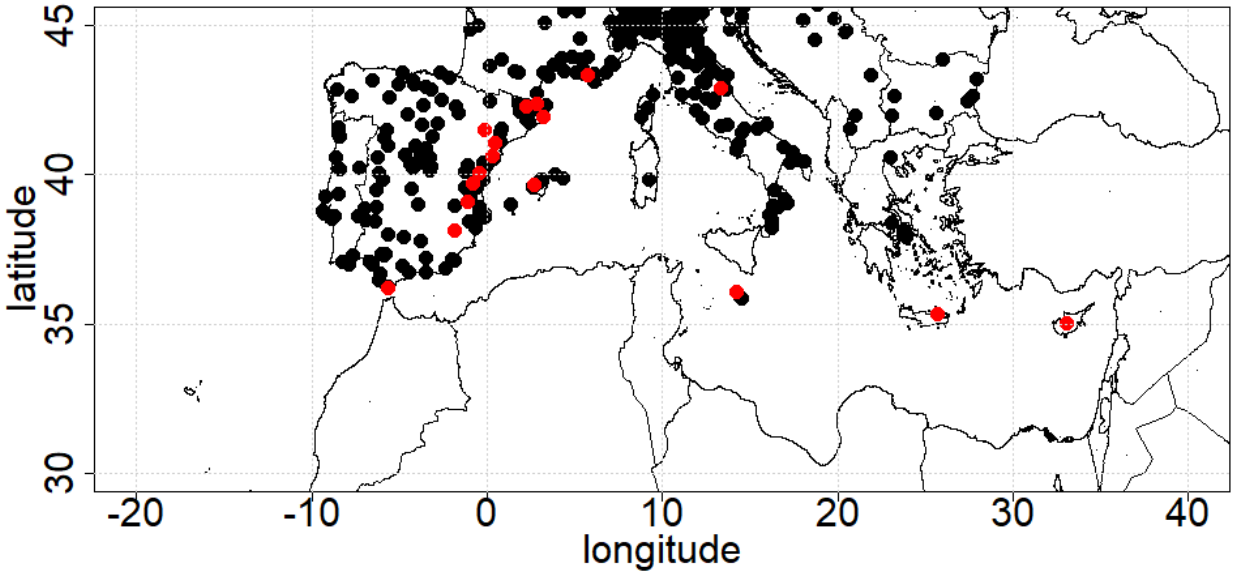

Figure 5.3. Available NRT surface ozone Airbase sites for period September-November 2019. With red cycles are denoted stations that fulfil the criteria shown in Table 2.

All PM10 and PM2.5 hourly available measurements (i.e. non-final validated observations) coincident with the model output are used for the 3-hourly evaluation. CAMS model outputs (PM10 and PM2.5) are bilinear interpolated in the horizontal to the station locations (see Figure 5.2).

Three-hourly values of PM10 and PM2.5 from AirBase and CAMS model outputs are used to check the model performance. Mean Bias (MB), Mean Normalised Mean Bias (MNMB), Fractional Gross Error (FGE), Root Mean Square Error (RMSE), Person correlation coefficient (r), and the number of data (NDATA), averaged over the study period are computed for this objective. This set of statistics is being computed for each selected site (shown in Figure 5.2).

Simulated Near-Real-Time (NRT) ozone mixing ratios are validated against observations provided by Airbase (http://acm.eionet.europa.eu/databases/airbase/). The data are downloaded through an FTP created by Météo France (ftp.cnrm-game-meteo.fr/TEST/). All available stations with surface ozone observations for period September-November 2019 are shown in figure 5.3.

The model performance has been carried out using all available stations in the Mediterranean that fulfil the criteria shown in Table 5.2. Table 5.1 shows names and coordinates for each one of the selected Mediterranean stations.

Model values have been interpolated linearly in the horizontal at the stations' location (see Table 5.1). In the vertical, simulated ozone concentrations have been extracted at the model level which matches the real altitude of the stations, which is equivalent to matching the mean pressure of model level and station. Validation scores (MNMB, r) are calculated for each station on a quarterly basis (DJF, MAM, JJA, SON). Time series plots show the model runs in comparison with the observations.

Table 5.1: Coordinates, elevation as, for each one of the selected Mediterranean stations.

Station Name	Stat_ID	Lon	Lat	Elevation (m)	Distance from the shore (km)
Al Cornocales	ES1648A	-5.66	36.23	189	16
Caravaka	ES1882A	-1.87	38.12	1	73
Zarra	ES0012R	-1.10	39.08	885	70
VIillar Del Arzobispo	ES1671A	-0.83	39.71	430	48
Cirat	ES1689A	-0.47	40.05	466	37
Bujaraloz	ES1400A	-0.15	41.51	327	60
Morella	ES1441A	-0.09	40.64	1150	51
Bc-La Senia	ES1754A	0.29	40.64	428	21
Ay-Gandesa	ES1379A	0.44	41.06	368	15
Ak-Pardines	ES1310A	2.21	42.31	1226	81
Hospital Joan March	ES1827A	2.69	39.68	172	3
Al-Agullana	ES1201A	2.84	42.39	214	25
Av-Begur	ES1311A	3.21	41.96	200	9
Plan Aups/Ste Baume	FR03027	5.73	43.34	675	21
Gharb	MT00007	14.20	36.07	114	31
Aliartos	GR0001R	23.11	38.37	110	18
Finokalia	GR0002R	25.67	35.32	250	4

Table 5.2: Criteria for the selection of stations in the Mediterranean.

1)	Station was selected from classes 1-2 in the O3 Joly-Peuch classification
2)	Station was identified as 1-2 in NO2 and NO Joly-Peuch classification when NOx data were available
3)	Data availability at each station to exceed 80% of all possible points during 2005-2012
4)	Statistically significant correlations between observed air temperature at 850hPa and surface ozone
5)	Station located within about 100 km from the shoreline of the Mediterranean

Airbase surface observations over Europe: ozone and NOx

The model performance has been evaluated using all available stations in the Europe that fulfil the criteria shown in Table 5.4. Table 5.3 shows names and coordinates for each one of the selected European stations.

Model values have been interpolated linearly in the horizontal at the stations' location (see Table 5.3). In the vertical, simulated ozone concentrations have been extracted at the model level which matches the real altitude of the stations, which is equivalent to matching the mean pressure of model level and station. Validation scores (MNMB, r) are calculated for each station on a quarterly basis (e.g. SON). Time series plots show the model runs in comparison with the observations.

Table 5.3: Station ID, Coordinates and elevation for each one of the selected European stations (period JJA 2019).

Stat_ID	Longitude	Latitude	Elevation		Stat_ID	Longitude	Latitude	Elevation
AT30103	14.867	48.18	465		ES1310A	2.214	42.312	1226
AT30202	15.919	48.106	581		ES1311A	3.213	41.959	200
AT30302	16.675	48.05	235		ES1379A	0.44	41.058	368
AT30403	16.523	48.392	260		ES1400A	-0.152	41.506	327
AT30502	15.047	48.879	570		ES1441A	-0.091	40.637	1150
AT31502	15.86	47.67	890		ES1489A	-3.231	42.875	911
AT31701	15.546	48.37	320		ES1491A	-2.704	43.406	116
AT53055	13.016	47.937	730		ES1531A	-4.253	43.153	650
AT80503	9.927	47.529	1020		ES1599A	-2.155	43.251	225
BETN063	4.668	50.655	145		ES1648A	-5.664	36.234	189
BETN066	6.002	50.629	295		ES1662A	-1.808	42.308	460
BETN073	4.988	50.503	160		ES1671A	-0.832	39.708	430
BETN085	6.002	50.303	490		ES1689A	-0.468	40.054	466
BETN093	5.235	50.274	265		ES1754A	0.288	40.643	428
BETN100	4.595	50.096	225		ES1793A	-6.734	37.104	31
BETN121	5.202	49.877	430		ES1802A	-3.468	40.909	995
BETN132	5.63	49.719	375		ES1806A	-3.221	40.288	795
CH0004R	6.979	47.049	1020		ES1827A	2.687	39.678	172
CH0005R	8.463	47.067	1031		ES1882A	-1.869	38.115	1
CH0019A	9.394	47.407	915		ES1883A	0.182	42.458	1005
CY0002R	33.058	35.038	532		FI00208	24.685	60.314	55
CZ0BKUC	16.086	48.881	334		FI00349	21.374	59.779	7
CZ0BMIS	16.724	48.792	245		FI00352	29.402	66.322	310
CZ0CCHU	13.615	49.068	1118		FI00356	24.112	67.967	566
CZ0CHVO	14.723	48.724	818		FI00357	28.303	68.477	262
CZ0CKOC	13.837	49.467	519		FI00428	31.047	63.143	235
CZ0ESVR	16.034	49.735	735		FR03027	5.727	43.335	682
CZ0HKRY	15.85	50.66	1001		FR07031	3.277	45.105	1040
CZ0JKMY	15.439	49.159	569		FR12020	0.18	43.63	240
CZ0JKOS	15.08	49.573	535		FR12029	0.845	43.884	222
CZ0KPRB	12.615	50.372	904		FR12031	1.822	43.441	260
CZ0LSOU	15.32	50.79	771		FR16302	7.13	48.493	770
CZ0MJES	17.19	50.242	625		FR20049	4.466	45.961	540
CZ0PPRM	12.678	49.67	740		FR22014	6.957	49.195	340
CZ0SONR	14.783	49.914	514		FR30028	7.011	48.051	1200
CZ0TBKR	18.539	49.503	890		FR35012	2.06	45.81	810
CZ0TCER	17.542	49.777	749		GB0013R	-3.717	50.598	119
CZ0URVH	13.42	50.58	840		GB0015R	-4.777	57.734	270
CZ0UTUS	13.328	50.377	322		GB0031R	-3.034	52.504	370
CZ0ZSNV	18.008	49.048	600		GB0033R	-3.206	55.862	180
DEBB053	14.015	52.564	88		GB0037R	-1.752	53.403	420
DEBB066	14.057	51.898	52		GB0043R	-4.691	51.782	160
DEBB075	13.124	52.484	39		GB0048R	-3.243	55.792	260
DEBW031	7.765	47.81	904		GB0745A	1.122	52.95	16

DEBY072	12.549	49.438	755		GB0838A	-0.772	52.554	145
DEHE024	9.775	51.292	610		GB0881A	-1.185	60.139	80
DEHE028	8.817	49.653	484		IE0001R	-10.241	51.938	10
DEHE050	9.271	51.361	489		IE0031R	-9.904	54.327	8
DEHE051	9.936	50.498	931		IE0090A	-6.883	54.066	170
DEHE052	8.446	50.222	811		IE0111A	-7.196	53.107	20
DEHE060	9.032	51.155	483		IT0842A	10.007	45.279	61
DEMV004	12.065	53.818	17		IT0989A	12.962	42.572	948
DEMV012	14.257	53.52	17		IT1474A	13.545	45.844	125
DEMV017	11.363	53.302	25		IT1665A	18.116	40.459	10
DENI031	8.091	53.596	2		IT1812A	9.497	45.913	1192
DENI051	10.612	51.758	939		IT1842A	13.337	42.901	1000
DESH008	10.241	54.093	45		IT1870A	11.643	45.29	18
DESH013	11.216	54.413	2		LT00051	26.004	55.463	180
DESN049	12.611	50.431	896		LT00052	24.29	54.092	130
DESN051	13.675	51.12	246		LT00053	21.887	56.008	155
DESN052	13.751	50.731	877		LU0103A	6.176	49.944	510
DESN053	12.953	50.428	1214		MK0042A	20.699	41.536	1333
DESN074	13.465	50.659	785		MT00007	14.197	36.067	114
DESN076	13.009	51.304	313		NO0015R	13.907	65.831	440
DESN079	14.75	51.285	148		NO0039R	8.877	62.782	210
DESN080	12.234	51.396	122		NO0043R	11.528	58.997	180
DEST039	10.618	51.799	1130		NO0052R	5.201	59.197	30
DETH026	10.375	50.562	450		NO0056R	11.074	60.373	280
DETH027	11.135	50.5	840		PL0002R	21.972	51.814	177
DETH042	10.867	51.333	420		PL0004R	17.535	54.754	2
DEUB001	8.308	54.925	12		PL0005R	22.038	54.125	157
DEUB004	7.908	47.913	1205		PL0014A	20.792	51.835	176
DEUB005	10.757	52.801	74		PL0077A	17.934	53.662	121
DEUB028	12.722	54.437	1		PL0094A	19.233	52.143	177
DEUB029	10.77	50.654	937		PL0105A	19.518	51.291	166
DEUB030	13.032	53.141	65		PL0121A	21.117	49.634	327
DK0031R	8.427	56.29	37		PL0128A	20.455	52.286	72
DK0054A	10.736	54.746	10		PL0150A	23.642	53.215	180
EE0009R	25.931	59.494	32		PL0182A	14.382	53.122	2
EE0011R	21.845	58.376	6		PL0247A	17.773	52.501	122
EE0016A	26.759	58.703	50		PT01047	-8.694	41.802	777
ES0001R	-4.351	39.547	917		PT01048	-7.791	41.371	1086
ES0005R	-8.924	42.721	685		PT02021	-8.101	40.641	741
ES0008R	-4.85	43.439	134		PT03096	-8.466	39.352	143
ES0009R	-3.143	41.274	1360		PT05012	-7.679	37.312	300
ES0010R	3.316	42.319	76		SE0005R	15.32	63.845	380
ES0012R	-1.101	39.083	885		SE0013R	21.063	67.879	524
ES0013R	-5.898	41.239	985		SE0014R	11.914	57.394	10
ES0014R	0.735	41.394	470		SE0032R	15.565	57.811	263
ES0296A	3.015	39.747	7		SE0035R	19.767	64.244	271
ES1201A	2.842	42.392	214		SE0039R	15.472	59.728	132

Table 5.4: Criteria for the selection of stations for Europe as a whole.

1)	Station was selected from classes 1-2 in the O3 Joly-Peuch classification
2)	Station was identified as 1-2 in NO2 and NO Joly-Peuch classification when NOx data were available
3)	Data availability at each station to exceed 80% of all possible points during 2005-2012

6 IAGOS aircraft measurements

The IAGOS Research Infrastructure (Petzold et al, 2015; http://www.iagos.org) uses sensors mounted on commercial aircraft to obtain in situ measurements of various chemical species in the atmosphere. All IAGOS-CORE aircraft are equipped with a package which provides volume mixing ratios of the trace gases ozone, CO, and water vapour, cloud particle number concentration, and meteorological measurements including temperature, pressure and winds. Further details on instruments and their operation can be found in Nédélec et al. (2015) for ozone and CO, and in (Helten et al. 1998, Neis et al, 2015, a-b, Smit et al., 2008, 2014) for water vapour. Data are stored every 4s throughout the flight and are used either as tropospheric profiles taken during landing and take-off or as horizontal trajectories in the upper troposphere-lower stratosphere (UTLS) obtained during the cruise part of the flight. The IAGOS network is shown in Figure 6.1. So far, the IAGOS fleet has visited 307 airports. More details on the frequency of the airports visited by IAGOS are available on the IAGOS data portal website via http://www.iagos.org. The airports are spread over latitudes ranging from -37°S (Melbourne) to 64°N (Fairbanks). Most airports serve large urban conglomerations where pollution would be expected to be high. Most airports are also located in coastal areas and are obviously free of vegetation. Otherwise, the airports are representative of a wide variety of environments. Petetin et al (2018) addressed the representativeness of IAGOS measurements in the lower troposphere and have found that in the first few hundred metres above the surface, IAGOS profiles can be considered as suburban or urban background stations shifting towards regional representativeness as altitude increases.

Data are transmitted when the aircraft arrives at its parking gate and are available for use in CAMS after a time-delay of a few days (ideally less than 3). This time-delay is to enable the project PI to give a first check of the data. For ozone and CO, this first stage in the QA/QC procedure is fully described in Nédélec et al. (2015). The measurement accuracy of ozone is estimated at ±[2 ppbv + 2%] and for CO ±[5 ppbv + 5%], and are independent of geographic location and altitude. IAGOS Capacitive Hygrometers (ICH) provide relative humidity data with respect to liquid water. The in-flight calibration method allows the provision of humidity measurements in near–real time with an uncertainty of ±8% RH at the surface and ±7% RH in the upper troposphere (Smit et al., 2008, 2014) with a detection limit for a water vapour mixing ratio of 10 ppmv (Kunz et al., 2008). Sometimes two aircraft arrive or depart from the same airport within 3 hours, which offers an opportunity to crosscheck the measurements from two different aircraft. Since 1994, about 8000 profile inter-comparisons (1 hour time difference) have been made and highlight the quality and internal consistency of the entire IAGOS data set for ozone and CO (Blot et al., 2021). Similarly, two aircraft may fly along a similar trajectory at cruise altitude enabling a crosscheck of the instruments in the UTLS. This happens less frequently (so far about 645 for a time difference of 1 hour) but is still an important check on the performance of the instruments.

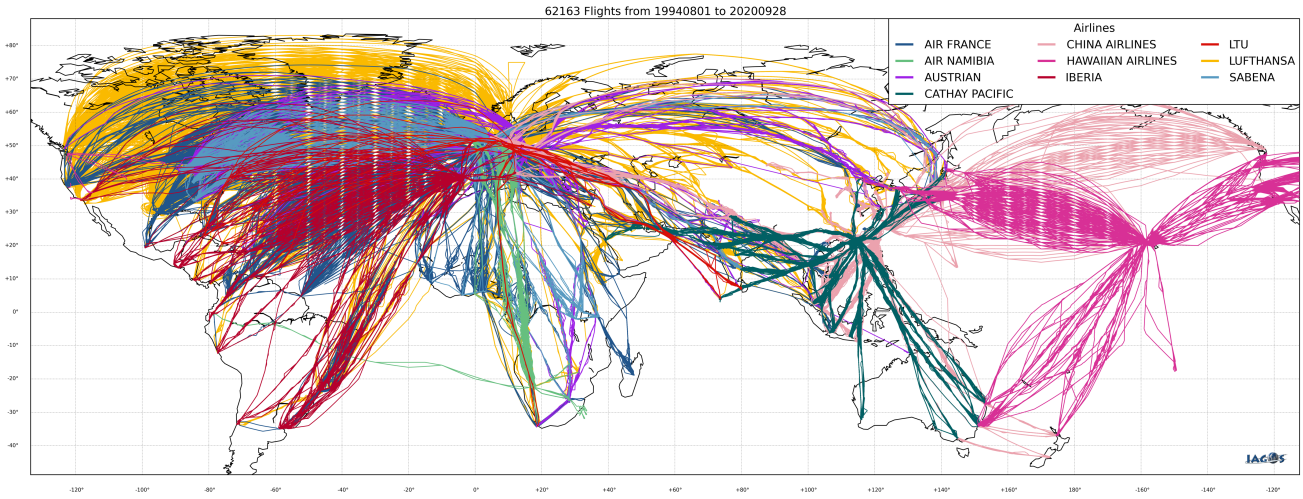

Figure 6.1. Flight tracks since the beginning of IAGOS (MOZAIC) in August 1994 until 28 September 2020.

Additionally, each instrument's zero and calibration factor are regularly checked in-flight. For ozone, this calibration is performed every two hours. Similarly, for CO checks are made every 20 minutes or if the temperature of the instrument increases by more than 1K. The purpose of these checks is primarily to check for instrument drift. For water vapour, an inflight calibration method corrects the potential drift of the sensor offset at zero relative humidity (Smit et al., 2008). At the end of their operational period (approximately 6 months for O3/CO, 2 months for H2O) the instruments are removed from the aircraft and calibrated in the laboratory. For ozone and CO this calibration is performed with a reference analyser, which is periodically crosschecked with a primary standard at the National Institute of Standards and Technology in France. For water vapour, the capacitive hygrometers are calibrated against a Lyman-α resonance fluorescence hygrometer (Kley and Stone, 1978) with respect to RH over liquid water (Helten et al., 1998; Smit et al., 2014). Due to the 6 months wait, these post-calibrated data (Level 2) are not available for use in the NRT reports but are usually ready for evaluation with the reanalysis. From the beginning of the MOZAIC program in 1994 (Marenco et al., 1998), the measurement quality control procedures have remained unchanged ensuring that the time-series are free of instrumental artefacts, which is vital for the evaluation of the reanalysis.

Validation Methodology

Global

Ozone, CO and water vapour profiles from IAGOS-CORE (in NRT) obtained during landing and take-off are used in the reports with additional profiles from IAGOS-CARIBIC used for the evaluation of the reanalysis. Frankfurt has the most consistent availability of data dating back to the beginning of MOZAIC in 1994. Other airports are included in the report if they are considered to be of interest and if the availability of data is good. For example, recently, there is a high frequency of flights to airports in the Gulf of Guinea (Lagos, Port Harcourt, Malabo) and West Africa (Luanda and Abuja) and frequent flights to the Arabian Peninsula (Muscat, Doha, Jeddah, Manama, Riyadh, Kuwait). Eastern North America (New York, Chicago, Philadelphia) and Asia (Taipei, Hong Kong) are also included.

In the current version of the processing code used for the comparisons with IAGOS, each observed profile (take-off/landing) for the different species (O3, CO, H2O) is compared with the profile extracted from the model's grid-box containing the airport and using the closest time step from the model. A daily mean is then calculated from these individual profiles for both observations and model analysis/forecast. In the validation reports the individual profiles, daily mean profiles, and seasonal time-series of the daily mean mixing ratios calculated for 5 different atmospheric layers. The layers are: the surface layer extending up to 950hPa, the boundary layer from 950-850 hPa and the free troposphere from 850hPa to the upper troposphere. The height of the tropopause (if encountered) is determined from the IAGOS temperature profiles and the upper troposphere (UT) is defined as being 1km below the tropopause and the lower stratosphere (LS) 1km above the tropopause.

A new processing code has been recently implemented for comparisons with IAGOS including not only profile data but also cruise-level data. In this code the collocation method uses 4D interpolation of the global model data to the IAGOS flight track. For each flight, IAGOS time series are first subsampled to a temporal resolution of 1 minute corresponding to about 15 km (originally 4s). The subsampled dataset is then used to interpolate the model in space and time to the subsampled points of the IAGOS flight. Profiles and cruise-level comparisons are done separately by extracting the adequate subsets from the collocated dataset. The improvement from the application of the 4D interpolation method in the profile comparisons is investigated. These procedures are routinely executed and the generation of new comparison plots, in particular for cruise data, is included in the validation reports.

Regional

Ozone and CO profiles from IAGOS-CORE (in NRT) obtained during landing and take-off at European airports are used. Observations in ppbv are converted to µg/m3 using the IAGOS temperatures and pressures. Frankfurt and Paris have up to four flights per day. Other airports such as Vienna and Amsterdam are visited more infrequently. The models are interpolated to the flight track using the closest hour to the time of the profile, and from the 24-, 48-, and 72-hour preceding forecasts.

7 MOPITT CO and IASI CO and ozone observations

The Infrared Atmospheric Sounding Interferometer (IASI) is a nadir looking thermal infrared (TIR) sounder instruments on-board the satellite MetOp-B. It is designed to measure the spectrum emitted by the Earth-atmosphere system in the TIR spectral range, using nadir geometry (Clerbaux et al., 2009). MetOp-B IASI has been launched in October 2012 (Hurtmans et al., 2012) and provides global Earth coverage twice a day (~ 09:30 and 21:30 local time), with a horizontal resolution of 12 km diameter footprint on the ground at nadir. We use MetOp-A CO total column data, version v20100815 from 1st October 2007 to 29 September 2014, version v20140922 from 30 September 2014, version v20191122 from 22nd November 2019 and MetOp-B version V6.5.0 data from 1 March 2020 onwards. These data have been processed at LATMOS using a retrieval code called FORLI (Fast Optimal Retrievals on Layers for IASI), developed at ULB (Université Libre de Bruxelles). The IASI CO product is available at https://cds-espri.ipsl.fr.

Following the recommendations of Hurtmans et. al., 2012 we filter the data with bias values lower/higher than -0.15/0.25 x 10^{-9} W/(cm^2 cm^{-1} sr) and an RMS larger than 2.7 x 10^{-9} W/(cm^2 cm^{-1} sr). Also, we filter the data with CO total column > 20 x 10^{18} molec/cm^2. And only the data with "super" quality flag is equal to 0 were used. The estimated bias of the IASI CO data is about 7% in the Northern Hemisphere and equatorial region and 11% in the Southern Hemisphere. In case of high CO concentrations, such as during fire events, bias can be up to 17% (George et al., 2009).

The IASI O_3 data are also available at https://iasi.aeris-data.fr. The IASI O_3 product from FORLI is a vertical profile retrieved on 40 layers between surface and 40 km, with an extra layer from 40 km to the top of the atmosphere (Boynard et al., 2016). The data product provides averaging kernels and relative total error profiles, on the same vertical grid. To avoid cloud contamination, retrievals are only performed for clear or almost-clear scenes with a fractional cloud cover below 13%, identified using the cloud information from the EUMETSAT operational processing (August et. al., 2012). A second filter is applied to remove observations with poor spectral fits (root mean square of the spectral fit residual higher than 3.5 x 10^{-8} W cm $^{-2}$ sr cm^{-1}). The full description of the FORLI-O_3 software and the optimal estimation method algorithm is given in Hurtmans et al. (2012).

For the validation we use IASI MetOp-B O_3 data with DOFS<2 and a ratio of the surface to 6 km O_3 partial column to the total O_3 column higher or equal to 0.085, which indicates too high O_3 in the troposphere. For the comparison with IASI data, the vertically integrated model O_3 data were transformed using IASI averaging kernels (see formula below, Rodgers, 2000) and selected corresponding to the satellite overpass time.

IASI O_3 total columns are consistent with GOME-2, Dobson, Brewer and SAOZ measurements with global mean differences up to 2% depending on the instrument. The comparison results between IASI against smoothed ozonesonde partial O_3 columns vary in altitude and latitude, with maximum standard deviation for the 300-150 hPa column 20-40% due to strong ozone variability and a priori uncertainty. Compared to ozonesonde data, the IASI product overestimates the O_3 abundance in the stratosphere (up to 20 % for the 150-25 hPa column) and underestimates the O_3 abundance in the troposphere (within 10 % for the mid-latitudes and ~ 18 % for the tropics). (Boynard et al., 2018).

The MOPITT instrument is mounted on-board the NASA EOS Terra satellite and has been operational since March 2000 (Deeter et al., 2010). It measures upwelling radiation in the thermal infrared spectral range using gas-filter correlation radiometry. At nadir view, the MOPITT instrument has a horizontal resolution of 22 x 22 km^2 and allows for global coverage within three days with overpass time at about 10:30 local time. The data used corresponds to the daytime CO total columns from the version 8 of the MOPITT thermal infrared product level 3. MOPITT V8 data are available at https://www2.acom.ucar.edu/mopitt.

For the validation, the modeled data are interpolated to the satellite overpass time and transformed from mass mixing ratios in kg/kg to volume mixing ratios, mole/mole:

The VMR of CO [ppbv] = 28.9644 / 28.0101 *1e9 * MMR CO [kg/kg]. The data is regridded to the same grid as used for the MOPITT gridded data (1x1 TM5), with conserved mass. The modeled profiles (X) are transformed by applying the satellite averaging kernels (A) and the a priori profile (X_a) according to the following equation (Rodgers, 2000) to create the profiles X^* appropriate for comparison with satellite data:

$$X \quad = X_a + A(X - X_a)$$

We should mention at this point, that a comparison of MOPITT V8 validation results calculated by applying the averaging kernels for each retrieval to the 'true' CO profile, with validation results based on long-term monthly-mean averaging kernels have revealed that the difference between the two is small (Merritt Deeter, private communication).

The averaging kernels indicate the sensitivity of the satellite measurement and retrieval system to the true CO profile, with the remainder of the information set by the a priori profile and retrieval constraints (Emmons, 2009; Deeter et al., 2010). The model CO total columns, used in the comparison with satellite observations, have been calculated using the profiles $\boldsymbol{X}^*$ which have the same vertical resolution and a-priori dependence as the satellite retrievals.

The averaging kernels indicate a low sensitivity near the surface and maximum sensitivity in the lower troposphere (4–6 km), where MOPITT shows slightly higher sensitivity compared to IASI (George et al., 2009).

The IASI sensitivity is the lowest over the cold surfaces of Antarctica and Greenland, especially during March-April-May season.

8 SCIAMACHY/GOME-2/TROPOMI NO2 and HCHO observations

The Scanning Imaging Spectrometer for Atmospheric Chartography (SCIAMACHY, Bovensmann et al., 1999) is an UV/visible/near infrared spectrometer, which operated on Envisat from August 2002 to March 2012 when the European Space Agency lost contact to the satellite. SCIAMACHY observed the light scattered in the atmosphere in nadir and limb geometry and also performed solar and lunar occultation measurements. Tropospheric trace gas columns can be derived from the nadir measurements at spatial resolution of 30 x 60 km^2 for most gases with global coverage achieved after 6 days of observations. Envisat was in a sun-synchronous orbit with a descending node equator crossing time of 10:00 LT. SCIAMACHY raw radiances and irradiances are calibrated and distributed by DLR, the level 1 data version used by the IUP, University of Bremen in house DOAS retrievals used for analysis of trace columns in this project correspond to V7.04. The DOAS analysis applied to the SCIAMACHY data is described by Richter et al. (2005) for NO_2 and by Wittrock et al. (2006) for HCHO.

The Global Ozone Monitoring Experiment-2 (GOME-2) is a nadir viewing UV/visible spectrometer observing scattered sunlight in the spectral range from 240 to 790 nm with moderate spectral resolution of 0.26 to 0.51 nm (Munro et al., 2016). The first GOME-2 operating on MetOp-A provides data since January 2007, the second instrument on MetOp-B since December 2012. The third instrument on MetOp-C provides data since early 2019. All three satellites are in sun-synchronous morning orbits with descending node equatorial crossing times of 09:30 LT. The spatial resolution of the instruments is 40 x 80 km^2 in nominal operation, providing nearly global coverage every day. For GOME-2 on MetOp-A this was changed to 40 x 40 km^2 in July 2013, improving spatial resolution at the expense of coverage.

Raw radiances and irradiances measured by the GOME-2 instruments are calibrated by EUMETSAT and the resulting level 1 data distributed in near real time (NRT) via EUMETCAST. Data is received at the IUP, University of Bremen and analysed for trace gas columns using in-house DOAS retrievals (Richter et al., 2011; Vrekoussis et al, 2010). The data sets used for CAMS validation are based on the NRT level 1 data and are not updated by the consolidated data, which is available at EUMETSAT after a few days or reprocessed data, which is provided by EUMETSAT at irregular intervals. The level 1 data version is therefore not consistent through the data set, meaning that different level 1 data versions are used for model validation. Data reception through EUMETCAST is sometimes interrupted for technical reasons or due to poor weather conditions leading to loss of connection. Most missing data is added within a few days, but some gaps remain in the IUP data set.

The TROPOspheric Monitoring Instrument (TROPOMI) is an UV/visible/near and short-wave infrared push-broom imaging spectrometer operating on board the Copernicus Sentinel-5 Precursor satellite since October 2017. Sentinel-5 is in sun-synchronous orbit with an equatorial crossing time of 13:30 LT in ascending node, has a swath of 2600 km and provides daily global coverage. Compared to SCIAMACHY and GOME-2 the spatial resolution is finer (3.5x7 km^2 at nadir before August 2019 and 3.5x5.5 km^2 afterwards), the signal to noise ratio is improved and the fraction of cloud free observations is larger due to the smaller footprint (Veefkind, 2012; https://sentinel.esa.int).

TROPOMI calibrated level 1 offline data are copied from the Copernicus Science Hub as soon as they become available. As the level 1 data version may change over the mission and no reprocessing is

performed, level 1 data from different processing versions may be used in the validation. NO_2 settings of the DOAS fit are similar to those used in Richter et al. (2011) for GOME-2, the HCHO retrievals are described in Alvarado et al. (2020).

As the European Space Agency lost contact to Envisat in April 2012, SCIAMACHY data is used for validation prior to that date and GOME-2/MetOp-A data is used for subsequent comparisons until the end of 2020. Comparisons to GOME-2/MetOp-A are not continued past that date due to instrument degradation. TROPOMI, GOME-2/MetOp-B and GOME-2/MetOp-C comparisons are provided since January 2019.

Tropospheric NO_2

Tropospheric NO_2 columns are computed from level 1 SCIAMACHY/GOME-2 and TROPOMI data using a three-step approach:

1) Applying the DOAS retrieval to measured spectra which yields the total slant column (molec/cm^2) using: (SCIAMACHY/GOME-2A) a MOZART-model based climatology as a-priori (see Richter et al., 2005); (TROPOMI/GOME-2C) CAMS osuite NO_2 as a-priori.

2) Correction of the stratospheric contribution by applying: (SCIAMACHY/GOME-2A) the reference sector correction approach; (TROPOMI/GOME-2C) the STREAM-B algorithm which is an IUP-Bremen version of the STREAM algorithm by Beirle et al. (2016).

3) Conversion into vertical columns by application of an air mass factor (molec/cm^2).

In addition, a chi-square limit of 5 x 10^{-3} is applied to the results of the DOAS fit and only observations with solar zenith angles between 0 and 85° are regarded. Only data with a FRESCO+ (Wang et al., 2008) cloud fraction smaller than 0.2 are used but no further cloud correction is applied. In the case of TROPOMI data, the cloud fraction is taken from the operational NO_2 product.

Monthly mean tropospheric NO_2 columns are associated with relative uncertainties of roughly 20% - 30% in polluted regions with an additional absolute uncertainty of 5 x 10^{14} molec/cm^2. These are broad error estimates only. Therefore, in future NRT reports, standard deviations derived from monthly mean values for each specific month will be added to the satellite time series of tropospheric NO_2 columns as a first estimate on how the model simulated values compare to satellite retrievals.

The data product used here has some limitations mostly due to the stratospheric correction, which can lead to negative NO_2 columns at high latitudes in spring for SCIAMACHY/GOME-2A as a result of the simplistic reference sector approach. The STREAM-B stratospheric correction method used for TROPOMI/GOME-2C leads to a negative offset in the current preliminary TROPOMI and GOME-2C data versions and will be improved by addition of tropospheric background values in the near future. For SCIAMACHY and GOME-2A, the air mass factors are based on a monthly climatology created from one year of MOZART model profiles and thus cannot reproduce short-term variations in meteorology or biomass burning activity. For TROPOMI and GOME-2C, the approach is different as the CAMS global NO_2 output interpolated to the time and location of the satellite overpass are used as a priori for the air mass factors, better reflecting actual atmospheric conditions.

Stratospheric NO_2

It is important to note that the SCIAMACHY/GOME-2/TROPOMI stratospheric columns are in fact total columns derived using a stratospheric air mass factor. To minimize the impact of the troposphere, only data over the clean Pacific region are used (180°E - 220°E). Still, the amount considered here as being stratospheric includes a weighted part of tropospheric NO_2.

A chi-square limit of 5×10^{-3} is applied to the results of the DOAS fit and only observations with solar zenith angles between 0 and 85° are regarded. No cloud screening is applied for stratospheric NO_2.

Monthly mean stratospheric NO_2 columns are associated with relative uncertainties of roughly 5 % - 10% and an additional absolute uncertainty of 1×10^{14} molec/cm^2 (these values are only valid over the clean Pacific). These are broad error estimates only. Therefore, in future NRT reports, standard deviations derived from monthly mean values for each specific month will be added to the satellite time series of stratospheric NO_2 columns as a first estimate on how the model simulated values compare to satellite retrievals.

Tropospheric HCHO

Tropospheric HCHO columns are computed under the assumption that stratospheric HCHO amounts are negligible. HCHO columns are derived from level 1 SCIAMACHY/GOME-2A/GOME-2B/TROPOMI data using the DOAS method. For SCIAMACHY and GOME-2A air mass factors are based on a static monthly climatology using land surface classification and biomass burning statistics to estimate the vertical HCHO profile. For TROPOMI and GOME-2B, the daily CAMS global HCHO profiles interpolated to the time and location of satellite overpass are used as a priori.

A chi-square limit of 2×10^{-3} is applied to the results of the DOAS fit from GOME-2A/GOME-2B data and only observations with solar zenith angles between 0 and 60° are used. For SCIAMACHY the solar zenith angle limits are the same, but the chi-square limit is 2.5×10^{-4}. For GOME-2A/GOME-2B, only data with a FRESCO+ cloud fraction lower than 0.2 are used but no further cloud correction is applied. For TROPOMI, the chi-square limit is 1×10^{-2}, the SZA limit is 75° and only data with cloud fractions below 0.2 are used without further cloud correction. As HCHO retrievals are subject to drifts and offsets, the values are normalized over the Pacific sector.

Monthly mean HCHO columns are associated with relative uncertainties of roughly 10% - 30% and an additional absolute uncertainty of 2×10^{15} molec/cm^2. As these uncertainty estimates are much larger than for NO_2, data are smoothed to reduce the impact of noise. The error estimates are broad values only. Therefore, in future NRT reports, standard deviations derived from monthly mean values for each specific month will be added to the satellite time series of tropospheric HCHO columns as a first estimate on how the model simulated values compare to satellite retrievals. HCHO column data in the region of the South Atlantic Anomaly are not valid and are therefore not regarded for model validation.

QA/QC procedures and processing

Quality assurance of the satellite data is based on application of the above-mentioned criteria for the fitting residual and the cloud fraction. While the first ensures that the spectral retrieval of the trace gas has a good quality, the second limits the data set to those observations with good sensitivity to the troposphere (not applied for stratospheric NO_2). In addition to these automated

tests, visual inspection of daily maps is used to remove orbits which have offsets, usually resulting from instrumental changes after power switch-off or from calibration problems. This is however rarely the case.

Treatment of model data

The first step consists in selecting the model output corresponding to the satellite overpass time (approx. 10:00 solar local time for SCIAMACHY, 09:30 for the GOME-2 instruments, 13:30 for TROPOMI). The model results are then integrated in the vertical to derive tropospheric and stratospheric vertical columns (molec/cm^2), as only vertical columns are retrieved from the satellite measurements and not concentrations at specific heights. For the separation of the stratosphere and troposphere, a latitude dependent tropopause height is used.

The approaches used for treating the model data differ for SCIAMACHY and the GOME-2 instruments on the one hand and TROPOMI on the other hand.

For SCIAMACHY/GOME-2A/B, the spatial resolutions of the models are coarser than that of the standard satellite product (0.125° x 0.125°). Thus, the daily satellite measurements are re-gridded to the corresponding model resolution of 0.4° for C-IFS runs. In this process, the average of all valid SCIAMACHY/GOME-2 grid boxes within one model grid box is taken without applying any area weighting, i.e., all satellite data are considered as long as part of it is located within the model box.

Finally, the model data is selected according to the existing satellite data, ensuring that both datasets consist of data for the same days at the same locations. This is important because for example SCIAMACHY data are not available at daily global coverage. In optimal conditions, the global coverage would be obtained every 6 days. Moreover, with the exception of SCIAMACHY HCHO, tropospheric columns are only determined for clear sky pixels, i.e., cloud fraction smaller than 20% according to the FRESCO+ data. For this reason, the daily model data previously selected for the overpass time are then matched to the available satellite data, which is already converted to the model resolution.

For TROPOMI and GOME-2C, model data are interpolated in space and time to each individual measurement. The resulting “orbital” model data are then treated just like the satellite measurements, applying the same quality and cloud filtering and gridding to the model resolution of 0.4° for C-IFS runs. In this process, the average of all valid TROPOMI measurements within one model grid box is taken without applying any area weighting, i.e., all satellite data are considered as long as their centre is located within the grid box.

In order to get sufficient signal to noise ratio and statistical representativeness, all data are considered as monthly averages only.

9 Aerosol and dust optical depth from AERONET

High quality aerosol optical properties are provided by the ground-based sun-/sky photometer networks of AERONET (Aerosol, Robotic NETwork; Holben, 2001: http://aeronet.gsfc.nasa.gov/) programme. The AERONET program provides a long-term, continuous and readily accessible public domain database of aerosol optical, microphysical and radiative properties for aerosol research and characterization, validation of satellite retrievals, validation of aerosol models, and synergism with other databases. The network imposes standardization of instruments, calibration, processing and distribution.

Holben et al. (1998) and Eck et al. (1999) found relative uncertainties for reference AERONET instruments better than 0.2–0.5 and 1.5% for field instruments in the visible and the near-infrared range (Ecket al., 1999; Schmid et al., 1999). This means an uncertainty due to calibration between 0.002 and 0.005 for reference instruments and 0.015 for instruments calibrated by means of intercomparison techniques and regular inter-annual checks in calibration laboratories.

Since October 2015, AERONET recommends the new CE318-T (Triple) instrument (see AERONET news at http://aeronet.gsfc.nasa.gov/), which has been designed to perform a complete cycle of diurnal photometric measurements during both daytime and night-time (Barreto et al., 2016). The CE318-T, with new improvements that permit to extend photometric information at night-time using the moon as a light source, will replace the standard AERONET Cimel sunphotometer.

In their comprehensive assessment evaluation of the new CE318-T, following the error propagation theory, Barreto et al. (2016) provided an estimation of the combined CE318-T AOD standard uncertainty for each calibration method. For the daylight period Barreto et al. (2016) expect similar values to those calculated for standard sunphotometer versions, ranging between 0.002 and 0.009 for reference instruments and 0.015 for field instruments. For the night-time period, Barreto et al. (2016) estimate AOD uncertainty values of 0.011–0.014 for visible channels (with the exception of 440 nm, with values up to 0.016 for higher phase angles) and 0.012–0.018 for near-IR channels. For field instruments calibrated using the Moon Ratio technique they found AOD uncertainty between 0.011 and 0.019. Using the new Sun Ratio technique (Barreto et al., 2016), higher uncertainties are expected: 0.012–0.015 (0.017) for visible (440 nm) channels and 0.015–0.021 for longer wavelengths. For instruments calibrated by means of the new Sun-Moon gain factor technique (Barreto et al., 2016), the uncertainties range from 0.016 to 0.019.

AERONET provides globally distributed observations of spectral aerosol optical depth (AOD), inversion products, and precipitable water in diverse aerosol regimes. AERONET has been operating under what we call Version 2 processing that we implemented in 2006 and was based on 2004 knowledge and expertise. The newest processing, Version 3, was released in 2015 after the entire database was reprocessed and real-time data processing became operational (http://aeronet.gsfc.nasa.gov/cgi-bin/print_web_data_v3). All Version 3 algorithms have been developed individually vetted and represent four main categories: aerosol optical depth (AOD) processing, inversion processing, database management and new products. The primary trigger for release of Version 3 lies with cloud screening of the direct sun observations and computation of AOD that will fundamentally change all data available for analysis and all subsequent retrieval products. Aerosol optical depth data are computed for three data quality levels: Level 1.0

(unscreened), Level 1.5 (cloud-screened), and Level 2.0 (cloud-screened and quality-assured). The main difference between Level 1.5 and Level 2.0 datasets, is that Level 1.5 dataset is corrected with the pre-calibration (performed to the photometer before start measuring on a site), while Level 2.0 data are corrected with pre- and post-calibration. The latter is applied once the photometer has been post-calibrated after having been measuring for about a year in an AERONET station. In many cases the differences between Level 1.5 and Level 2.0 data are very small, less than the associated AOD uncertainty, however undetected cloud contamination may give bias to level 1.5 data.

Currently, the network is composed by more than 300 sunphotometers around the world (http://aeronet.gsfc.nasa.gov/Site_Lists/site_index.html). AERONET-Europe Central Facility provides instrument calibration and data processing of the new CE318-T photometers for the night period, within ACTRIS-2 project.

9.1 Method for comparison of AOD at global scale

Global model evaluation is performed regularly to document the CAMS aerosol performance. AeroCom type evaluation is generated every second week of a given month since April 2011. Version 3 Level 1.5 NRT Aeronet Data are obtained from the NASA Goddard webserver. Standard score tables, maps, scatterplots, bias maps, time series comparison and histograms are made available through the AeroCom web interface http://aerocom.met.no/cgi-bin/aerocom/surfobs_annualrs.pl?PROJECT=CAMS. The performance of the o-suite and e-suite can this way be compared to other model simulations, such as earlier MACC model versions, the CAMS reanalysis or the AeroCom Median from an international multi-model ensemble.

The analysed variables consist of the total aerosol optical depth (AOD) at 550 nm and the Angstöm coefficient. Since sun photometers measure AOD at 500 nm, an Angström coefficient is obtained from 440nm and 670nm AOD values and is used to obtain from AOD@500nm an approximate AOD@550nm value. Mountain sites above 1000 m are excluded from comparison because model orography often does not reflect real orography. The 3-hourly model data are retrieved finally on the days when valid, clear-sky Aeronet observations in the model grid are reported. No observation is available on cloudy days and during night. Depending on region and season sampling frequency at a given station may vary largely from absent to daily observation through a full month. Coherent pairs of valid daily observation from model and sun photometer are retained at each station. To further filter out possibly cloud contaminated NRT data, daily Aeronet data are rejected when the measured Ångström coefficient is less than 0.2 and if, on the same day, the observation is twice as large as the corresponding CAMS o-suite model value. The varying fluctuating network comprises ca 300 sites. A site location map of stations with valid observations in 2020 is provided in figure 9.1.

Valid daily data from all stations over the globe are used to form the comparison basis for a given month. Standard score tables, maps, scatterplots, bias maps, time series comparison, histograms and site location maps are made available through the AeroCom web interface http://aerocom.met.no/cgi-bin/aerocom/surfobs_annualrs.pl?PROJECT=CAMS for each month. Site location maps and time series plots can be used to trace back which data went into statistical performance parameters for a given month. The performance of the o-suite and e-suite can in this

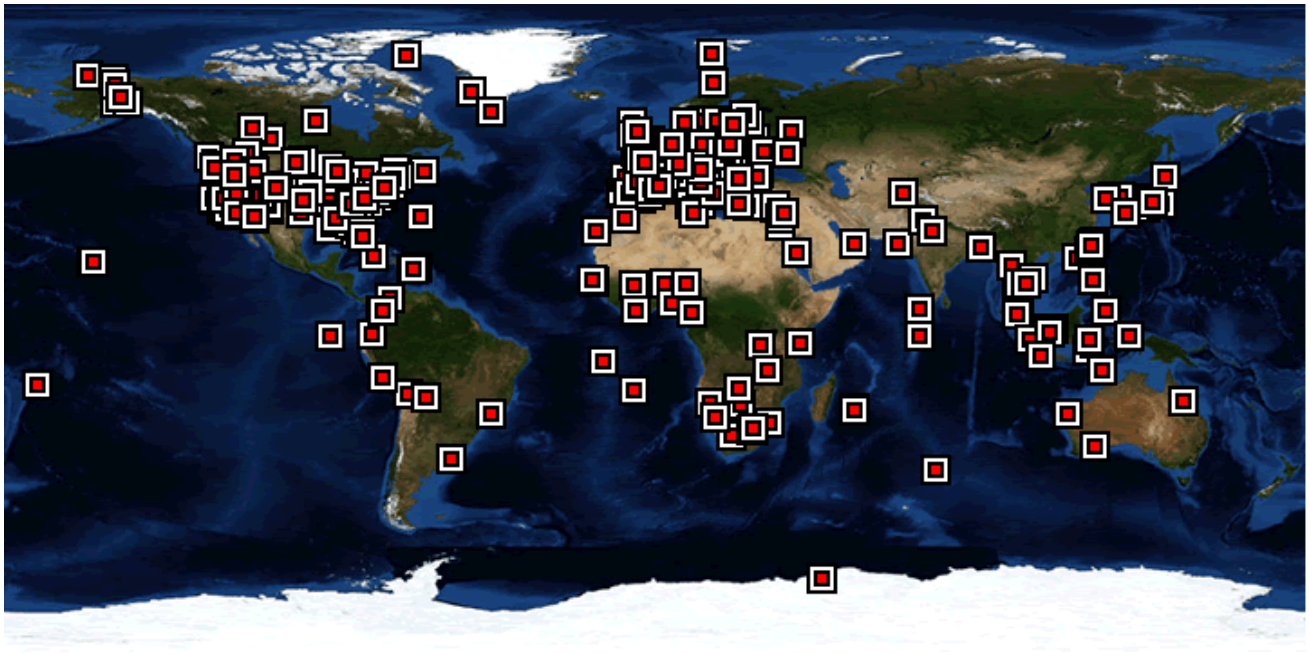

Figure 9.1: Sites with sun photometers reporting version 3 level 1.5 Aeronet data in 2020. Image extracted from the NASA-AERONET website (https://aeronet.gsfc.nasa.gov).

way be compared to other model simulations, such as earlier MACC model versions, the MACC reanalysis, or the AeroCom Median from an international multi-model ensemble.

9.2 Method for comparison of AOD and DOD over Northern Africa, Middle East and Europe

For the regional validation over Northern Africa, Middle East and Europe, we used AERONET sites inside the following box domain: longitude 25ºW to 60ºE and latitude 0º to 65ºN. For 2019, we used AOD observations at 550 nm from 67 selected AERONET sites.

Cloud-screened direct-sun data (Level 1.5) between 440 and 870nm under cloud-free conditions are used. Quantitative evaluations of the modelled AOD are conducted. The AOD at 550 nm is derived from data between 440 and 870 nm following the Ångström's law. Because AERONET data are acquired at 15-min intervals on average, all measurements within ±90 min of the models' outputs are used for the 3-hourly evaluation.

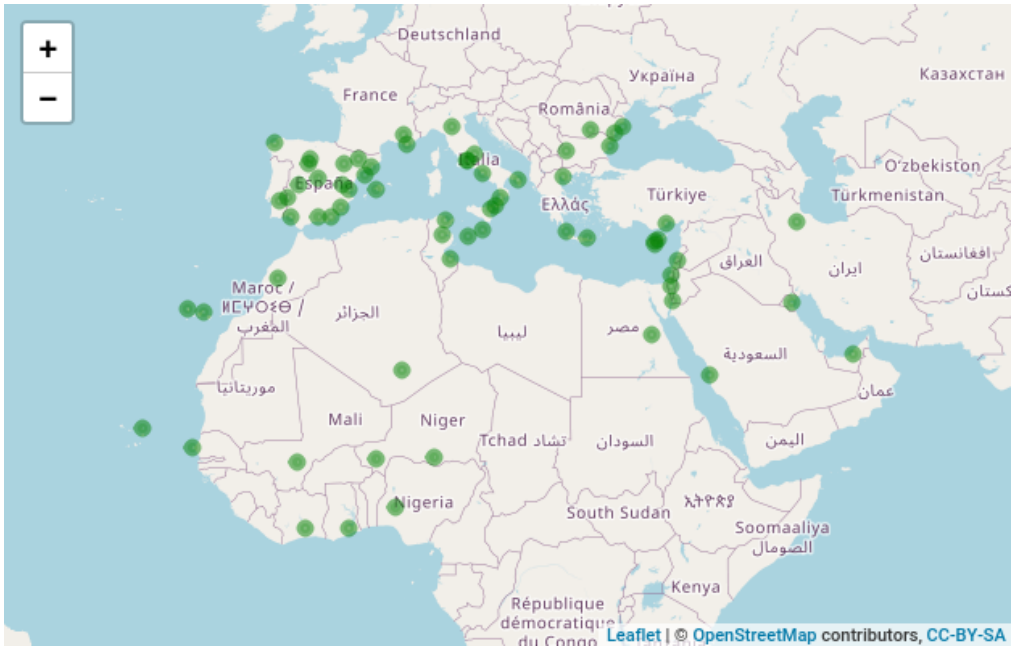

Figure 9.2: Map of the selected 67 AERONET sites considered in the CAMS validation for the year 2020.

The dust content is difficult to verify because bulk optical observations are not specific for dust. Since AOD is the degree to which a mixture of atmospheric aerosols prevents the transmission of light by absorption or scattering, we had to determine the criteria for filtering data to ensure that most of the AOD is influenced by mineral dust. Our first approach was to discriminate AOD observations clearly dominated by dust using Ångström's exponent (AE) as filter because it is inversely related to the average size of the particles: the smaller the particles are associated the larger AE. AE ranges normally from ~ 4 corresponding to molecular extinction to ~ 0 corresponding to coarse-mode aerosols (sea-salt and mineral dust) indicating a non-AOD wavelength dependence (O'Neill et al., 2003). Values of AE > 1.2 indicates significant presence of fine-mode particles (biomass burning or urban aerosols) (Basart et al., 2009). Quantitative evaluations of the modelled dust AOD (DOD) over North Africa-Middle East-Europe regional domain (whose locations are depicted in Figure 9.2) are conducted for dust-dominated conditions following Basart et al. (2009); i.e., when the AE≤ 0.75. All data with AE larger than 1.2 are considered free of dust (DOD = 0 is assumed). Values of AE between 0.75 and 1.2 are associated with mixed aerosols and are not included in the analysis. The AOD at 550 nm is derived from data between 440 and 870 nm following the Ångström's law.

In case of aerosol dust evaluation, a second methodology to discriminate DOD is being implemented. This second methodology is based in the fact that direct-sun AOD AERONET processing includes the Spectral Deconvolution Algorithm (SDA) retrievals (O'Neill et al., 2003). The SDA algorithm yields fine (sub-micron) and coarse (super-micron) AOD at a standard wavelength of 500 nm (AOD-fine and AOD-coarse, respectively). However, the amplitude of the errors of the derived parameters varies as the inverse of the total AOD. In addition to measurement errors, there are errors in the AOD retrieval due to the uncertainty in the assumed values of the spectral curvature in each mode (O'Neill et al., 2001), which are most critical in coarse mode dominated conditions. Moreover, some of the AERONET sites have not been available the SDA Level 2.0. At those sites where the SDA products are available, the dust AOD evaluation will be complemented

with AOD-coarse, which is fundamentally associated with maritime/oceanic aerosols and desert dust. Since sea-salt is related to low AOD (< 0.03; Dubovik et al., 2002) and mainly affects coastal stations, high AOD-coarse values are mostly related to mineral dust.

According to Cuevas et al. (2015), by using the criterion of AOD-coarse from the SDA retrieval, while the number of paired data points in the MACC-II-AERONET evaluation experienced no significant changes in the Sahara and the Sahel, this number grew significantly in other regions, especially in the dust transport corridors such as the Mediterranean regions, the North-western Maghreb and the Subtropical North Atlantic. Concerning long-range transport areas (i.e., North Atlantic and the Mediterranean), the AE filter applied to direct-sun AOD observations (AE < threshold value) selects pure desert dust intrusions. Desert dust events in these regions are sporadic and consequently the number of observations is very low. The MNMB showed varying results, improving in some regions and worsens in others in comparison with direct-sun DOD observations (Cuevas et al., 2015). Summarizing both methodologies have advantages and disadvantages, depending on the region where DOD is evaluated.

Both methodologies to filter AERONET DOD will be used in CAMS DOD evaluation. CAMS model outputs (dust AOD at 550nm) are bilinear interpolated in the horizontal at the stations' location. 3-hourly values of DOD from AERONET and CAMS model outputs are used to check the model performance. Mean Bias (MB), Mean Normalised Mean Bias (MNMB), Fractional Gross Error (FGE), Root Mean Square Error (RMSE), Person correlation coefficient (r), and the number of data (NDATA), averaged over the study period are computed for this objective. This set of statistics is being computed for each AERONET site and for selected regions distributed in desert dust source (i.e., Sahara, Sahel and Middle East) and transport regions.

10 Method for comparison of DOD against Multi-model Median from SDS-WAS

The Sand and Dust Storm Warning Advisory and Assessment System (SDS-WAS) is a project of the World Meteorological Organization (WMO) with the mission to enhance the ability of countries to deliver timely, high-quality sand and dust storm forecasts, observations, information and knowledge to end users. The Regional Center for Northern Africa, Middle-East and Europe (hereafter RC NAMEE or RC, http://sds-was.aemet.es/), hosted by the State Meteorological Agency of Spain (AEMET) and the Barcelona Supercomputing Center (BSC), supports a network of research and operational partners implementing the objectives of the SDS-WAS program in the region.

The DOD multi-model Median SDS-WAS product is obtained on a daily basis from the dust prediction models participating on the SDS-WAS model intercomparison (see the latest list of the model in the following link: http://sds-was.aemet.es/forecast-products/dust-forecasts/), which are

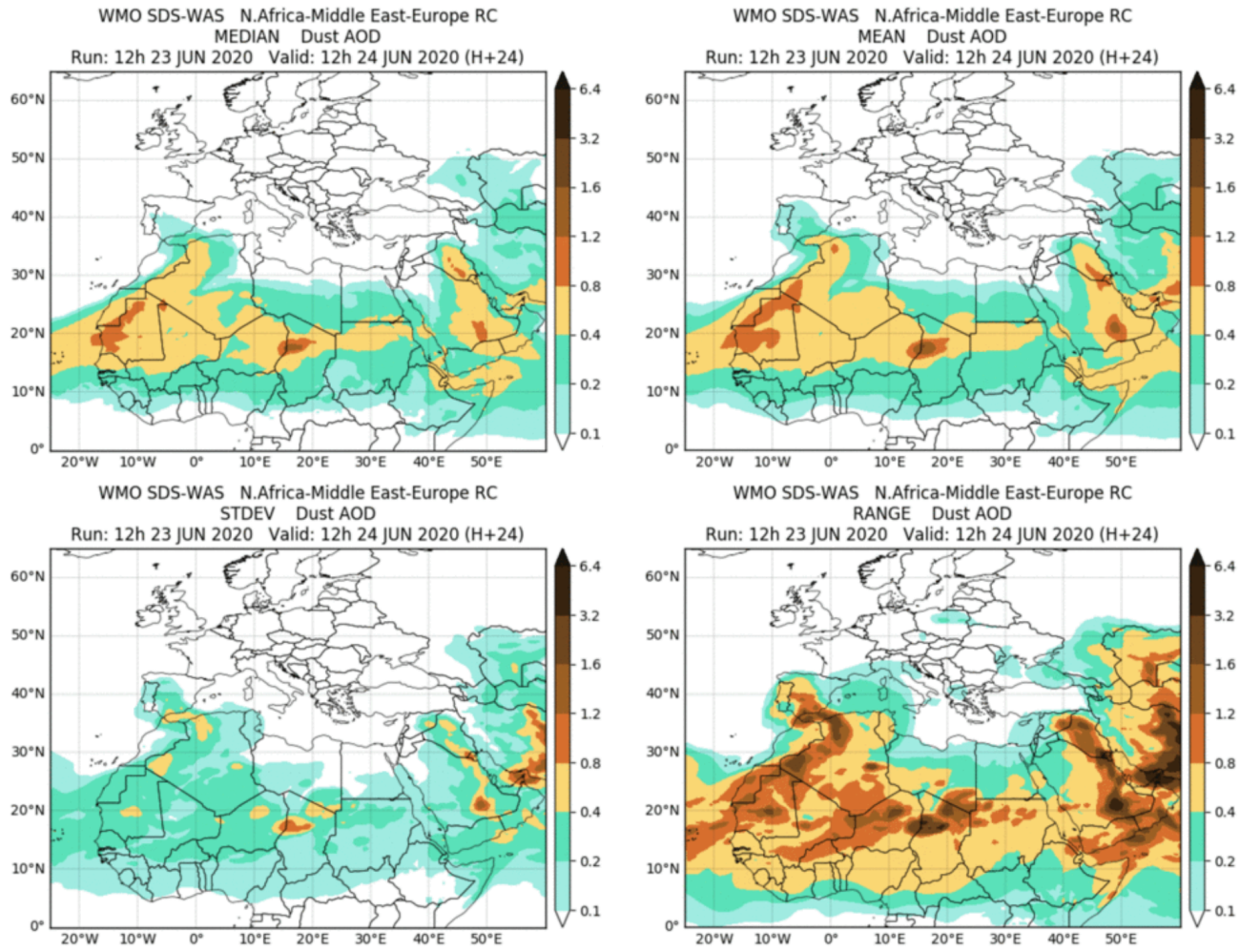

Figure 10.1: The DOD multi-model Median SDS-WAS product for 23 June 2020 at 12UTC, 24h forecast (http://sds-was.aemet.es/forecast-products/dust-forecasts/multimodel-products)

downloaded from the Sand and Dust Storm Warning Advisory and Assessment System (SDS-WAS) Regional Center for Northern Africa, Middle East and Europe (see Figure 10.1). The dust model products exchange includes forecasts of dust optical depth at 550 nm (DOD) with lead times up to 72 h, based on 00 UTC or 12 UTC runs. The output frequency is of 3 hours. The model outputs are bi-linearly interpolated to a common grid mesh of 0.5º x 0.5º to create the DOD multi-model Median SDS-WAS product. More details of the generation of the SDS-WAS multi-model products can be found in the following link: http://sds-was.aemet.es/forecast-products/dust-forecasts/multimodel-products.

11 DWD network ceilometers

11.1 DWD Ceilometer network

The German Meteorological Service (DWD) operates more than 110 CHM15K ceilometers as cloud base height monitors and aerosol profilers in its synoptic observations network. The low-cost/low-power elastic lidar systems, manufactured by Lufft (http://lufft.com – formerly by Jenoptik GmbH) evolved from cloud base height monitors into operational systems which allow to follow the planetary boundary layer (PBL) and aerosol layers in the free troposphere. With aid of nearby AOD measurements (Heese et al, 2010) or by absolute calibration (Wiegner et al., 2012) profiles of the particle backscatter or extinction coefficient can be inferred. The CHM15K uses a diode-pumped Nd:YAG solid state laser (1064 nm) and an off-axis Newton-type receiving telescope. Limited by the overlap between the laser beam and the telescope field of view, the signal can be used from about 0.4-10 km above ground with a vertical resolution of 15 m. For calibrated optical properties, the raw temporal resolution of 15s has to be averaged over at least 5 min.

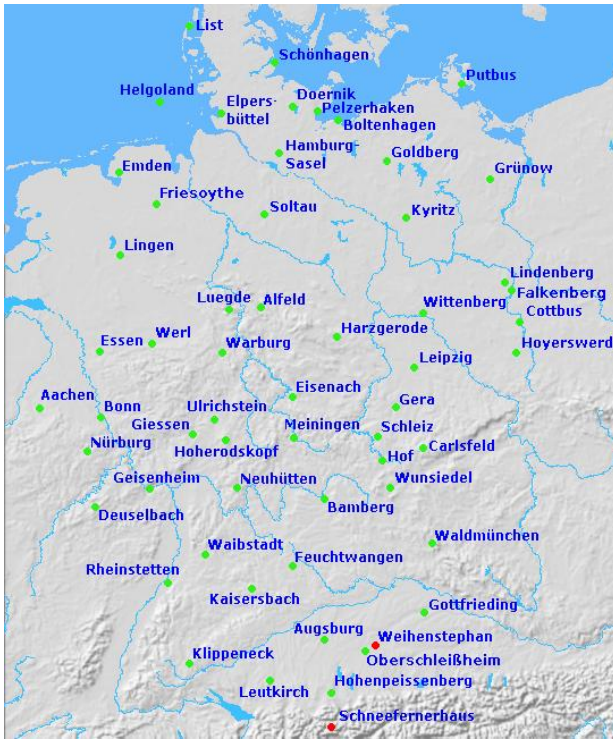

Ceilometer network of the German Meteorological Service (DWD)

11.2 (Attenuated) Backscatter Profiles

IFS data

Daily netcdf files with mass mixing ratios of the prognostic aerosol variables (14 variables in the case of 46R1), surface pressure, temperature, geopotential and boundary layer heights are retrieved from the MARS archive for both, the o-suite and the control run. The mass mixing ratios are converted to (attenuated) backscatter coefficients ($m^{-1}sr^{-1}$ or $(Mm)^{-1}sr^{-1}=10^{-6}m^{-1}sr^{-1}$) as follows: First, mass mixing ratios m, [kg/kg] are converted to mass concentrations c_m [kg/m^{-3}] by multiplication with air density, which is calculated from pressure and temperature. The extinction coefficient α, [m^{-1} or $(Mm)^{-1}=10^{-6}m^{-1}$] of each aerosol type is calculated by multiplying the mass concentrations with pre-calculated specific mass-extinction ratios σ^*_e, [m^2/g], depending on wavelength and relative humidity. The contribution of molecular scattering is considered using the Rayleigh formula. The backscatter coefficients β, [$m^{-1}sr^{-1}$] are finally obtained by dividing the extinction coefficients of each aerosol type by the respective lidar ratios S, [sr]. The attenuated backscatter coefficient

$\beta^*(r) = \beta(r)exp\{-2\int_0^r \alpha(r')dr'\} = \frac{Pr^2}{C_L}$, [$m^{-1}sr^{-1}$] is the backscatter coefficient degraded by the extinction between ceilometer and altitude r, whereby $\beta=\beta_m+\beta_p$ and $\alpha= \alpha_m+ \alpha_p$ are each composed of the molecule and particle contributions, and C_L is the lidar constant. The total backscatter coefficient is the sum of the individual aerosol types' backscatter coefficients.

The calculations of the conversion factors from mass to optical properties are based on Mie Theory. Refractive indices of the 11 aerosol types and their humidity dependency, their densities, specific mass-backscatter ratios and lidar ratios were extracted from the IFS aerosol code of LOA/LMD-Z or the respective auxiliary files. Where we were missing information, we calculated them with literature values taken from Boucher and Anderson (1995), Köpke et al. (1997), O'Dowd et al. (1997) Reddy et al. (2005) using the OPAC/GADS software package and database as in the IFS to ensure consistency (Morcrette et al, 2008, 2009).

The mass → backscatter conversion should better be a post-processing step at ECMWF ((attenuated) backscatter stored in MARS). Handling of the corresponding regional model output has still to be defined.

Table 11.1. Parameters requested from the ECMWF archive.

ECMWF-IFS aerosol optical (@1064 nm) and MARS-request parameters, if specified @ 70, 80, 90% rh.

Prognostic Variable	MARS -ID	Refr-Index	ρ [g/cm³]	σ^*_e [m²/g][B]	LR
DUST (0.03-0.55 µm)	4.210	1.48 + 6·10⁻³i (*)	2.61	2.6321 1.49(*)	78(*)
DUST (0.55-0.9 µm)	5.210			0.8679 1.61(*)	48(*)
DUST (0.9-20 µm)	6.210			0.4274 0.44(*)	13(*)
Hydrophilic BLACK CARBON	10.210	1.75 + 0.45i (*)	1.00	9.412	168(*)
Hydrophilic ORGANIC MATTER(#)	8.210	Bio: 1.44+0.001i(K) Anth: 1.55+0.001i(K)	1.769	5.502(#) 1.9/2.5/4.3(*)	46/49/57(*)
Hydrophobic BLACK CARBON	9.210	1.75 + 0.45i (*)	1.00	9.412	168(*)
Hydrophobic ORGANIC MATTER(#)	7.210	Bio: 1.44+0.001i(K) Anth: 1.55+0.001i(K)	1.769	5.502(#) 1.9/2.5/4.3(*)	46/49/57(*)
SEA-SALT (0.03-0.5 µm) (#)	1.210	1.51 + 2·10⁻⁴i (40%, SR) 1.42 + 4·10⁻⁵i (80%, SR) 1.36 + 5·10⁻⁸i (**)	1.183	3.0471 2.1/3.2/4.9(*)	65/76/73(*)
SEA-SALT (0.5-5 µm) (#)	2.210			0.3279 0.47/0.57/0.79	15/15/18(*)
SEA-SALT (5-20 µm) (#)	3.210			0.0924 0.13/0.15/0.21	15/15/9.5
SULPHATE(#)	11.210	1.60 + 0.0i (40%, SR) 1.44 + 0.0i (80%, SR)	1.769	6.609 2.6/3.5/6.0(*)	45/49/56(*)
CO	123.210	H2O, gas absorptions assumed t.b. negligible @1064 nm			
O3	203.210				
NO	27.217				
NO2	121.210				

(*) from LOA/LMD-z FTN code of O. Boucher
(SR) from S. Remy (ECMWF) for λ = 1.064 or 1.1 µm
(**) from Levoni et al, Appl. Optics, 36,30,1997
(B) from Benedetti et al, 2009
(#) depends on r.h.,
(K) valid for 532 nm Kim & Paulsen, ACP,13,7711ff, 2013 and to Nakayama et al, JGR,120,15,2015 (Imag-part), real-part with moderate wavelength dependence, imag-part strongly increasing with wavelength

Table 11.2. German Ceilometer stations.

Station	lat	lon	alt	Station	lat	lon	alt	Station	lat	lon	alt
list	55.01	8.41	26	lindenberg_	52.21	14.12	123	meiningen	50.56	10.38	450
leck	54.79	8.95	7	lindenberg	52.21	14.13	101	hoherodskopf	50.51	9.22	743.3
schoenhagen	54.64	10.02	2	falkenberg	52.17	14.12	73	carlsfeld	50.43	12.61	897
schleswig	54.53	9.55	43	magdeburg	52.1	11.58	85	nuerburg	50.36	6.87	485
putbus	54.37	13.48	39.5	alfeld	51.97	9.8	143.9	hof	50.31	11.88	565.1
st-peter-ording	54.33	8.6	5	wittenberg	51.89	12.65	105	wunsiedel	50.03	11.97	622.3
helgoland	54.18	7.89	4	Luegde	51.87	9.27	258	neuhuetten	50.01	9.43	339.5
doernick	54.17	10.35	26.3	wernigerode	51.85	10.77	240	geisenheim	49.99	7.95	110.2
pelzerhaken	54.09	10.88	1	cottbus	51.78	14.32	69	bamberg	49.88	10.92	240
elpersbuettel	54.07	9.01	3	harzgerode	51.65	11.14	404	deuselbach	49.76	7.06	480.5
boltenhagen	54	11.19	15	doberlug	51.65	13.58	100	waldmuenchen	49.39	12.69	498.8
quickborn	53.73	9.88	14	werl	51.58	7.89	84.8	waibstadt	49.3	8.91	236.6
norderney	53.71	7.15	11	warburg	51.51	9.11	235.8	berus	49.28	6.63	363
hamburg	53.65	10.11	35	hoyerswerda	51.45	14.25	115.9	feuchtwangen	49.16	10.37	475.1
goldberg	53.61	12.1	58	essen	51.41	6.97	150	rheinstetten	48.97	8.33	116.1
waren	53.52	12.67	70	leipzig	51.32	12.45	138	kaisersbach	48.92	9.69	488.7
emden	53.39	7.23	0	kahlerasten	51.18	8.49	839	gottfrieding	48.66	12.54	350.4
gruenow	53.32	13.94	55.9	goerlitz	51.16	14.96	240	augsburg	48.43	10.94	461.4
friesoythe	53.05	7.9	5.7	eisenach	51	10.36	312.4	weihenstephan	48.4	11.7	477.1
soltau	52.96	9.8	75.6	gera	50.88	12.13	311	oberschleissheim	48.24	11.55	484
kyritz	52.94	12.41	40	aachen	50.8	6.03	231	klippeneck	48.11	8.76	973.4
lingen	52.52	7.31	22	chemnitz	50.79	12.87	420	schauinsland	47.91	7.91	1205
genthin	52.39	12.16	35	ulrichstein	50.75	9.02	350.3	hohenpeissenberg	47.8	11.01	977
potsdam_alt	52.38	13.06	81	bonn	50.74	7.19	159	leutkirch	47.8	10.03	671.7
potsdam	52.38	13.06	81	schmuecke	50.66	10.77	948	hohenpeiss-ICOS	47.8	11.01	992
lindenbergtest	52.3	14.12	115	giessen	50.6	8.65	202.7	garmisch	47.48	11.07	719
braunschweig	52.29	10.45	81	schleiz	50.57	11.81	501	schneefernerhaus	47.42	10.97	2650

Aerosol representation in the IFS model

The 11 prognostic aerosol types, handled by the IFS model, are described in Morcrette et al. (2008, 2009), but the treatment of humidity deserves particular attention. The IFS model transports and provides aerosols in the dry state, but at each time step grows them according to relative humidity in order to calculate the relevant optical properties in the cases of sulphate, hydrophilic organic carbon and sea salt. (Though there is 'hydrophilic black carbon', its optical properties are not distinguished from those of the hydrophobic fraction.) However, no interaction of the humidity dependent growth with microphysical processes, no re-distribution between size bins (i.e. physical growth due to water uptake) nor chemical or phase transformations is taken into account. The output fields are valid for the very time of output and at the model grid point, i.e. no temporal or spatial averaging is included.

Ceilometer Data

Daily ncdf files with profiles every 15s from >110 German stations are stored as Pr^2 (=range-corrected intensity) by DWD (cf. table 11.2). These data are averaged to hourly means (nc-operators) and converted to (attenuated) backscatter ($Pr^2 \rightarrow \beta^*$) with aid of calibration constants (C_L: $\beta^*_{,ceilo\text{-}x}=Pr^2 \cdot C_{L,ceilo\text{-}x}$), which are regularly determined/updated for each instrument under manually to look up needed favourable conditions, like cloudiness, to ensure the necessary quality of aerosol backscatter coefficients. Initially, only stations are selected for evaluation which are less than 20 km distant from a model grid point and whose real altitudes correspond to the model orography (surface level 60) within Δalt<100m in order to avoid vertical re-sampling issues. No averaging of ceilometer data over stations is performed for continuity reasons. The calibration constant C_L contains all system-specific parameters, occurring in the elastic lidar equation, such that the received power can directly be related to the attenuated backscatter coefficient β^* ($P=C_L*1/r^2*\beta^*$, where the usual attenuation term exp{-2·AOT} is omitted).

Interpolation/resampling

Vertical Level altitudes (above model orography – L60) are calculated as barometric height, based on surface pressure p_s and sigma-hybrid-coefficients a_k, b_k: $p_k(n,j,i) = a_k + b_k*p_s(n,j,i)$ (for level centres). Then ceilometer profiles are simply resampled at the model levels, recognizing the height over m.s.l., without interpolation or application of any averaging kernels. Until the handling of stations, where model orography deviates significantly from real altitude, is clear, these are excluded.

Uncertainties

Ceilometers: Error of the ceilometers' β^*–profiles is composed of contributions from SNR and calibration (no assumptions about particles required for β^* – only on instrument stability). Absorptions can be neglected at the 1.064µm wavelength. Laser degradation, ageing of the optical components, pollution or snow on the output window 'only' reduces the SNR, but miss-alignment and other malfunctions can lead to not quantifiable errors in the operational (24/7) instruments. Usually $\Delta\beta^*_n \approx$20-50% can be reached under favorable atmospheric conditions. No measurement is possible above/beyond beam blocking clouds, during strong precipitation or fog.

Model: Here largest evaluation uncertainties arise from synchronization/co-location, particularly in the vertical, strong gradients in presence of temporal or spatial shifts, the conversion of physical to optical quantities, dynamics, etc. (model uncertainty estimate based on AN/FC covariance or from assimilation).

11.3 Boundary layer heights (BLH)

ECMWF data

The planetary boundary layer height (or mixing layer height) z0 is retrieved from MARS to daily ncdf-files by cronjob, both for o-suite and ctrl. The FC steps 0,3,6,9,...,21 are based on the daily 00 UT analysis. The IFS model associates the BLH with a certain value (0.25) of the bulk Richardson number, which characterizes the degree of turbulence. The vertical stability is estimated using the difference between a level and the lowest level. Several issues with this approach are described by e.g. v. Engeln and Teixeira (2013), related to the Richardson number being based on ratios of both dynamic and thermodynamic vertical gradients rather than of temperature and/or humidity as such, the use of dry varis in cloudy situations, and the fact that the Richardson number as a measure of local turbulence is often unable to properly characterize the turbulent properties of convective boundary layers. Turbulent kinetic energy, which could better be used, however, is rarely used in global models and as such is not available (comp. Engeln and Teixeira, 2013). CAMS model level geopotential heights are used to characterize the model-station height difference.

Ceilometer data

The BLH observations are taken as provided by the firmware, implemented in the CHM15k ceilometers. It is calculated from the backscatter intensities of the ceilometer range corrected signal (Pr2) by means of a wavelet transform algorithm, developed by Teschke and Pönitz (2010). In principle, the BLH detection is a pattern recognition problem, which is based on the assumption that the vertical distribution of aerosol can be used as a tracer for boundaries. This, however, is not always the case. The absolute value of the backscatter is typically not needed since the relevant information seems to be completely coded in the gradient (but possibly of different orders) of the backscatter profile (Teschke and Pönitz, 2010). Up to 3 layers are reported, the highest of which is identified with the top of the convective ML during daytime and the lowest one to the stable BL at night-time. Haeffelin et al. (2012) investigated limitations and capabilities of existing mixing height retrieval algorithms by comparing different retrieval techniques. They found "no evidence that the first derivative, wavelet transform, and two-dimensional derivative techniques result in different skills to detect one or multiple significant aerosol gradients" (Haeffelin et al., 2012). Generally, there is no perfect way to determine the height of the ML, both in observations and models, and the appropriateness of each method depends on the topic being investigated. The inferred MH may not be realistic in cases with multiple layers, low clouds/fog, missing aerosol gradients, precipitation and intense long-range transport of e.g. Saharan dust. These data can be rejected according to spatial inhomogeneity or temporal discontinuity. For a first approximation, if data are missing due to meteorological conditions or are spurious at individual stations, these are disregarded by discussing median MLH instead of means.

Uncertainties

From the 3 BLH, reported by the CHM15k-Nimbus, simply the uppermost is used. Since yet no quality or plausibility flag is available, the uncertainty cannot be quantified. Thus, the evaluation is semi-quantitative, only, but yields significance through using median values instead of means.

12 Contribution from NDACC

NDACC is a cross-border international research network of remote sounding stations (Fig. 12.1 and 12.2). It is a major contributor to the World Meteorological Organisation (WMO) GAW programme, and it works under the auspices of United Nations Environment Programme (UNEP) and the International Ozone Commission (IO3C). Relying on a strong involvement of European partners and efficient collaboration with partners worldwide, the network started operations officially in 1991, but a few data records extend back to the 1970s and even to the 1950s. At present time it includes more than 70 high-quality, remote-sensing research stations/sites distributed worldwide for (i) observing and understanding the physical / chemical state of the stratosphere and troposphere, and (ii) assessing the impact of stratospheric changes on the underlying troposphere and on global climate.

Validation of CAMS model data using observations from the NDACC network (ndacc.org) for a selected number of instruments (see below) was developed during the NORS EU project (Demonstration Network Of ground-based Remote Sensing observations in support of the Copernicus Atmospheric Service, EU FP7 project) (De Mazière et al., 2012, 2013), see http://nors.aeronomie.be and nors-server.aeronomie.be. The instruments used are

- Fourier Transform InfraRed (FTIR)
- MicroWave Radiatiometers (MWR)
- UV-Visible Differential Optical Absorption Spectroscopy (DOAS) and multi-axis DOAS or MAXDOAS
- Differential Absorption Lidar Technique (LIDAR)

For more information on the different instruments, see http://www.ndsc.ncep.noaa.gov/instr/ and see Figure 12.3. For a detailed description of each measurement technique, retrieval methods, reported uncertainties, data processing and filtering is found in the NORS data user guide deliverable http://nors.aeronomie.be/projectdir/PDF/NORS_D4.2_DUG.pdf. Below a brief description is found per instrument technique and the typical measurement uncertainties.

The NORS server validated O_3 using FTIR, MWR, UVVIS DOAS and LIDAR measurements, CO and CH4 using FTIR measurements, tropospheric H_2CO, NO_2 and aerosol using UVVIS DOAS and stratospheric NO_2 using FTIR measurements (the latter is not fully harmonized on NDACC). The validation server was halted end of 2019 and its functionality is transferred to the CAMS84 validation server https://global-evaluation.atmosphere.copernicus.eu.

All NDACC available stations submitting data in the GEOMS HDF file format are used in the validation server. There is no a-posteriori data filtering for the NRT validation reports, apart from an obvious filtering on corrupted NDACC data. The CAMS27 contract provides support to NDACC PI's to deliver quality measurement data to the public NDACC archive within one month after measurement. In 2019 selected DOBSON instruments are also supported in CAMS27 (see Fig 12.1) and will be used to validate the CAMS ozone product as soon as a sufficiently long (1 year) of data is available.

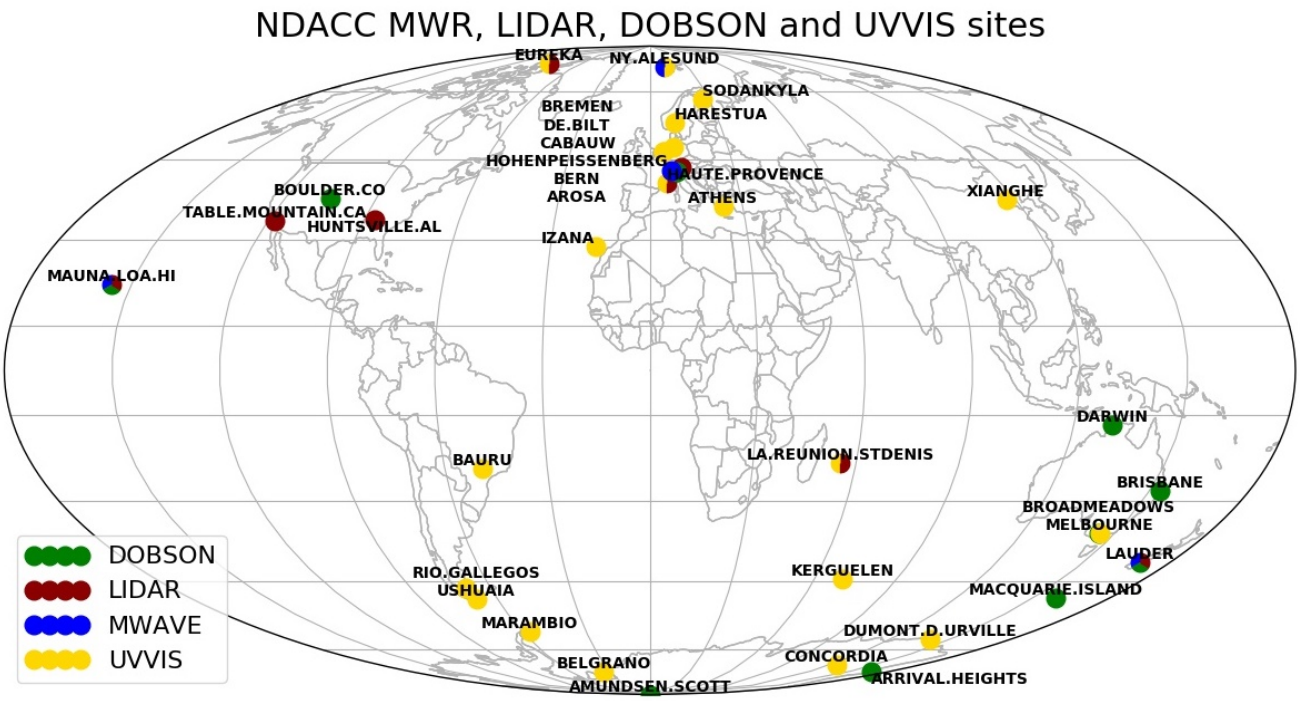

Figure 12.1: NDACC stations for LIDAR, MWR, DOBSON and UVVIS instruments. Stations submitting HDF with recent measurements (within past 2 years) are indicated.

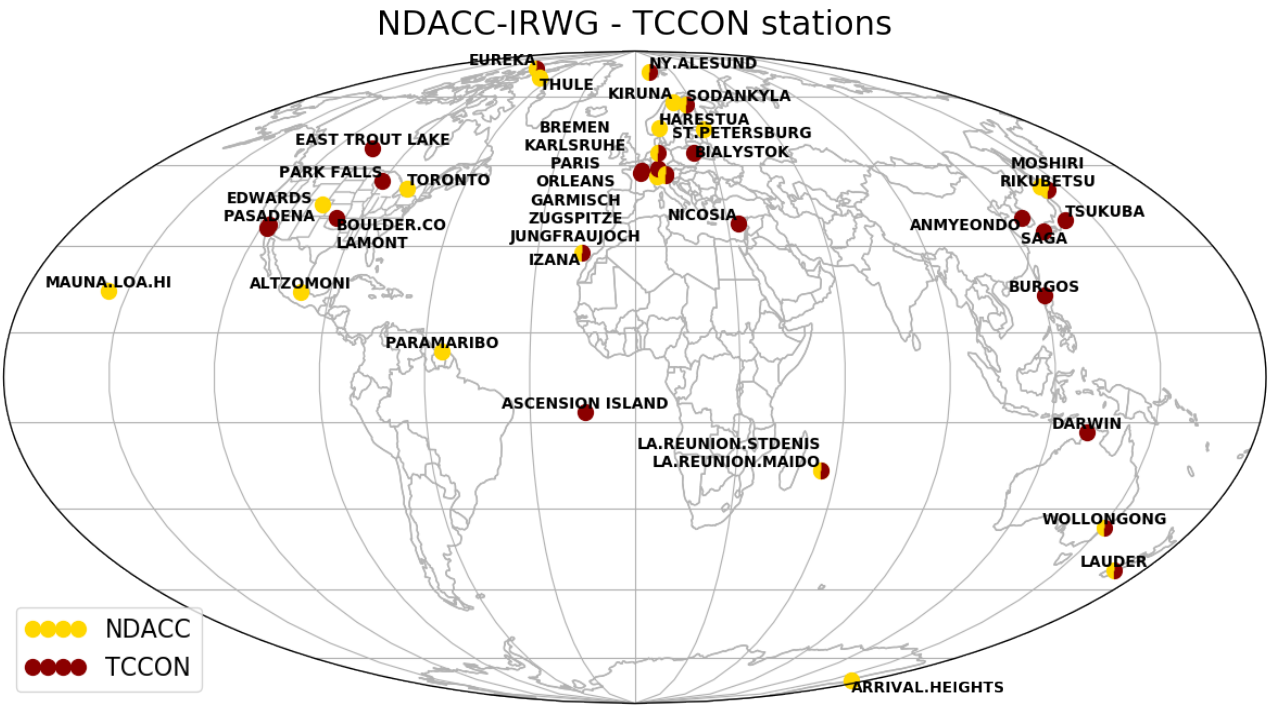

Figure 12.2: NDACC FTIR stations (yellow) submitting data in HDF format; TCCON stations are indicated in red (some stations measure for both TCCON and NDACC). The TCCON stations at Reunion, Orleans and Nicosia submit data in Rapid Delivery mode.

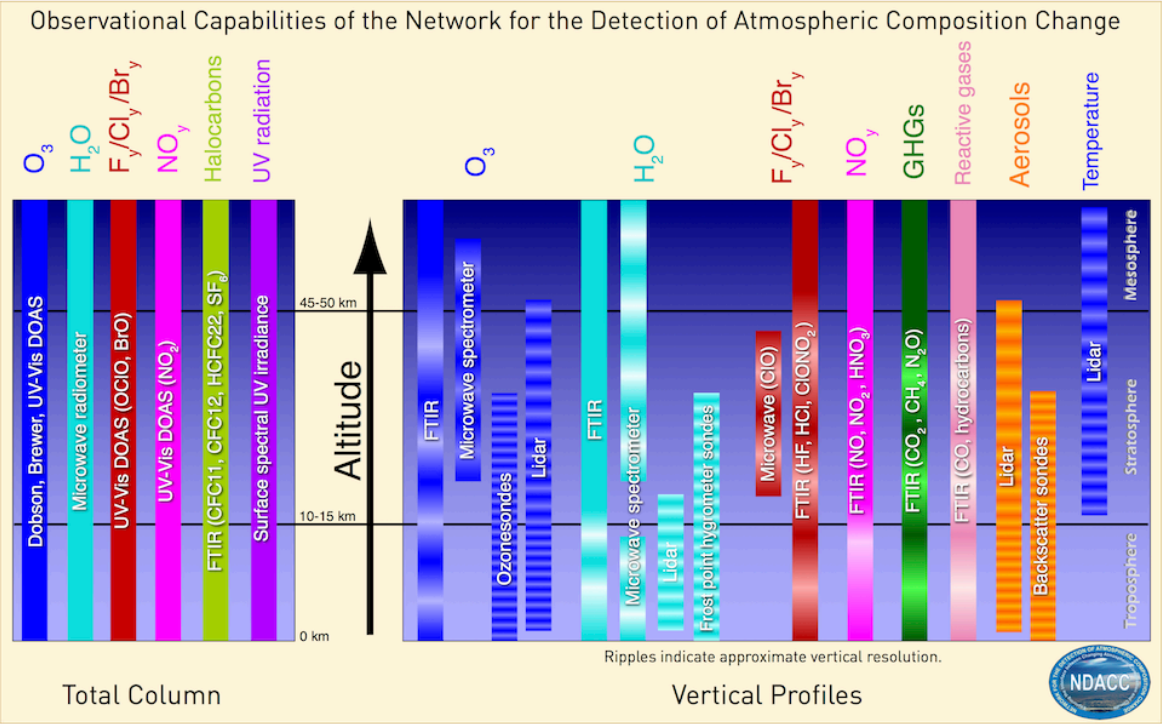

Figure 12.3: Overview of NDACC observational capabilities (picture taken from http://www.ndsc.ncep.noaa.gov).

Measurements are validated against model data if the difference between the measurement time and validity time of the model data is not greater than a pre-defined threshold value (1/2h for MWR O_3 and UVVIS H_2CO measurements, 3h for NDACC all FTIR measurements except NO_2 (1/4h) and TCCON data (1/3h), etc.) according to the variability of the measured species and availability of the data. Using the model vertical pressure grid and the model geopotential surface height, a vertical height grid for the model is constructed. Next, a model profile is obtained at the site location using a bilinear interpolation for the surrounding model grid points (for FTIR measurements, the model profile is extracted along the line of sight).

The target model data is regridded to the measurement vertical grid using a mass-conserving interpolation (i.e. layer height weighted regridding for number density profiles). Finally, the regridded model profile is smoothed using the averaging kernels (except for O_3 LIDAR measurements, where smoothing is not applicable); see below for some example kernel matrices. From this smoothed model profile, the desired partial columns are calculated and compared against the measurements. A detailed description of the validation methodology is described in Langerock et al (2015).

12.1 Validation with NDACC Microwave radiation measurements (MWR)

Microwave radiation measurements use a FFT spectrometer to record the pressure- broadened ozone line spectra at 142 GHz with a bandwidth of 1 GHz. Measurements are available every 30' and sensitivity typically start at 25km.

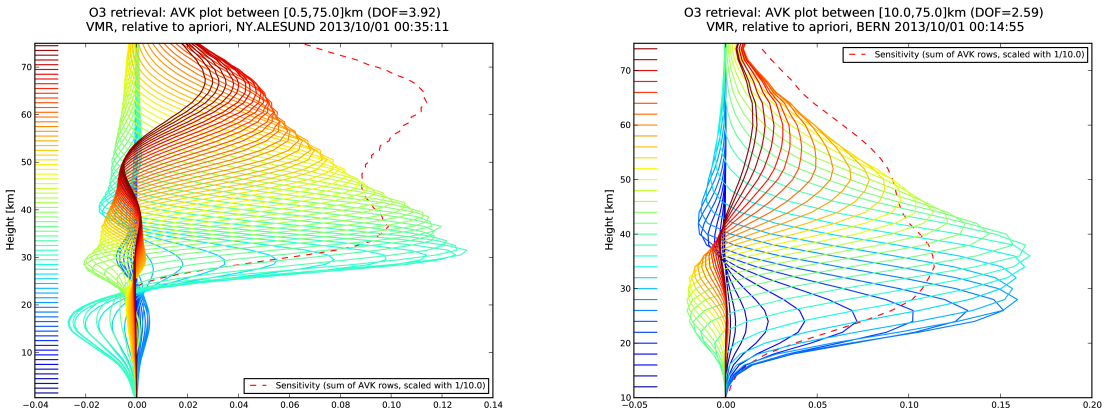

Figure 12.4: Typical averaging kernels for the Ground-based MWR stations of the NDACC network: sensitivity lies between ±20km and ±80km.

Figure 12.4 shows typical averaging kernels and from the measurement's sensitivity (dashed red line). In the validation, the profile comparisons are restricted to an altitude range between 20 and 60km: above and below this height range the instrument has no sensitivity or the model does not provide data. The typical uncertainty for the stratospheric columns is 5-10% (Hocke, 2007; Kämpfer, 2013; Peter, 1997).

12.2 Validation with Fourier Transform InfraRed measurements (FTIR) from NDACC and TCCON

FTIR measurements of O_3, CH_4, CO_2, HCHO and CO are taken by a Michelson-type interferometer, looking directly at the centre of the sun (or moon). The FTIR NDACC data does not contain CO_2, and TCCON CH_4, CO and CO_2 data used in CAMS validation reports.

The validation of the model data against these observations is basically the same as for MWR measurements. The only difference is that for FTIR measurements, model data are validated against measurements that are within an interval of one time-step around the time of model output.

The NDACC FTIR data consists of total columns (mol/cm^2), as well as VMR and partial columns (mol/cm^2) per atmospheric layer defined on a height grid (km). The averaging kernel illustrate that these FTIR instruments can only be used up to +/-60km, as the instrument has only little or no sensitivity above. Measurement uncertainties are site and target dependent, and are typically of the order of 3% (CO, O_3 and CH_4) to 13% (HCHO) (ISSI, 2012, Vigouroux 2018) for total columns.

TCCON FTIR data consists of dry air averaged columns (xgas, mol/mol) only. TCCON reports a column averaging kernel and the smoothing equation transforms the model profile to a column value. The precision for CH4 is approximately 0.3%, for CO 1% and for CO2 the precision is 0.25%.

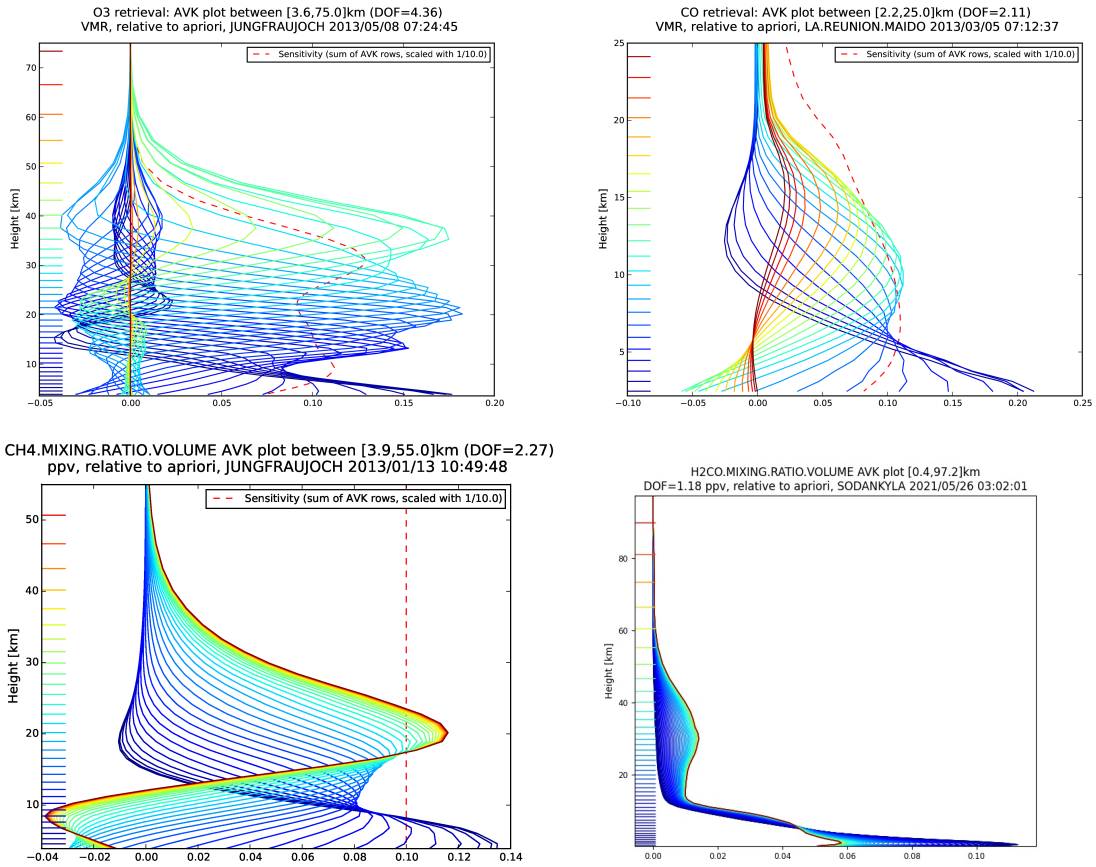

Figure 12.5 Example of AVK's in VMR/VMR units for ozone (left top) and CO (top right), methane (bottom left) and formaldehyde (bottom right). The dashed curve in the right plot represents the sensitivity curve, which vanishes at between 50 and 60km for ozone. CO measurements are sensitive up to 25km.

12.3 Validation with NDACC NO2, O3, H2CO and Aerosol UVVIS DOAS measurements

In a Multi-AXis or MAX-DOAS instrument, light is guided into the spectrometer by a telescope that can be pointed at the sun or at different parts of the sky. Depending on the instrument and application, different operation modes can be used:

1. Zenith sky operation for total columns, stratospheric profiles and tropospheric columns with low sensitivity

2. Direct sun operation for total columns and in combination with scattered light observations for atmospheric profiles

3. Multi-Axis operation with multiple viewing directions above the horizon for tropospheric profiles and (if azimuthal pointing is possible) horizontal gradients.

UVVIS (MAX-)DOAS ((Multi-Axis) Differential Optical Absorption Spectrometer) measures scattered sunlight at different elevation angles above the horizon. Measurements are sensitive to clouds and provide good tropospheric profile under homogeneous cloud conditions see Gielen et al., (2014). UVVIS DOAS (zenith measurements) also measure stratospheric O_3 and NO_2, which are column only

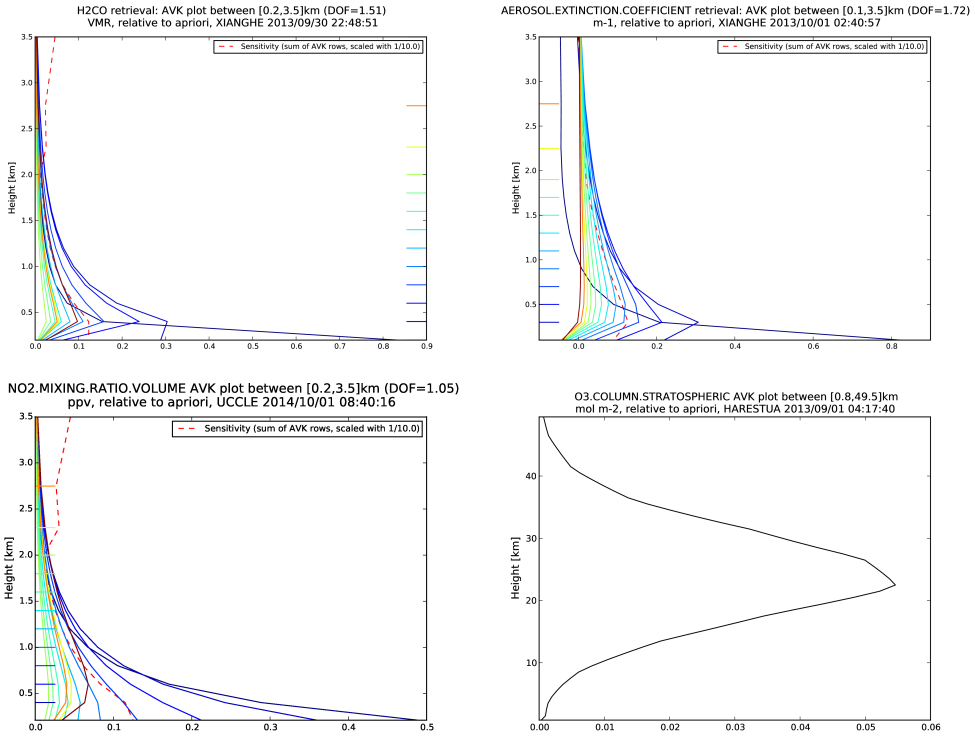

Figure 12.6. A typical UVVIS DOAS OFFAXIS AVK for H_2CO and NO_2 (VMR/VMR) and Aerosol extinction profile (m^{-1}) retrievals. The measurement is sensitive below 1km. For the UVVIS ozone zenith sky measurements (only column data) the column AVK is shown.

data. Uncertainties are site and target dependent and may range from 5-10-20% (Clemer et al., 2010; Connor et al., 1994; Eskes and Boersma, 2003; Frieß et al., 2006).

12.4 Validation with NDACC Light Detection And Ranging measurements (LIDAR)

LIDAR measurements used in this report were also collected in the framework of the NORS project (http://nors.aeronomie.be). The lidar (Light Detection And Ranging) technique (http://ndacc-lidar.org/) is a remote sensing measurement technique using the scattering properties of light by gases, liquids, and solids in order to infer their physical or chemical properties (Godin et al., 1994; McGee et al., 1993). A laser beam is sent into the atmosphere. The light is scattered by the atmospheric molecules and particles, and a fraction is collected back on the ground with a telescope. Since the lidar comprises the light source itself, the lidar technique is known as an 'active remote sensing' technique.

There are currently 30 lidar instruments worldwide contributing to NDACC. These instruments use three different lidar techniques to retrieve atmospheric temperature, ozone and aerosol properties:

- typically 30-80 km, down to 10 km if using Raman channels
- typically 20-40 km
- typically 10-45 km in the stratosphere, 1-10 km in the troposphere

Because the transition from L1 to L2 data is not based on optimal estimation, the measurement data does not contain AVK and no smoothing is applied to the model profile. To align the number density profiles of both model and measurement, a mass-conserving regridding technique is used. For temperature, a layer thickness weighted mean is calculated to convert the lidar profile to the coarser model grid. The typical uncertainty on the partial column data 15km<45km is 3% and, the profile NB uncertainties range from ~1% at 20km to 30% at 50km.

12.5 Validation with NDACC Dobson spectrometers (DOBSON)

NDACC PI's only started delivering measurement data in GEOMS format in 2019 (selected PI's have joined the CAMS27 rapid delivery effort). The validation methodology is straightforward (direct column to column comparison). As soon as a sufficiently long time series (one year) of data is available, the DOBSON stations delivering GEOMS data will be included in the NDACC validation contribution in CAMS84. The details of the validation setup (co-location, selection of DOBSON measurements depending on wavelength pairs A-D) will be determined when a sufficiently long time series is available in GEOMS format.

Depending on the wavelength pair used in the measurement, the uncertainty ranges from values of the order of 1% to 7% (Kohler2018; Evans2008).

13 Limb-scanning satellite instruments

13.1 Validation with OMPS-LP observations of O_3

The Ozone Mapping and Profiler Suite (OMPS) is composed of three instruments aboard Suomi National Polar-orbiting Partnership (S-NPP) satellites: the Nadir Mapper (OMPS-NM), the Nadir Profiler (OMPS-NP) and the Limb Profiler (OMPS-LP).

For the validation of the CAMS stratospheric ozone product, we use the level 2 daily retrievals from the OMPS-LP instrument (LP-L2-O3-DAILY product), release 2, version 2.5. This dataset starts on 10 February 2012 and is currently delivered in NRT with a latency of about 5 days at https://ozoneaq.gsfc.nasa.gov/data/omps/.

OMPS-LP is an ultraviolet-visible instrument designed to retrieve ozone concentration profiles from the tropopause up to 60 km during daytime. It views the Earth's limb looking backwards along the orbit track, using three parallel vertical slits. One slit is aligned with the orbit track. The two other two slits are pointed 4.25° to each side but they are not used any more for version 2.5. OMPS-LP delivers daily about 2500 ozone profiles, scanning the globe with a solar zenith angle lower than 85°, thus limiting the polar coverage during the polar night. The observations are screened according to the readme document (Johnson and DeLand, 2017).

According to a performance evaluation (Jaross et al., 2014), it is noticed that the Limb instrument operates mostly as designed and basic performance meets or exceeds the original design criteria.

The initial version of LP-L2-O3-DAILY (release 1) has been replaced by a new version (release 2) in July 2014, with several changes. Preliminary results of comparison of this release with AURA MLS (Xu et al. 2014) show a good agreement: "… an example of the results obtained when we compare LP ozone data with MLS ozone data for a monthly average in February 2014. Zonal mean differences are generally less than ±10% between 10 km and 60 km over all latitudes, with some larger differences only below 20 km in the tropics." However, some consistent differences between results from the three slits are noted: left slit ozone values are typically 5-10% higher than centre slit values above ~40 km and are ~10% lower between 15-20 km in the tropics. Similarly, right slit ozone values are typically 5-10% lower than centre slit values above ~40 km and are ~10% higher between 15-20 km in the tropics. There is no clear evidence of which slit may give the most accurate absolute results.

In the LP-L2-O3-DAILY product, separate retrievals are performed (for overlapping altitude ranges) using radiance data at ultraviolet (UV) and visible (VIS) wavelengths, and a combined ozone profile (VIS retrieval between 0-26.5 km, UV between 27.5-60.5 km) for each event is created from these individual retrievals. Note that no merging procedure is applied for the combined profile; these discontinuities are clearly visible in profiles in the northern latitudes. Approximately 2000 valid profiles are generated daily, from 85° South to 85° North but for to solar zenith angle lower than 85° thus limiting the polar coverage during the polar night. Each profile is also reported in volume mixing ratio format on a regular pressure grid. To this end, the retrieval uses temperature and pressure profiles from NASA Global Modelling and Assimilation Office (GMAO) GEOS-5 FP-IT Np gridded data (on 42 pressure levels up to 0.1hPa, at 0.5° latitude x 0.625° longitude horizontal

resolution, every 3 hours). For each data value a precision value is reported based on the estimated standard deviation derived from the diagonal of the covariance matrix of the optimal estimation solution for the retrieval.

The first step of the validation procedure consists in mapping the model data in the observations space.

The observations used for the validation are selected according to quality and usability criteria usually defined in accompanying documentations of the dataset. For the OMPS-LP LP-L2-O3-DAILY product, all the successfully retrieved O_3 volume mixing ratio on the altitude grid are used.

The model data are converted to volume mixing ratio, downgrade to a 2°x2° horizontal regular grid and interpolated along the time dimension using the CAMS 6-hourly analyses or forecasts. These interpolated data are mapped to the observation space by bilinear interpolation for the horizontal dimension and a vertical interpolation on the observations altitude grid. These model-at-observation (MAO) data, along with indicators of observation quality, are saved for the validation processing.

The second step of the validation builds statistics, in different latitude bands, on the observation datasets, the MAO datasets and their differences. The quality indicators in the datasets allow the selection of matching data in all datasets.

Alternative retrieval of OMPS-LP by U. Saskatchewan: it could be interesting to use an alternative retrieval, which is done by the team delivering Odin/OSIRIS data. This has not yet been explored because this dataset seem updated only twice per year (as of 9 March 2020). URL: https://research-groups.usask.ca/osiris/data-products.php#OSIRISLevel2DataProducts ftp://odin-osiris.usask.ca/OMPS-LP/Level2/o3/1.1.0/ (username: osirislevel2user; password: hugin)

13.2 Validation with ACE-FTS observations of O_3

ACE-FTS is one of the two instruments on the Canadian satellite mission SCISAT-1 (first Science Satellite), ACE (Bernath et al., 2005). It is a high spectral resolution Fourier transform spectrometer operating with a Michelson interferometer. Vertical profiles of atmospheric parameters such as temperature, pressure and volume mixing ratios of trace constituents are retrieved from the occultation spectra, as described in (Boone et al., 2005) with a vertical resolution of maximum 3-4 km. Level 2 ozone retrievals are used as an independent reference data set to validate the distribution of stratospheric ozone in the analyses and forecasts generated by CAMS.

It must be noted that the low spatio-temporal sampling of ACE-FTS (due to the solar occultation technique) does not deliver profiles in all latitude bands for each month. There are also two periods during the year where there are no measurements for a duration of almost 3 weeks due to the fact that the spacecraft is in constant sunlight: June and December (Hughes and Bernath, 2012).

As shown on fig. 13.1, there are four periods per year, lasting about 1 month (northern hemisphere: April, June, August, December; southern hemisphere: February, June, October, December) with no occultation poleward of 60°. At very high β angles (the angle between the orbital plane of the satellite and the Earth-Sun direction > 57°), it is common practice to skip more than half of the

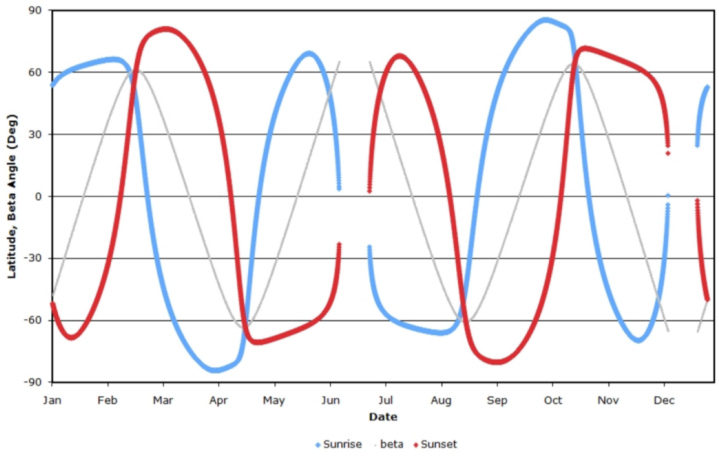

Figure 13.1. Occultation latitudes for ACE for one year on orbit. The red and blue lines indicate locations for sunrise and sunset occultations, respectively. The grey line shows the beta angle associated with the measurement. Note that by design, the latitudes of the ACE observations repeat every year, but the longitude of the occultations change from year to year. Copied from fig. 4 in Hughes and Bernath (2012).

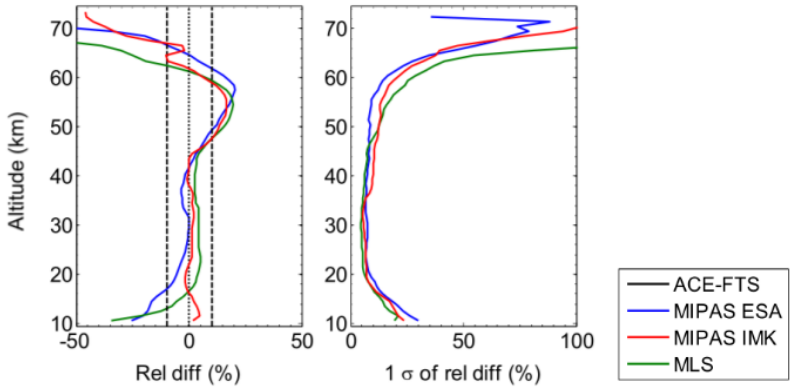

Figure 13.2. O_3 comparisons using coincidence criteria of within 3 h and 350 km. The left panel shows the mean of the relative differences (ACE-FTS minus other instrument) in percent, and the standard deviations of the relative differences in percent. Copied from fig. 2 in Sheese et al. (2017).

available measurement opportunities to avoid exceeding onboard storage capacities and overlapping command sequences. Therefore, the number of observations in the tropics is significantly lower than in the polar regions.

Teigtmeier et al. (2013) performed an intercomparison of ozone climatologies by satellite limb sounders including ACE-FTS (v2.2) and showed that the ACE-FTS climatology agreed well with those of the other instruments in the lower and mid-stratosphere but had a positive offset in the upper stratosphere. This was confirmed by Sheese et al. (2017) using a comparison of coincident ozone profiles between the latest version of ACE-FTS (3.5), Aura-MLS 3.3/3.4 (which is assimilated in CAMS o-suite and reanalysis) and MIPAS (which is assimilated in the CAMS reanalysis). The ACE-FTS data used as independent reference in CAMS-84 is typically within ±5% of mid-stratospheric MIPAS and MLS data and exhibits a positive bias of 10 to 20% in the upper stratosphere–lower mesosphere.

So far, version 3.6 was used for the validation of CAMS while the new version 4.1 is available since July 2020 (Boone et al., 2020). ACE-FTS v3.6 ozone profiles were delivered with a latency of two

days but the complete dataset with necessary quality flags was available only with ~45 days latency. However, since Janury 2021, the v3.6 retrieval is no more processing (reason unknow yet). The latency for v4.1 seems to be around two weeks, but this will need to be confirmed. Note that ACE-FTS, being a scientific mission, the processing of the retrieval can vary from time to time. Consequently, the use of v4.1 will be implemented in the coming weeks and this document provides information on both versions of the L2 retrieval.

The v3.6 ozone profiles used for the validation are selected according to quality and usability criteria usually defined in accompanying documentation of the dataset (Walker et al., 2017). The comparison also uses the quality flags provided along with the retrieval values, hence filtering out physically unrealistic outliers (at any altitude) and profiles known to be affected by instrument or processing errors. The v4.1 profiles are, on the other hand, provided after filtering so no additional filtering is applied. For both versions, all the O_3 volume mixing ratio successfully retrieved on the altitude grid are used. ACE-FTS retrieval in done one a kilometric altitude grid but the retrieval also provides the pressure profiles. This latter is used to interpolate the CAMS product on the ACE-FTS vertical grid.

Since ACE-FTS has limited sampling, any climatological comparison will show large sampling errors. This explains the rather large negative offset in the polar regions between ACE-FTS and the Multi-Instrument Mean of the SPARC Data Initiative (Tegtmeier et al., 2013, fig.2). Sheese et al. (2017) also showed the large diurnal biases appearing in comparisons between ACE-FTS sunrise (sunset) and MIPAS/MLS daytime (night-time) profiles.

The first step of the validation procedure consists in mapping the model data in the observations space: the model data are converted to volume mixing ratio, downgrade to a 2°x2° horizontal regular grid and interpolated along the time dimension using the CAMS 6-hourly analyses or forecasts. These 3-D distributions are mapped to the observation space by bilinear interpolation for the horizontal dimension and a vertical interpolation on the observation altitude grid. Hence there are no sampling biases in CAMS-84 validation (see also Lefever et al., 2015). These model-at-observation (MAO) data, along with indicators of observation quality, are saved for further processing.

The second step of the validation builds statistics, in different latitude bands, on the observation datasets, the MAO datasets and their differences. The quality indicators in the datasets allow the selection of matching data in all datasets.

13.3 Validation with SAGE III/ISS observations of O_3

SAGE III onboard the International Space Station (ISS) is a solar occultation instrument enabling high-precision vertical profiles of O_3 but with limited sampling and no coverage of the polar regions. Wang et al. (2020) have validated the v5.1, showing that among the three SAGE III/ISS solar occultation retrievals, the “AO3” ozone product shows the best accuracy and precision. Hence this is the product used for validation in CAMS-84. The mean biases of AO3 ozone by SAGE III/ISS are less than 5% for ~15–55 km in the mid-latitudes and ~20–55 km in the tropics, increasing to ~10% near the tropopause; its precision of is ~3% for altitudes 20–40 km, degrading to ~10–15% in the lower mesosphere (~55 km), and ~20–30% near the tropopause (McCormick et al., 2020; Wang et al., 2020).

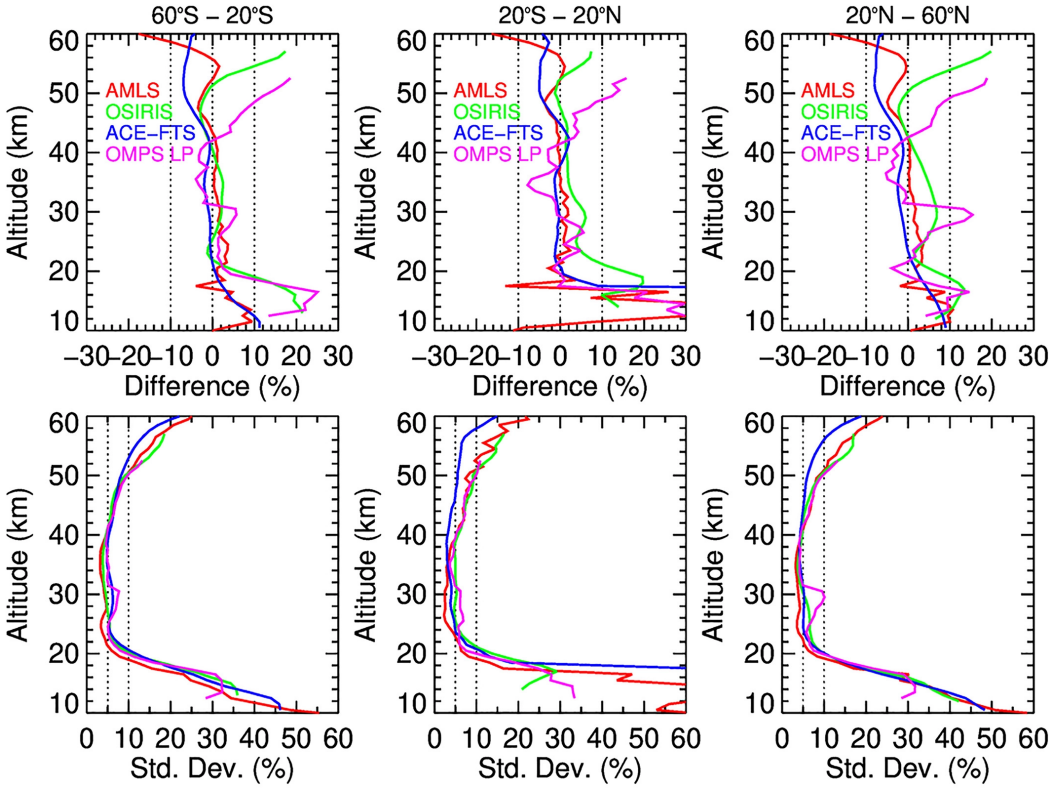

Figure 13.3. Mean differences (top) and standard deviations (bottom) between SAGE III/ISS AO3 against Aura MLS (red), ACE-FTS (blue), OSIRIS (green), and OMPS LP (pink) in three wide latitude bands (20°-60°S, 20°S-20°N, 20°-60°N). Copied from fig. 11 in Wang et al. (2020).

A comparison of SAGE III/ISS v5.1 AO3 products with corresponding ozone products from MLS, OSIRIS, ACE-FTS and OMPS-LP is presented in figure 13.3; and a yearly coverage (for 2019) is presented in figure 13.5.

The v5.1 observations used for the validation are selected according to quality and usability criteria defined in the version 2 of the SAGE III/ISS Data Product User Guide (https://asdc.larc.nasa.gov/documents/sageiii-iss/guide/DPUG-G3B-2-0.pdf). However, this version is no more processed since February 28, 2021, while the new v5.2 has been recently released (7 June 2017 – present). The CAMS validation of stratospheric ozone will thus start using this new version in the MAM 2021 report. According to Kizer et al. (2021), AO3 ozone products show little change from v5.1 to v5.2 and continue to show good agreement with coincident measurements from the ozonesondes. However, v5.2 profiles are not more smoothed by the retrieval team (see Fig. 13.4 and the version 3 of the Date Product User Guide https://asdc.larc.nasa.gov/documents/sageiii-iss/guide/DPUG-G3B.docx). The use of v5.2 will thus be evaluated in the MAM 2021 report.

The first step of the validation procedure consists in mapping the model data in the observations space. The model data are converted to volume mixing ratio, downgrade to a 2°x2° horizontal regular grid and interpolated along the time dimension using the CAMS 6-hourly analyses or forecasts. These interpolated data are mapped to the observation space by bilinear interpolation for the horizontal dimension and a vertical interpolation on the observation altitude grid. These MAO data, along with indicators of observation quality, are saved for further processing.

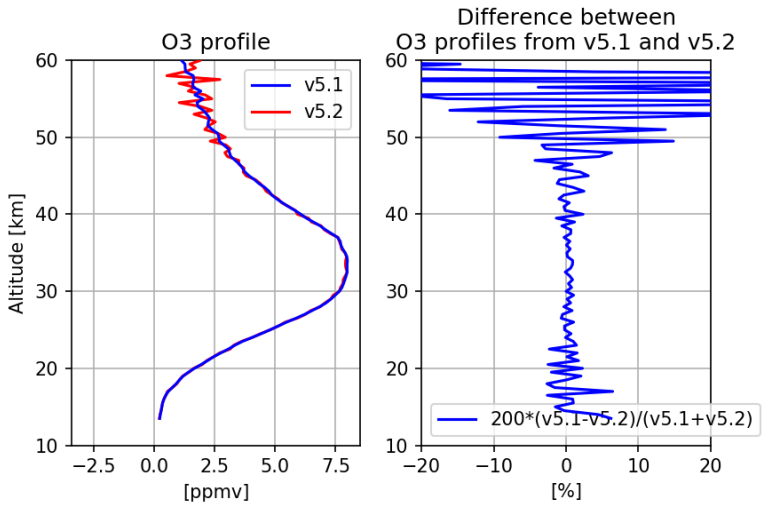

Figure 13.4. Left: Daily mean ozone profiles (ppmv) of SAGE III/ISS sunrise occultations on January 1, 2021, from version 5.1 (blue line) and 5.2 (red line). Right: Difference between both profiles normalized by their mean (%).

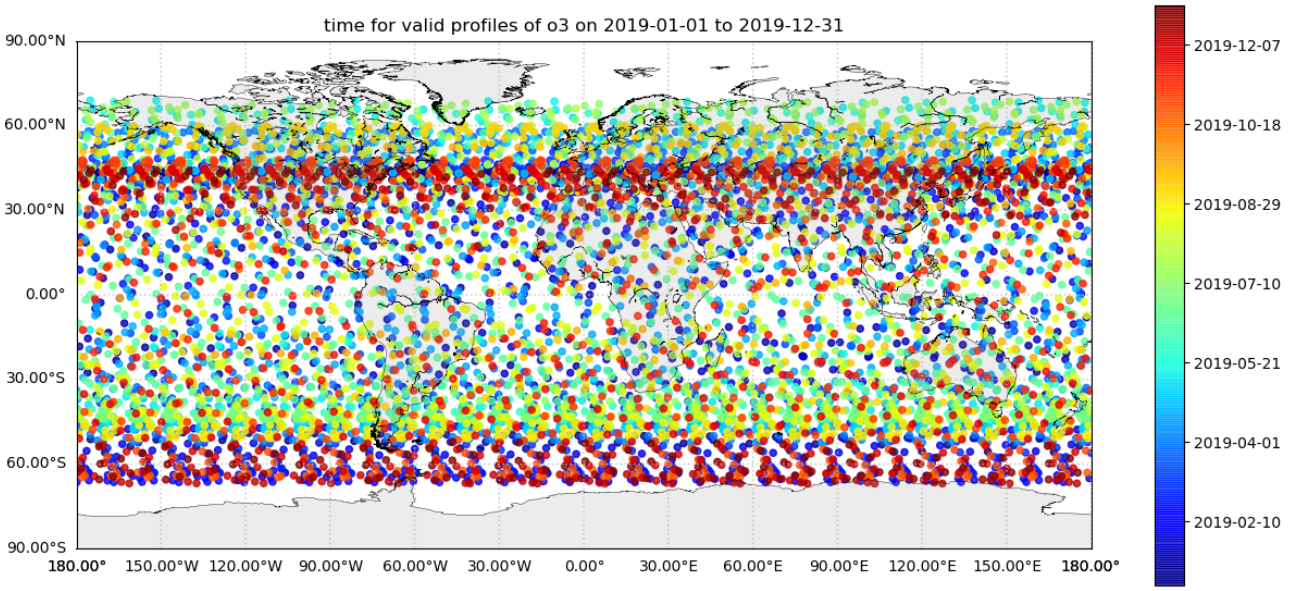

Figure 13.5. Spatial coverage of SAGE III/ISS AO3 in the year 2019. Each profile with valid values is represented by a dot color-coded according to the time in the year (from January, blue, to December, red).

The second step of the validation builds statistics, in different latitude bands, on the observation datasets, the MAO datasets and their differences. The quality indicators in the datasets allow the selection of matching data in all datasets.

14 Greenhouse gas observations with TCCON

The Total Carbon Column Observing Network (TCCON) is a network of ground-based Fourier Transform Spectrometers that record spectra of the sun in the near-infrared. TCCON currently consists of 26 stations distributed around the world. The TCCON data products are column-averaged dry air mole fractions of CO_2, CH_4, N_2O, HF, CO, H_2O, and HDO.

The data processing is performed by a common software package maintained at Caltech/NASA JPL (Wunch et al., 2011). The raw data are called interferograms. An interferogram is the measured intensity of the electromagnetic radiation versus the optical path difference of the light coming from the fixed and moving mirror. These interferograms are then processed by a standardised code (I2S), which corrects the interferograms for solar intensity variations, ghosts and phase errors, and then uses a fast Fourier transformation to compute the spectra. The retrieval of the column abundances is done by the column scaling algorithm GFIT. The retrieval package contains the spectral line list needed for the retrieval. In a post processing routine. the column abundances are converted to column averaged dry air mole fractions by division by the O_2 column involving airmass corrections and a scaling to account for differences to the WMO reference scale. The final product consists of the corrected column average mole fractions and their uncertainties together with averaging kernel and a priori. Additional auxiliary data will also be provided.

The processed data is delivered to Caltech, USA, where a final QA/QC is performed before uploading the data to the TCCON data archive. User guides, documentation describing the methods and evaluation are provided, along with appropriate information necessary for using the data to evaluate models and other measurements (e.g., averaging kernels, a priori profiles, error description, etc.). The format of the data is NetCDF. The data become publicly available no later than one year after the measurements are recorded. Several sites choose to release their data sooner. Within validation projects it has been shown that the final data can be made available 3 months after the measurement.

The TCCON stations at Reunion, Orleans and Nicosia, Cyprus (formerly Bialystok) submit data in Rapid Delivery (RD) mode. This data is available 3-5 days after the measurement. It is retrieved at the TCCON site and then directly delivered to home institution. The RD data will undergo an automated quality check, but not the thorough TCCON quality check. The lag time of 3-5 days mainly arises from the availability of the pressure-temperature profiles.

The validation is done in the same way as the NDACC FTIR validation and is described in 12.2.

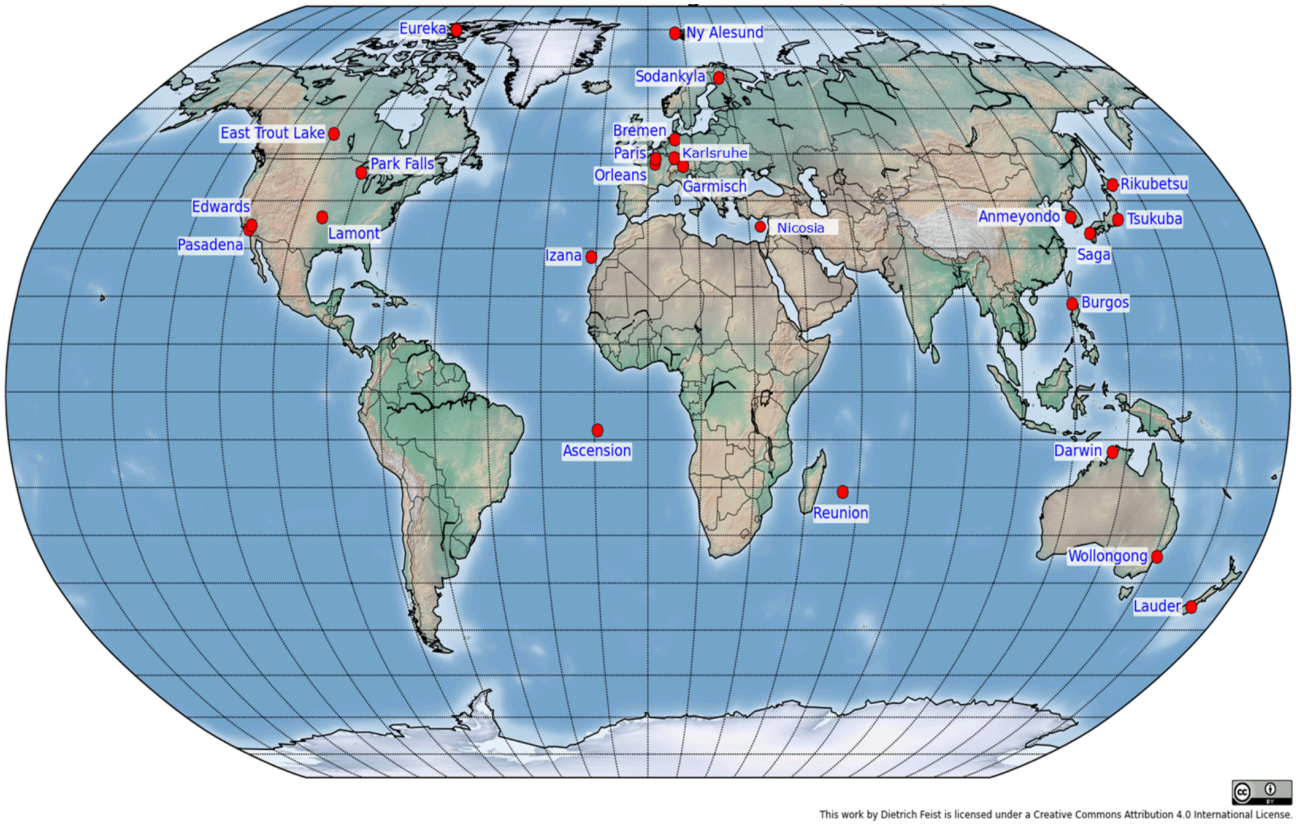

Figure 2: Map of operational TCCON sites in 2019.

15 ICOS CO_2/CH_4 surface observations

On November 2015, the European Commission has officially established the Integrated Carbon Observation System (ICOS ERIC). The ICOS European Research Infrastructure Consortium currently involved 12 European countries: Belgium, Czech Republic, Denmark, Finland, France, Germany, Italy, Netherlands, Norway, Sweden, Switzerland, United Kingdom. Spain announced in December 2019 its intention to join ICOS with four atmospheric stations.

ICOS is a distributed research infrastructure that provides harmonized European-wide measurements on carbon cycle, on greenhouse gas emissions and on atmospheric concentrations of greenhouse gases. The ICOS RI integrates atmosphere, ecosystem and ocean greenhouse gas monitoring networks in order to provide the observational basis for a full European carbon balance and its trends. Standardized measurements are carried out throughout Europe at tall atmospheric towers and ecosystem sites from the Artic to the Mediterranean, as well as on ocean platforms and vessels covering the North Atlantic, the Mediterranean Sea and the Baltic Sea. Each network is coordinated by its Thematic Centre responsible for data integration and processing, centralized quality control, network training and data transmission. The Atmosphere Thematic Centre (ATC) is based in at LSCE, France.

The stations are going through a labelling process, which started in January 2016. So far 34 atmospheric stations (figure 15.1) are engaged in this process, and all of them will provide data in near real time by the end of 2020 at the latest. The protocols of the measurements and data processing are performed according to the ICOS specifications (Laurent et al., 2017). So far, all the measurements are done using cavity ring-down spectroscopy (CRDS) analysers (Yver Kwok et al., 2015). Each instrument is regularly (at least once a month) calibrated against reference gases linked to the WMO scales. In addition, two target gases are used for the quality control of the dataset and uncertainty assessment. The objective of the ICOS program is to reach the compatibility of measurements recommended by WMO: ±0.1 ppm for CO2 and ±2 ppb for CH4 (WMO/GAW report N°213, 2013).

The dataset is processed with a standardized algorithm (Hazan et al., 2016). After an automatic check of several parameters, the time series are validated by the station PIs within a three months period after the data acquisition. The model/observation comparison is based on hourly means, without any data selection to separate for example the influence of local from larger scale emissions. An algorithm to identify and isolate short-term spikes has been implemented in the data processing (El Yazidi et al., 2018). The validation of the model will be done using hourly means without the spikes associated to local sources which cannot be represented by the model. Each station is compared with the closest grid location of the model. In the horizontal no interpolation is done. For some coastal stations, like Finokalia, we may have to use the closest oceanic model grid-box. In the vertical the observations are compared to the data extracted at the same elevation above the surface, and at the real altitude above sea level.

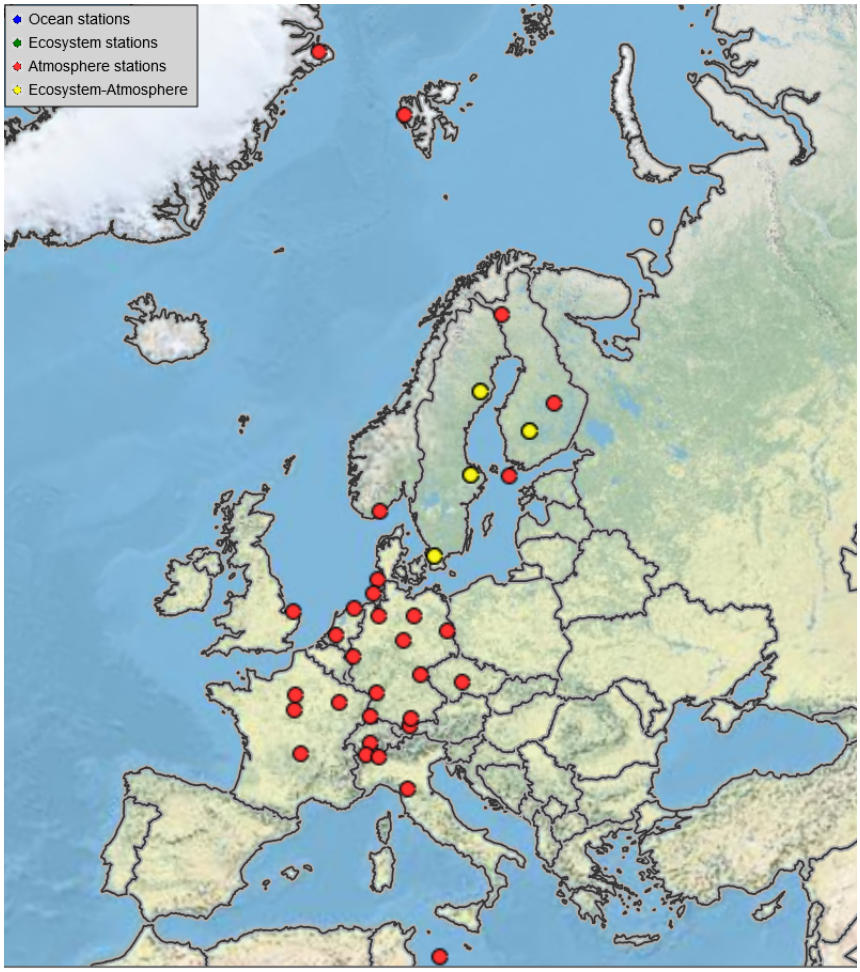

Figure 15.1. Map of the ICOS atmospheric stations engaged in the labelling process. Station at La Réunion Island not shown on this map.

By default we use the model data extracted at the sea level altitude of the monitoring site, except if the model altitude of the grid cell corresponding to the location of the site is higher than the station altitude. At the moment the measurement errors are negligible compared to the representativeness error. In order to improve the comparability of observations with model the CAMS-26 project proposes to implement a baseline and regional data selection, aiming to separate the observations according to their representativeness, and to detect synoptic and seasonal CO2/CH4 anomalies. As part of the CAMS-26 project ICOS is also extending the near real time access to CO and Radon observations.

In addition to the CO2 and CH4 data provided in near real time by ICOS in Europe, we propose to use stations outside Europe from the RAMCES network with one station is the Indian Ocean (Amsterdam Island) and 5 tropical sites (Lamto, French Guiana, Chacaltaya, La Réunion, Marocoo). Those data are available also in near-real time. The OBSPACK international dataset, is now updated two to four times per year (for CO2), and consequently can be used for the NRT reports. So far this data set was used only for the validation of the CO2 and CH4 reanalysis. By extending the NRT validation by using near real time CO2 dataset available in the OBSPACK-NRT updates, we will benefit from stations located in North America, tropical site, and airborne measurements from the

CONTRAIL project. Finally regular AIRCORE measurements (CO2, CH4, CO), up to 25 km, are performed at the ICOS Trainou tall tower and will be used when available.

16 Acknowledgements

We wish to acknowledge the provision of NRT GAW observational data by: Institute of Atmospheric Sciences and Climate (ISAC) of the Italian National Research Council (CNR), South African Weather Service, National Centre for Atmospheric Science (NCAS, Cape Verde), National Air Pollution Monitoring Network (NABEL) (Federal Office for the Environment FOEN and Swiss Federal Laboratories for Materials Testing and Research EMPA), Atmospheric Environment Division Global Environment and Marine Department Japan Meteorological Agency, Chinese Academy of Meteorological Sciences (CAMS), Alfred Wegener Institut, Umweltbundesamt (Austria), National Meteorological Service (Argentina), Umweltbundesamt (UBA, Germany)

We are grateful to the numerous operators of the Aeronet network and to the central data processing facility at NASA Goddard Space Flight Center for providing the NRT sun photometer data, and especially Ilya Slutker and Brent Holben for sending the data.

The authors thank to all researchers, data providers and collaborators of the World Meteorological Organization's Sand and Dust Storm Warning Advisory and Assessment System (WMO SDS-WAS) for Northern Africa, Middle East and Europe (NAMEE) Regional Node. Also special thank to Canary Government as well as AERONET, MODIS, U.K. Met Office MSG, MSG Eumetsat and EOSDIS World Viewer principal investigators and scientists for establishing and maintaining data used in the activities of the WMO SDS-WAS NAMEE Regional Center (http://sds-was.aemet.es/).

We wish to acknowledge the provision of ozone sonde data by the World Ozone and Ultraviolet Radiation Data Centre established at EC in Toronto (http://woudc.org), by the Data Host Facility of the Network for the Detection of Atmospheric Composition Change established at NOAA (http://ndacc.org), by the Norwegian Institute for Air Research (http://nilu.no) and by the National Aeronautics and Space Administration (https://www.nasa.gov).

The data used in this publication were obtained from institute or PI as part of the Network for the Detection of Atmospheric Composition Change (NDACC) and are publicly available (see http://www.ndacc.org).

The authors acknowledge the NOAA Earth System Research Laboratory (ESRL) Global Monitoring Division (GMD) for the provision of ground-based ozone concentrations.

The MOPITT CO data were obtained from the NASA Langley Research Center ASDC. We acknowledge the LATMOS IASI group for providing IASI CO data.

SCIAMACHY lv1 radiances were provided to IUP by ESA through DLR/DFD.

GOME2 lv1 radiances were provided to IUP by EUMETSAT.

TROPOMI S-5P level 1 data were provided to IUP through the EU Copernicus program.

The authors acknowledge Environment and Climate Change Canada for the provision of Alert ozone data and Sara Crepinsek – NOAA for the provision of Tiksi ozone data. Surface ozone data from the Zeppelin Mountain, Svalbard are from www.luftkvalitet.info. Surface ozone data from the Villum Research Station, Station Nord (VRS) were financially supported by "The Danish Environmental

Protection Agency" with means from the MIKA/DANCEA funds for Environmental Support to the Arctic Region. The Villum Foundation is acknowledged for the large grant making it possible to build VRS in North Greenland.

We acknowledge the National Aeronautics and Space Administration (NASA), USA for the OMPS Level-2 data (http://npp.gsfc.nasa.gov/omps.html), and the SAGE III-ISS ozone data https://eosweb.larc.nasa.gov/project/sageiii-iss/sageiii-iss_table.

We thank the Canadian Space Agency and ACE science team for providing level 2 data retrieved from ACE-FTS on the Canadian satellite SCISAT-1.

The European Environment Information and Observation Network (Eionet) Air Quality portal provides details relevant for the reporting of air quality information from EU Member States and other EEA member and co-operating countries. This information is submitted according to Directives 2004/107/EC and 2008/50/EC of the European Parliament and of the Council.

We are grateful to the IAGOS operators from the various institutes which are members of IAGOS-AISBL (http://www.iagos.org). The authors also acknowledge the strong support of the European Commission, Airbus, and the airlines (Lufthansa, Air France, Austrian, Air Namibia, Cathay Pacific, Iberia, China Airlines and Hawaiian Airlines so far) which have carried the MOZAIC or IAGOS equipment and undertaken maintenance since 1994. In the last 10 years of operation, MOZAIC has been funded by INSU-CNRS (France), Météo-France, Université Paul Sabatier (Toulouse, France) and Research Center Jülich (FZJ, Jülich, Germany). IAGOS has been additionally funded by the EU projects IAGOS-DS and IAGOS-ERI. The MOZAIC–IAGOS database (http://www.iagos-data.fr) is supported by AERIS (CNES and INSU-CNRS). Data are also available via the AERIS web site www.aeris-data.fr.

We acknowledge the provision of CO_2/CH_4 data from SNO-RAMCES/ICOS network coordinated by LSCE/OVSQ (CEA-CNRS-UVSQ, Université Paris-Saclay), as well as Laboratorio de Física de la Atmósfera (UMSA, Bolivia), Environmental Chemical Processes Laboratory (ECPL/UoC, Greece), Station Géophysique de LAMTO, Ivory Coast), C-CAPS/NUIG/EPA (Ireland), BIRA-IASB (Belgium) and the following research institutes in France: LaMP/OPGC, P2OA/LA/OMP, OPE/ANDRA, OHP/PYTHEAS, OPAR/LACY/OSUR, UMR EcoFoG, IPEV, IRD.

The TCCON site at Orleans is operated by the University of Bremen and the RAMCES team at LSCE (Gif-sur-Yvette, France). The TCCON site at Bialystok is operated by the University of Bremen. Funding for the two sites was provided by the EU-project ICOS-INWIRE and the University of Bremen. The TCCON site at Réunion is operated by BIRA-IASB, in cooperation with UReunion and is funded by BELSPO in the framework of the Belgian ICOS program.

TCCON references:

Hazan, L., J. Tarniewicz, M. Ramonet, O. Laurent and A. Abbaris **(2016)**. *Automatic processing of atmospheric CO_2 and CH_4 mole fractions at the ICOS Atmosphere Thematic Centre*. Atmospheric Measurement Techniques 9(9): 4719-4736.

Blumenstock, T., F. Hase, M. Schneider, O. E. García, and E. Sepúlveda. 2017. "TCCON data from Izana (ES), Release GGG2014.R1." CaltechDATA. doi:10.14291/tccon.ggg2014.izana01.r1.

De Mazière, M., M. K. Sha, F. Desmet, C. Hermans, F. Scolas, N. Kumps, J.-M. Metzger, V. Duflot, and J.-P. Cammas. 2017. "TCCON data from Réunion Island (RE), Release GGG2014.R1." CaltechDATA. doi:10.14291/tccon.ggg2014.reunion01.r1.

Deutscher, N. M., J. Notholt, J. Messerschmidt, C. Weinzierl, T. Warneke, C. Petri, and P. Grupe. 2017. "TCCON data from Bialystok (PL), Release GGG2014.R1." CaltechDATA. doi:10.14291/tccon.ggg2014.bialystok01.r1/1183984.

Dubey, M. K., B. G. Henderson, D. Green, Z. T. Butterfield, G. Keppel-Aleks, N. T. Allen, J.-F. Blavier, C. M. Roehl, D. Wunch, and R. Lindenmaier. 2017. "TCCON data from Manaus (BR), Release GGG2014.R0." CaltechDATA. doi:10.14291/tccon.ggg2014.manaus01.r0/1149274.

Dubey, M. K., R. Lindenmaier, B. G. Henderson, D. Green, N. T. Allen, C. M. Roehl, J.-F. Blavier, et al. 2017. "TCCON data from Four Corners (US), Release GGG2014.R0." CaltechDATA. doi:10.14291/tccon.ggg2014.fourcorners01.r0/1149272.

Feist, D. G., S. G. Arnold, N. John, and M. C. Geibel. 2017. "TCCON data from Ascension Island (SH), Release GGG2014.R0." CaltechDATA. doi:10.14291/tccon.ggg2014.ascension01.r0/1149285.

Goo, T.-Y., Y.-S. Oh, and V. A. Velazco. 2017. "TCCON data from Anmeyondo (KR), Release GGG2014.R0." CaltechDATA. doi:10.14291/tccon.ggg2014.anmeyondo01.r0/1149284.

Griffith, D. W. T., N. M. Deutscher, V. A. Velazco, P. O. Wennberg, Y. Yavin, G. Keppel-Aleks, R. A. Washenfelder, et al. 2017. "TCCON data from Darwin (AU), Release GGG2014.R0." CaltechDATA. doi:10.14291/tccon.ggg2014.darwin01.r0/1149290.

Griffith, D. W. T., V. A. Velazco, N. M. Deutscher, C. Paton-Walsh, N. B. Jones, S. R. Wilson, R. C. Macatangay, G. C. Kettlewell, R. R. Buchholz, and M. O. Riggenbach. 2017. "TCCON data from Wollongong (AU), Release GGG2014.R0." CaltechDATA. doi:10.14291/tccon.ggg2014.wollongong01.r0/1149291.

Hase, F., T. Blumenstock, S. Dohe, J. Groß, and M.ä. Kiel. 2017. "TCCON data from Karlsruhe (DE), Release GGG2014.R1." CaltechDATA. doi:10.14291/tccon.ggg2014.karlsruhe01.r1/1182416.

Iraci, L. T., J. R. Podolske, P. W. Hillyard, C. Roehl, P. O. Wennberg, J.-F. Blavier, J. Landeros, et al. 2017. "TCCON data from Edwards (US), Release GGG2014.R1." CaltechDATA. doi:10.14291/tccon.ggg2014.edwards01.r1/1255068.

—. 2017. "TCCON data from Indianapolis (US), Release GGG2014.R1." CaltechDATA. doi:10.14291/tccon.ggg2014.indianapolis01.r1/1330094.

Kawakami, S., H. Ohyama, K. Arai, H. Okumura, C. Taura, T. Fukamachi, and M. Sakashita. 2017. "TCCON data from Saga (JP), Release GGG2014.R0." CaltechDATA. doi:10.14291/tccon.ggg2014.saga01.r0/1149283.

Kivi, R., P. Heikkinen, and E. Kyrö. 2017. "TCCON data from Sodankylä (FI), Release GGG2014.R0." CaltechDATA. doi:10.14291/tccon.ggg2014.sodankyla01.r0/1149280.

Liu, Cheng, Wei Wang, and Youwen Sun. 2018. "TCCON data from Hefei (PRC), Release GGG2014.R0." CaltechDATA. doi:10.14291/tccon.ggg2014.hefei01.r0.

Morino, I., N. Yokozeki, T. Matsuzaki, and M. Horikawa. 2017. "TCCON data from Rikubetsu (JP), Release GGG2014.R2." CaltechDATA. doi:10.14291/tccon.ggg2014.rikubetsu01.r2.

Morino, I., T. Matsuzaki, and M. Horikawa. 2017. "TCCON data from Tsukuba (JP), 125HR, Release GGG2014.R2." CaltechDATA. doi:10.14291/tccon.ggg2014.tsukuba02.r2.

Morino, Isamu, Voltaire A. Velazco, Akihiro Hori, Osamu Uchino, and David W. T. Griffith. 2018. "TCCON data from Burgos, Ilocos Norte (PH), Release GGG2014.R0." CaltechDATA. doi:10.14291/tccon.ggg2014.burgos01.r0.

Notholt, J., C. Petri, T. Warneke, N. M. Deutscher, M. Palm, M. Buschmann, C. Weinzierl, R. C. Macatangay, and P. Grupe. 2017. "TCCON data from Bremen (DE), Release GGG2014.R0." CaltechDATA. doi:10.14291/tccon.ggg2014.bremen01.r0/1149275.

Notholt, J., T. Warneke, C. Petri, N. M. Deutscher, C. Weinzierl, M. Palm, and M. Buschmann. 2017. "TCCON data from Ny Ålesund, Spitsbergen (NO), Release GGG2014.R0." CaltechDATA. doi:10.14291/tccon.ggg2014.nyalesund01.r0/1149278.

Pollard, David Frank, John Robinson, and Hisako Shiona. 2019. "TCCON data from Lauder (NZ), Release GGG2014.R0." CaltechDATA. doi:10.14291/tccon.ggg2014.lauder03.r0.

Sherlock, V., B. Connor, J. Robinson, H. Shiona, D. Smale, and D. F. Pollard. 2017. "TCCON data from Lauder (NZ), 120HR, Release GGG2014.R0." CaltechDATA. doi:10.14291/tccon.ggg2014.lauder01.r0/1149293.

—. 2017. "TCCON data from Lauder (NZ), 125HR, Release GGG2014.R0." CaltechDATA. doi:10.14291/tccon.ggg2014.lauder02.r0/1149298.

Strong, K., S. Roche, J. E. Franklin, J. Mendonca, E. Lutsch, D. Weaver, P. F. Fogal, J. R. Drummond, R. Batchelor, and R. Lindenmaier. 2018. "TCCON data from Eureka (CA), Release GGG2014.R3." CaltechDATA. doi:10.14291/tccon.ggg2014.eureka01.r3.

Sussmann, R., and M. Rettinger. 2017. "TCCON data from Garmisch (DE), Release GGG2014.R2." CaltechDATA. doi:10.14291/tccon.ggg2014.garmisch01.r2.

—. 2018. "TCCON data from Zugspitze (DE), Release GGG2014.R1." CaltechDATA. doi:10.14291/tccon.ggg2014.zugspitze01.r1.

Té, Y., P. Jeseck, and C. Janssen. 2017. "TCCON data from Paris (FR), Release GGG2014.R0." CaltechDATA. doi:10.14291/tccon.ggg2014.paris01.r0/1149279.

Warneke, T., J. Messerschmidt, J. Notholt, C. Weinzierl, N. M. Deutscher, C. Petri, and P. Grupe. 2017. "TCCON data from Orléans (FR), Release GGG2014.R0." CaltechDATA. doi:10.14291/tccon.ggg2014.orleans01.r0/1149276.

Wennberg, P. O., C. M. Roehl, D. Wunch, G. C. Toon, J.-F. Blavier, R. Washenfelder, G. Keppel-Aleks, N. T. Allen, and J. Ayers. 2017. "TCCON data from Park Falls (US), Release GGG2014.R1." CaltechDATA. doi:10.14291/tccon.ggg2014.parkfalls01.r1.

Wennberg, P. O., C. M. Roehl, J.-F. Blavier, D. Wunch, and N. T. Allen. 2017. "TCCON data from Jet Propulsion Laboratory (US), 2011, Release GGG2014.R1." CaltechDATA. doi:10.14291/tccon.ggg2014.jpl02.r1/1330096.

Wennberg, P. O., D. Wunch, C. M. Roehl, J.-F. Blavier, G. C. Toon, and N. T. Allen. 2017. "TCCON data from Caltech (US), Release GGG2014.R1." CaltechDATA. doi:10.14291/tccon.ggg2014.pasadena01.r1/1182415.

—. 2017. "TCCON data from Lamont (US), Release GGG2014.R1." CaltechDATA. doi:10.14291/tccon.ggg2014.lamont01.r1/1255070.

Wennberg, P. O., D. Wunch, Y. Yavin, G. C. Toon, J.-F. Blavier, N. T. Allen, and G. Keppel-Aleks. 2017. "TCCON data from Jet Propulsion Laboratory (US), 2007, Release GGG2014.R0." CaltechDATA. doi:10.14291/tccon.ggg2014.jpl01.r0/1149163.

Wunch, D., J. Mendonca, O. Colebatch, N. T. Allen, J.-F. Blavier, S. Roche, J. Hedelius, et al. 2017. "TCCON data from East Trout Lake, SK (CA), Release GGG2014.R1." CaltechDATA. doi:10.14291/tccon.ggg2014.easttroutlake01.r1.

Wunch, D., Toon, G. C., Sherlock, V., Deutscher, N. M., Liu, C., Feist, D. G., & Wennberg, P. O. (2015). The Total Carbon Column Observing Network's GGG2014 Data Version. Tech. rep., California Institute of Technology, Pasadena. doi:10.14291/tccon.ggg2014.documentation.R0/1221662.

17 References

Alvarado, L. M. A., Richter, A., Vrekoussis, M., Hilboll, A., Kalisz Hedegaard, A. B., Schneising, O., and Burrows, J. P.: Unexpected long-range transport of glyoxal and formaldehyde observed from the Copernicus Sentinel-5 Precursor satellite during the 2018 Canadian wildfires, Atmos. Chem. Phys., 20, 2057–2072, https://doi.org/10.5194/acp-20-2057-2020, 2020.

August, Thomas, Dieter Klaes, Peter Schlüssel, Tim Hultberg, Marc Crapeau, Arlindo Arriaga, Anne O'Carroll, Dorothée Coppens, Rose Munro, Xavier Calbet, IASI on Metop-A: Operational Level 2 retrievals after five years in orbit, Journal of Quantitative Spectroscopy and Radiative Transfer, Volume 113, Issue 11, 2012, p 1340-1371, ISSN 0022-4073, https://doi.org/10.1016/j.jqsrt.2012.02.028.

Bai, K., Li, K., Guo, J., Yang, Y., & Chang, N. ‐B., Filling the gaps of in situ hourly PM2.5 concentration data with the aid of empirical orthogonal function analysis constrained by diurnal cycles, Atmospheric Measurement Techniques, 13(3), 1213‐1226. https://doi.org/10.5194/amt-13-1213-2020, 2020.

Barreto, Á., Cuevas, E., Granados-Muñoz, M.-J., Alados-Arboledas, L., Romero, P. M., Gröbner, J., Kouremeti, N., Almansa, A. F., Stone, T., Toledano, C., Román, R., Sorokin, M., Holben, B., Canini, M., and Yela, M.: The new sun-sky-lunar Cimel CE318-T multiband photometer – a comprehensive performance evaluation, Atmos. Meas. Tech., 9, 631-654, doi:10.5194/amt-9-631-2016, 2016.

Basart, S., Pérez García-Pando, C., Cuevas, E., Baldasano Recio, J. M., & Gobbi, P. (2009). Aerosol characterization in Northern Africa, Northeastern Atlantic, Mediterranean basin and Middle East from direct-sun AERONET observations. Atmospheric chemistry and physics, 9(21), 8265-8282.

Beirle, S., Hörmann, C., Jöckel, P., Liu, S., Penning de Vries, M., Pozzer, A., Sihler, H., Valks, P., and Wagner, T.: The STRatospheric Estimation Algorithm from Mainz (STREAM): estimating stratospheric NO_2 from nadir-viewing satellites by weighted convolution, Atmos. Meas. Tech., 9, 2753–2779, https://doi.org/10.5194/amt-9-2753-2016, 2016.

Bernath, P. F., McElroy, C. T., Abrams, et al.: Atmospheric Chemistry Experiment (ACE): Mission overview, Geophys. Res. Lett., 32, L15S01, doi:10.1029/2005GL022386, 2005.

Blot, R., Nedelec, P., Boulanger, D., Wolff, P., Sauvage, B., Cousin, J.-M., Athier, G., Zahn, A., Obersteiner, F., Scharffe, D., Petetin, H., Bennouna, Y., Clark, H., and Thouret, V.: Internal consistency of the IAGOS ozone and carbon monoxide measurements for the last 25 years, Atmos. Meas. Tech., 14, 3935–3951, https://doi.org/10.5194/amt-14-3935-2021, 2021.

Boone, C.D., Nassar, R., Walker, K. A., Rochon, Y., McLeod, S.D., Rinsland, C. P., and Bernath, P. F.: Retrievals for the atmospheric chemistry experiment Fourier-transform spectrometer, Appl. Optics IP, 44, 7218–7231, doi:10.1364/AO.44.007218, 2005.

Boynard, A., Hurtmans, D., Koukouli, M. E., Goutail, F., Bureau, J., Safieddine, S., Lerot, C., Hadji-Lazaro, J., Wespes, C., Pommereau, J.-P., Pazmino, A., Zyrichidou, I., Balis, D., Barbe, A., Mikhailenko, S. N., Loyola, D., Valks, P., Van Roozendael, M., Coheur, P.-F., and Clerbaux, C.: Seven years of IASI ozone retrievals from FORLI: validation with independent total column and vertical profile measurements, Atmos. Meas. Tech., 9, 4327–4353, https://doi.org/10.5194/amt-9-4327-2016, 2016.

Boynard, A., Hurtmans, D., Garane, K., Goutail, F., Hadji-Lazaro, J., Koukouli, M. E., Wespes, C., Vigouroux, C., Keppens, A., Pommereau, J.-P., Pazmino, A., Balis, D., Loyola, D., Valks, P., Sussmann, R., Smale, D., Coheur, P.-F., and Clerbaux, C.: Validation of the IASI FORLI/EUMETSAT ozone products using satellite (GOME-2),

ground-based (Brewer–Dobson, SAOZ, FTIR) and ozonesonde measurements, Atmos. Meas. Tech., 11, 5125–5152, https://doi.org/10.5194/amt-11-5125-2018, 2018.

Brewer, A. and J. Milford (1960), The Oxford Kew ozonesonde, Proc. Roy. Soc.London, Ser. A, 256, 470, 1960.

Boucher, O., Anderson, T.L., General circulation model assessment of the sensitivity of direct climate forcing by anthropogenic sulfate aerosols to aerosol size and chemistry. Journal of Geophysical Research: Atmospheres 1995;100(D12):26117-26134.

Bovensmann, H., Burrows, J. P., Buchwitz, M., Frerick, J., Noël, S., Rozanov, V. V., Chance, K. V. and Goede, a. P. H.: SCIAMACHY: Mission Objectives and Measurement Modes, J. Atmos. Sci., 56(2), 127–150, doi:10.1175/1520-0469(1999)056<0127:SMOAMM>2.0.CO;2, 1999.

Clémer, K., Van Roozendael, M., Fayt, C., Hendrick, F., Hermans, C., Pinardi, G., Spurr, R., Wang, P., and De Mazière, M.: Multiple wavelength retrieval of tropospheric aerosol optical properties from MAXDOAS measurements in Beijing, Atmos. Meas. Tech., 3, 863-878, 2010.

Clerbaux C., A. Boynard, L. Clarisse, M. George, J. Hadji-Lazaro, H. Herbin, D. Hurtmans, M. Pommier, A. Razavi, S. Turquety, C. Wespes, and P.-F. Coheur, Monitoring of atmospheric composition using the thermal infrared IASI/MetOp sounder, Atmos. Chem. Phys., 2009.

Christensen, J.H., Brandt, J., Frohn, L.M. and Skov, H., Modelling of mercury with the Danish Eulerian Hemispheric Model, Atm. Chem. Phys. 4, 2251-2257, 2004.

Connor, B. J., Siskind, D. E., Tsou, J. J., Parrish, A., and Remsberg, E. E.: Ground-based microwave observations of ozone in the upper stratosphere and mesosphere, J. Geophys. Res., 99 (D8), 16,757-16,770, 1994.

Cuevas, E., Camino, C., Benedetti, A., Basart, S., Terradellas, E.,Baldasano, J. M., Morcrette, J. J., Marticorena, B., Goloub,P., Mortier, A., Berjón, A., Hernández, Y., Gil-Ojeda, M.,and Schulz, M.: The MACC-II 2007–2008 reanalysis: atmospheric dust evaluation and characterization over northern Africa and the Middle East, Atmos. Chem. Phys., 15, 3991–4024, doi:10.5194/acp-15-3991-2015, 2015.

Deeter, M. N., Emmons, L. K., Edwards, D. P., Gille, J. C., and Drummond, J. R.: Vertical resolution and information content of CO profiles retrieved by MOPITT, Geophys. Res. Lett., 31, L15112, doi:10.1029/2004GL020235, 2004.

Deeter, M. N., et al., The MOPITT version 4 CO product: Algorithm enhancements, validation, and long-term stability, J. Geophys. Res., 115, D07306, doi:10.1029/2009JD013005, 2010.

Deeter M. N., Martinez-Alonso S., Edwards D. P., Emmons L. K., Gille J. C., Worden H. M., Pittman J. V., Daube B. C., Wofsy S. C.: Validation of MOPITT Version 5 thermal-infrared, near-infrared, and multispectral carbon monoxide profile retrievals for 2000–2011, J. Geoph. Res., 118, 12, 2013.

Deeter M. N., Martinez-Alonso S., Edwards D. P., Emmons L. K., Gille J. C., Worden H. M., Sweeney C., Pittman J. V., Daube B. C., and Wofsy S. C.: The MOPITT Version 6 product: algorithm enhancements and validation, Atmos. Meas. Tech, 7, 3623-3632, 2014

Deeter M. N., David P. Edwards, Gene L. Francis, John C. Gille, Sara Martínez-Alonso, Helen M. Worden, and Colm Sweeney, A climate-scale satellite record for carbon monoxide: the MOPITT Version 7 product, Atmospheric Measurement Techniques, Vol. 10 Issue 7, p2533-2555, 2017.

de Mazière, M., et al., D8.1 NORS Validation server user requirements document, available as NORS deliverable at http://nors.aeronomie.be/, 2012.

de Mazière, M., etal., D4.2 NORS Data user guide, 2013, available as NORS deliverable at http://nors.aeronomie.be/, 2013

Deshler, T., J.L. Mercer, H.G.J. Smit, R. Stubi, G. Levrat, B.J. Johnson, S.J. Oltmans, R. Kivi, A.M. Thompson, J. Witte, J. Davies, F.J. Schmidlin, G. Brothers, T. Sasaki (2008) Atmospheric comparison of electrochemical cell ozonesondes from different maufacturers, and with different cathode solution strengths: The Balloon Experiment on Standards for Ozonsondes. J. Geophys. Res.113, D04307, doi:10.1029/2007JD008975

Dubovik, O., Holben, B., Eck, T. F., Smirnov, A., Kaufman, Y. J., King, M. D., Tanré, D., & Slutsker, I. (2002). Variability of Absorption and Optical Properties of Key Aerosol Types Observed in Worldwide Locations, Journal of the Atmospheric Sciences, 59(3), 590-608.

Dupuy, E., et al.: Validation of ozone measurements from the Atmospheric Chemistry Experiment (ACE), Atmos. Chem. Phys., 9, 287-343, doi:10.5194/acp-9-287-2009, 2009.

Eck, T., Holben, B., Reid, J. S., Dubovik, O., Smirnov, A.,O'Neill, N. T., Slutsker, I., and Kinne, S.: Wavelength dependence of the optical depth of biomass burning urban and desert dust aerosols, J. Geophys. Res., 104, 31333–31349, doi:10.1029/1999JD900923, 1999.

*El Yazidi, A., M. Ramonet, P. Ciais, G. Broquet, I. Pison, A. Abbaris, D. Brunner, S. Conil, M. Delmotte, F. Gheusi, F. Guerin, L. Hazan, N. Kachroudi, G. Kouvarakis, N. Mihalopoulos, L. Rivier and D. Serca **(2018)**. Identification of spikes associated with local sources in continuous time series of atmospheric CO, CO2 and CH4. Atmospheric Measurement Techniques 11(3): 1599-1614.*

Emmons, L. K., D. P. Edwards, M. N. Deeter, J. C. Gille, T. Campos, P. Nédélec, P. Novelli, and G. Sachse, Measurements of Pollution In The Troposphere (MOPITT) validation through 2006, Atmos. Chem. Phys., 9, 1795-1803, 2009.

Engeln, Axel von, and João Teixeira, A Planetary Boundary Layer Height Climatology Derived from ECMWF Reanalysis Data, Journal of Climate 2013 26:17, 6575-6590, 2013.

Eskes, H. J., and Boersma, K. F.: Averaging kernels for DOAS total-column satellite retrievals, Atmos. Chem. Phys., 3, 1285–1291, 2003.

Eskes, H., Huijnen, V., Arola, A., Benedictow, A., Blechschmidt, A.-M., Botek, E., Boucher, O., Bouarar, I., Chabrillat, S., Cuevas, E., Engelen, R., Flentje, H., Gaudel, A., Griesfeller, J., Jones, L., Kapsomenakis, J., Katragkou, E., Kinne, S., Langerock, B., Razinger, M., Richter, A., Schultz, M., Schulz, M., Sudarchikova, N., Thouret, V., Vrekoussis, M., Wagner, A., and Zerefos, C.: Validation of reactive gases and aerosols in the MACC global analysis and forecast system, Geosci. Model Dev., 8, 3523-3543, doi:10.5194/gmd-8-3523-2015, 2015.

Evans, R. D: Operations Handbook: Ozone Observations with a Dobson Spectrophotometer, Volume 183 of Global Atmosphere Watch, WMO 2008.

Fisher, R. A. (1936). "The Use of Multiple Measurements in Taxonomic Problems" (PDF). Annals of Eugenics. 7 (2): 179–188. doi:10.1111/j.1469-1809.1936.tb02137.x.

Frieß U., Monks, P.S., Remedios, J.J., Rozanov, A., Sinreich, R., Wagner, T. and Platt, U.: MAX- DOAS O4 measurements: A new technique to derive information on atmospheric aerosols: 2. Modeling studies, J. Geophys. Res. 111, D14203, doi:10.1029/2005JD006618, 2006.

George M., C. Clerbaux, D. Hurtmans, S. Turquety, P.-F. Coheur, M. Pommier, J. Hadji-Lazaro, D. P. Edwards, H. Worden, M. Luo, C. Rinsland, and W. McMillan: Carbon monoxide distributions from the IASI/METOP mission: evaluation with other space-borne remote sensors, Atmos. Chem. Phys., 9, 8317-8330, 2009.

Gielen, C., Van Roozendael, M., Hendrick, F., Pinardi, G., Vlemmix, T., De Bock, V., De Backer, H., Fayt, C., Hermans, C., Gillotay, D., and Wang, P.: A simple and versatile cloud-screening method for MAX-DOAS retrievals, Atmos. Meas. Tech., 7, 3509-3527, doi:10.5194/amt-7-3509-2014, 2014.

Godin, S., G. Mégie and J. Pelon, Geophys. Res. Lett., 1989, 16(16), 547–550. H. Nakane, N. Sugimoto, S. Hayashida, Y. Sasano and I. Matsui, Five years lidar observation of vertical profiles of stratospheric ozone at NIES, Tsukuba (36N, 140E), Proc. 17th ILRC, Sendai, Japan, 1994.

Guo, J., Xia, F., Zhang, Y., Liu, H., Li, J., Lou, M., He, J., Yan, Y., Wang, F., Min, M., and Zhai, P.: Impact of diurnal variability and meteorological factors on the PM2.5-AOD relationship: Implications for PM2.5 remote sensing, Environ. Pollut., 221, 94–104, https://doi.org/10.1016/j.envpol.2016.11.043, 2017.

Haeffelin, M., Angelini, F., Morille, Y., Martucci, G., O'Dowd, C. D., Xueref-Rémy, I., Wastine, B., Frey, S., and Sauvage, L.: Eval- uation of mixing depth retrievals from automatic profiling li- dars and ceilometers inview of future integrated networks in Eu- rope, Bound.-Lay. Meteorol., 143, 49–75, doi:10.1007/s10546- 011-9643-z, 2012.

Hazan, L., J. Tarniewicz, M. Ramonet, O. Laurent and A. Abbaris (2016). Automatic processing of atmospheric CO_2 and CH_4 mole fractions at the ICOS Atmosphere Thematic Centre. Atmospheric Measurement Techniques 9(9): 4719-4736.

Heese, B., Flentje, H., Althausen, D., Ansmann, A., and Frey, S.: Ceilometer lidar comparison: backscatter 5 coefficient retrieval and signal-to-noise ratio determination, Atmos. Meas. Tech., 3, 1763–1770, doi:10.5194/amt-3-1763-2010, 2010.

Heidam, N.Z., Christensen, J.H., Skov, H., Wåhlin, P., Monitoring and modelling of the atmospheric Environment in Greenland. A review., Sci. Total Environ., 331 No. 1-3, 5-28, 2004.

Helten, M., Smit, H. G. J., Strater, W., Kley, D., Nédélec, P., Zoger, M., and Busen, R.: Calibration and performance of automatic compact instrumentation for the measurement of relative humidity from passenger aircraft, J. Geophys. Res., 103, 25643-25652, https://doi.org/10.1029/98JD00536, 1998.

Hocke, K.: Homogenisation of the ozone series of the microwave radiometers SOMORA and GROMOS, IAP Research Report, No. 2007-04-MW, Institut für angewandte Physik, Universität Bern, 2007.

Hugues, R and Bernath, P. F: ACE Mission Information for Public Data Release, Document Nr ACE-SOC 0025, June 2012, https://ace.uwaterloo.ca/ACE-FTS_v2.2/ACEFTSPublicReleaseDocumentation.pdf

Holben, B. N., Eck, T. F., Slutsker, I., Tanré, D., Buis, J. P., Setzer, A., Vermote, E., Reagan, J. A., Kaufman, Y. J., Nakajima, T., Lavenu, F., Jankowiak, I., and Smirnov A.: AERONET – a federated instrument network and data archive for aerosol characterization, Remote Sens. Environ., 66, 1–16, 5529, 5533, 5537, 5544, 1998.

Hurtmans D., Coheur P.-F., Wespes C., Clarisse L., Scharf O., Clerbaux C., Hadji-Lazaro J., George M., Turquety S.: FORLI radiative transfer and retrieval code for IASI, J. Quantitative Spectroscopy and Radiative Transfer, 113, 11, 2012.

ISSI, 2012: Schneider, Matthias, Philippe Demoulin, Ralf Sussmann, and Justus Notholt, Fourier Transform Infrared Spectrometry, Chapter 6 in Monitoring Atmospheric Water Vapour, Ground-Based Remote Sensing and In-situ Methods, ISSI Scientific Report Series, Vol. No. 10 (Editor Niklaus Kämpfer), Springer, DOI 10.1007/978-1-4614-3909-7, 2012, ISBN 978-1-4614-3908-0, 2013.

Jaross, G., Bhartia, P.K., Chen, G., Kowitt, M., Haken, M., Chen, Z., Xu, Ph., Warner, J., Kelly, T., OMPS Limb Profiler instrument performance assessment, J. Geophys. Res. Atmos 119, 2169-8996, 2014.

Johnson, J. and Deland, M., README document for the Suomi-NPP OMPS LP L2 O3 daily product, NASA GES DISC, 31 p, 2017. https://snpp-omps.gesdisc.eosdis.nasa.gov/data/SNPP_OMPS_Level2/OMPS_NPP_LP_L2_O3_DAILY.2/doc/README.OMPS_NPP_LP_L2_O3_DAILY.2.pdf

Joly, Mathieu and Vincent-Henri Peuch, Objective classification of air quality monitoring sites over Europe, Atmospheric Environment 47, 111-123, https://doi.org/10.1016/j.atmosenv.2011.11.025, 2012.

Kämpfer, N.: Monitoring Atmospheric Water Vapour: Ground-Based Remote Sensing and In-situ Methods, ed.: Niklaus Kämpfer, vol.: 10, series: ISSI Scientific Report Series, Springer New York, http://dx.doi.org/10.1007/978-1-4614-3909-7, 2012, ISBN 978-1-4614-3908-0, 2013.

Kobayashi, J. and Y. Toyama: On various methods of measuring the vertical distribution of atmospheric ozone (III) - Carbon iodine type chemical ozonesonde-. Pap. Met. Geophys., 17, 113-126, 1966.

Köhler, U., Nevas, S., McConville, G., Evans, R., Smid, M., Stanek, M., Redondas, A., and Schönenborn, F.: Optical characterisation of three reference Dobsons in the ATMOZ Project – verification of G. M. B. Dobson's original specifications, Atmos. Meas. Tech., 11, 1989-1999, https://doi.org/10.5194/amt-11-1989-2018, 2018.

Komhyr, W.D.: Electrochemical concentration cells for gas analysis, Ann.Geoph., 25, 203-210, 1969.

Köpke, P., Hess, M., Schult, I., Shettle, E., Global aerosol data set. Max-Planck-Institut für Meteorologie Hamburg, Germany, 1997.

Kizer, S., Flittner, D., Roell, M., Damadeo, R., Roller, C., Hurst, D., Hall, E., Jordan, A., Cullis, P., Johnson, B. and Querel, R.: Stratospheric Aerosol and Gas Experiment III on the International Space Station (SAGE III/ISS) Newly Released V5.2 Validation of Ozone and Water Vapor Data, EGU 2021, PICO presentation EGU21-8481, https://presentations.copernicus.org/EGU21/EGU21-8481_presentation.pdf

Kunz, A., Spelten, N., Konopka, P., Müller, R., Forbes, R. M., and Wernli, H.: Comparison of Fast In situ Stratospheric Hygrometer (FISH) measurements of water vapor in the upper troposphere and lower stratosphere (UTLS) with ECMWF (re)analysis data, Atmos. Chem. Phys., 14, 10803–10822, https://doi.org/10.5194/acp-14-10803-2014, 2014.

Lambert, J.-C., Atmospheric Service Validation Protocol, Version 2, 28 May 2013, MACC-II document MACCII_MAN_DEL_D153.1_20130528_Lambert_V2.pdf .

Langerock, B., De Mazière, M., Hendrick, F., Vigouroux, C., Desmet, F., Dils, B., and Niemeijer, S.: Description of algorithms for co-locating and comparing gridded model data with remote-sensing observations, Geosci. Model Dev., 8, pp 911-921, doi:10.5194/gmd-8-911-2015, 2015.

Laurent, O.: ICOS Atmospheric Station Specifications, Version 1.3, (https://icos-atc.lsce.ipsl.fr/filebrowser/download/69422), 2017.

Lefever, K.; van der R., A; Baier, F.; Christophe, Y.; Errera, Q.; Eskes, H.; Flemming, J.; Inness, A.; Jones, L.; Lambert, J.-C.; Langerock, B.; Schultz, M. G.; Stein, O.; Wagner, A. & Chabrillat, S.: Copernicus stratospheric ozone service, 2009--2012: validation, system intercomparison and roles of input data sets. Atmos. Chem. Phys., 15 , 2269-2293, doi: 10.5194/acp-15-2269-2015, 2015.

Li, L., Zhang, J., Qiu, W., Wang, J., and Fang, Y.: An ensemble spatiotemporal model for predicting PM2.5 concentrations, Int. J. Environ. Res. Pub. He., 14, 549, https://doi.org/10.3390/ijerph14050549, 2017.

Liu, F., van der A, R. J., Eskes, H., Ding, J., and Mijling, B.: Evaluation of modeling NO_2 concentrations driven by satellite-derived and bottom-up emission inventories using in situ measurements over China, Atmos. Chem. Phys., 18, 4171–4186, https://doi.org/10.5194/acp-18-4171-2018, 2018.

Logan, J., An analysis of ozonesonde data for the troposphere: Recommendations for testing 3-D models and development of a gridded climatology for tropospheric ozone, J. Geophys.Res, 104, pp. 16,115-16,149, 1999.

Marenco, A., V. Thouret, P. Nédélec, H. Smit, M. Helten, D. Kley, F. Karcher, P. Simon, K. Law, J. Pyle, G. Poschmann, R. Von Wrede, C. Hume and T. Cook, Measurement of ozone and water vapor by Airbus in-service aircraft: The MOZAIC airborne program, An overview, J. Geophys. Res., 103, 25,631-25,642, 1998.

McCormick, M. P., Lei, L., Hill, M. T., Anderson, J., Querel, R. and Steinbrecht, W.: Early results and validation of SAGE III-ISS ozone profile measurements from onboard the International Space Station, Atmos. Meas. Tech., 13(3), 1287–1297, doi:10.5194/amt-13-1287-2020, 2020.

McGee, T.J., M. Gross, R. Ferrare, W. S. Heaps and U. N. Singh, Geophys. Res. Lett., 1993, 20, 955– 958.

Morcrette, J.J., Beljaars, A., Benedetti, A., Jones, L., Boucher, O., Sea-salt and dust aerosols in the ECMWF IFS model. Geophysical Research Letters 2008; 35(24). L24813.

Morcrette, J.J., Boucher, O., Jones, L., Salmond, D., Bechtold, P., Beljaars, A., Benedetti, A., Bonet, A., Kaiser, J.W., Razinger, M., Schulz, M., Serrar, S., Simmons, A.J., So_ev, M., Suttie, M., Tompkins, A.M., Untch, A., Aerosol analysis and forecast in the european centre for medium range weather forecasts integrated forecast system: Forward modeling. Journal of Geophysical Research: Atmospheres 2009; 114(D6), D06206.

Munro, R., Lang, R., Klaes, D., Poli, G., Retscher, C., Lindstrot, R., Huckle, R., Lacan, A., Grzegorski, M., Holdak, A., Kokhanovsky, A., Livschitz, J. and Eisinger, M.: The GOME-2 instrument on the Metop series of satellites: instrument design, calibration, and level 1 data processing – an overview, Atmos. Meas. Tech., 9(3), 1279–1301, doi:10.5194/amt-9-1279-2016, 2016.

Nédélec P., Blot R., Boulanger D., Athier G., Cousin J-M., Gautron B., Petzold A., Volz-Thomas A. and Thouret V., Instrumentation on commercial aircraft for monitoring the atmospheric composition on a global scale: the IAGOS system, technical overview of ozone and carbon monoxide measurements, MOZAIC-IAGOS special issue, Tellus B 2015, 67, 27791, http://dx.doi.org/10.3402./tellusb.v67.27791

Neis, P., Smit, H. G. J., Krämer, M., Spelten, N., and Petzold, A.: Evaluation of the MOZAIC Capacitive Hygrometer during the airborne field study CIRRUS-III, Atmos. Meas. Tech., 8, 1233–1243, https://doi.org/10.5194/amt-8-1233-2015, 2015a.

Neis, P., Smit, H. G. J., Rohs, S., Bundke, U., Krämer, M., Spelten, N., Ebert, V., Buchholz, B., Thomas K., and Petzold, A.: Quality assessment of MOZAIC and IAGOS capacitive hygrometers: insights from airborne field studies, Tellus B: Chemical and Physical Meteorology, 67:1, DOI: 10.3402/tellusb.v67.28320, 2015b.

O'Dowd, C.D., Lowe, J.A., Smith, M.H., Davison, B., Hewitt, C.N., Harrison, R.M.. Biogenic sulphur emissions and inferred non-sea-salt sulphate cloud condensation nuclei in and around antarctica. Journal of Geophysical Research: Atmospheres 1997; 102(D11):12839-12854.

Oltmans, S.J. and Komhyr, W.D. (1986). Surface ozone distributions and variations from 1973-1984 measurements at the NOAA geophysical monitoring for climatic change baseline observatories.. Journal of Geophysical Research 91: doi: 10.1029/JD091iD04p05229. issn: 0148-0227

Oltmans, SJ and Levy II, H, Surface ozone measurements from a global network, Atmos. Environ., 28, 9-24, 1994.

O'Neill, N. T., Eck, T. F., Holben, B. N., Smirnov, A., Dubovik, O., Royer, A.: Bi-modal size distribution influences on the variation of Angstrom derivatives in spectral and optical depth space, J. Geophys. Res., vol. 106, 9787-9806, 2001.

O'Neill, N. T., Eck, T. F., Smirnov, A., Holben, B. N. and Thulasiraman, S., Spectral discrimination of coarse and fine mode optical depth, J. Geophys. Res., 108, 4559, 2003.

Peter, R.: The Ground-based Millimeter-wave Ozone Spectrometer - GROMOS, IAP Research Report, No. 1997-13, Institut für angewandte Physik, Universitaät Bern, 1997.

Petetin, H., Jeoffrion, M.; Sauvage, B.; Athier, G.; Blot, R.; Boulanger, D.; Clark, H.; Cousin, J.-M.; Gheusi, F.; Nedelec, P.; Steinbacher, M.; Thouret, V.: Representativeness of the IAGOS airborne measurements in the lower troposphere. Elementa Science of the Anthropocene, 6 (1), pp. 23, 2018.

Petzold A., V. Thouret, C. Gerbig, A. Zahn, C. A.M. Brenninkmeijer, M. Gallagher, M. Hermann, M. Pontaud, H. Ziereis, D. Boulanger, J. Marshall, P. Nédélec, H. G.J. Smit, U. Friess, J.-M. Flaud, A. Wahner, J.-P. Cammas, A. Volz-Thomas, Global-scale atmosphere monitoring by in-service aircraft current achievements and future prospects of the European Research Infrastructure IAGOS, Tellus B 2015, 67, 28452, http://dx.doi.org/10.3402/tellusb.v67.28452.

Pumphrey, H. C., M. L. Santee, N. J. Livesey, M. J. Schwartz, and W. G. Read: Microwave Limb Sounder observations of biomass-burning products from the Australian bush fires of February 2009, Atmos. Chem. Phys., 11, 6285-6296, 2011.

Reddy, M.S., Boucher, O., Bellouin, N., Schulz, M., Balkanski, Y., Dufresne, J.L., Pham, M.. Estimates of global multicomponent aerosol optical depth and direct radiative perturbation in the laboratoire de meteorologie dynamique general circulation model. Journal of Geophysical Research: Atmospheres 2005; 110(D10), D10S16.

Richter, A., Burrows, J. P., Nüss, H., Granier, C. and Niemeier, U.: Increase in tropospheric nitrogen dioxide over China observed from space., Nature, 437(7055), 129–32, doi:10.1038/nature04092, 2005.

*Richter, A., Begoin, M., Hilboll, A., and Burrows, J. P.: An improved NO2 retrieval for the GOME-2 satellite instrument, Atmos. Meas. Tech. , **4**, 1147-1159, doi:10.5194/amt-4-1147-2011, 2011*

Rodgers, C. D.: Inverse Methods for Atmospheric Sounding, Theory and Practice, World Scientific, Singapore, 2000.

Schmid, B., Michalsky, J., Halthore, R., Beauharnois, M., Harisson,L., Livingston, J., Russell, P., Holben, B., Eck, T., and Smirnov, A.: Comparison of aerosol optical depth from four solar radiometers during the fall 1997 ARM intensive observation period, J. Geophys. Res., 26, 2725–2728, 1999.

*Sheese, P. E.; Walker, K. A.; Boone, C. D.; Bernath, P. F.; Froidevaux, L.; Funke, B.; Raspollini, P. & von Clarmann, T.: ACE-FTS ozone, water vapour, nitrous oxide, nitric acid, and carbon monoxide profile comparisons with MIPAS and MLS. J. Quant. Spect. Rad. Transfer, **186**, 63 – 8, doi:10.1016/j.jqsrt.2016.06.026, 2017.*

Skov, H., Hertel, O. Bech Poulsen, M., Christensen, J.H. and Nordstrøm C. The dynamics of gaseous elemental mercury and ozone at Villum Research Station, Station Nord. Under preparation March 2019 for Atmos. Chem. Phys.

Skov, H., Christensen, J., Goodsite, M.E., Heidam, N.Z., Jensen, B., Wåhlin, P. and Geernaert, G., The fate of elemental mercury in Arctic during atmospheric mercury depletion episodes and the load of atmospheric mercury to Arctic, Environ. Sci. Technol. 38, 2373-2382, 2004.

Smit, H.G.J.: Ozonesondes, in Encyclopedia of Atmospheric Sciences, edited by J. Holton, J. Pyle, and J. Curry, pp. 1469-1476, Academic Press, London, 2002.

Smit, H.G.J., W. Straeter, B.J. Johnson, S.J. Oltmans, J. Davies, D.W. Tarasick, B. Hoegger, R. Stubi, F.J. Schmidlin, T. Northam, A.M. Thompson, J.C. Witte, I. Boyd: Assessment of the performance of ECC-ozonesondes under quasi-flight conditions in the environmental simulation chamber: Insights from the Juelich Ozone Sonde Intercomparison Experiment (JOSIE), J. Geophys. Res. 112, D19306, doi:10.1029/2006JD007308, 2007.

Smit, H. G. J., Volz-Thomas, A., Helten, M., Paetz, W., and Kley, D.: An In-Flight Calibration Method for Near-Real-Time Humidity Measurements with the Airborne MOZAIC Sensor. J. Atmos. Oceanic Technol., 25, 656–666, https://doi.org/10.1175/2007JTECHA975.1, 2008.

Smit, H.G.J.: Quality Assurance and Quality Control for Ozonesonde Measurements in GAW. WMO/GAW No. 201, World Meteorological Organisation, Geneva, 2013.

Smit, H. G. J., Rohs, S., Neis, P., Boulanger, D., Krämer, M., Wahner, A., and Petzold, A.: Technical Note: Reanalysis of upper troposphere humidity data from the MOZAIC programme for the period 1994 to 2009, Atmos. Chem. Phys., 14, 13241–13255, https://doi.org/10.5194/acp-14-13241-2014, 2014.

Seckmeyer G., A. Bais, G. Bernhard, M. Blumthaler, C.R. Booth, K. Lantz, R.L. McKenzie, P. Disterhoft, and A. Webb (2006), Instruments to measure solar ultraviolet radiation Part 2: Broadband instruments measuring erythemally weighted solar irradiance. Draft available at: http://www.wmo.ch/ web/arep/reports/gaw164_final_draft.pdf, WMO/GAW No. 164 World Meteorological Organisation, Geneva.

Staehelin, J.: Global atmospheric ozone monitoring. WMO Bulletin, Volume 57 (1), Geneva, 2008

Stauffer, R. M., Thompson, A. M., Kollonige, D. E., Witte, J. C., Tarasick, D. W., Davies, J., et al. (2020). A post-2013 dropoff in total ozone at a third of global ozonesonde stations: Electrochemical concentration cell instrument artifacts? Geophysical Research Letters, 47, e2019GL086791.

Tegtmeier, S.; Hegglin, M. I. et al. : SPARC Data Initiative: A comparison of ozone climatologies from international satellite limb sounders. J. Geophys. Res.: Atmos., 118, 12,229-12,247, doi:10.1002/2013JD019877, 2013.

Teschke, G. and K. Poenitz, 2010: On the retrieval of aerosol (mixing) layer heights on the basis of ceilometer data. International Symposium for the Advancement of Boundary Layer Remote Sensing. 28.-30.06.2010. Paris.

Thompson, A. M., Witte, J. C., Sterling, C.,Jordan, A., Johnson, B. J., Oltmans, S. J.,Thiongo, K. (2017). First reprocessing of Southern Hemisphere Additional Ozonesondes (SHADOZ) ozone profiles (1998–2016): 2. Comparisons with satellites and ground-based instruments. Journal of Geophysical Research: Atmospheres, 122, 13,000–13,025. https://doi.org/10.1002/2017JD027406, 2017.

Veefkind, P., et al TROPOMI on the ESA Sentinel-5 Precursor: A GMES mission for global observations of the atmospheric composition for climate, air quality and ozone layer applications, Remote Sensing of the Environment, doi:10.1016/j.rse.2011.09.027, 2012.

Vigouroux, C., Bauer Aquino, C. A., Bauwens, M., Becker, C., Blumenstock, T., De Mazière, M., García, O., Grutter, M., Guarin, C., Hannigan, J., Hase, F., Jones, N., Kivi, R., Koshelev, D., Langerock, B., Lutsch, E., Makarova, M., Metzger, J.-M., Müller, J.-F., Notholt, J., Ortega, I., Palm, M., Paton-Walsh, C., Poberovskii, A., Rettinger, M., Robinson, J., Smale, D., Stavrakou, T., Stremme, W., Strong, K., Sussmann, R., Té, Y., and Toon, G.: NDACC harmonized formaldehyde time series from 21 FTIR stations covering a wide range of column abundances, Atmos. Meas. Tech., 11, 5049–5073, https://doi.org/10.5194/amt-11-5049-2018, 2018

Vrekoussis, M., Wittrock, F., Richter, A. and Burrows, J. P.: GOME-2 observations of oxygenated VOCs: what can we learn from the ratio glyoxal to formaldehyde on a global scale?, Atmos. Chem. Phys., 10(21), 10145–10160, doi:10.5194/acp-10-10145-2010, 2010.

Walker, K., Jones, S., Sheese, P., Boone, C. and P. Bernath: ACE – FTS Atmospheric Chemistry Experiment. Data usage guide and file format description for ACE-FTS level 2 data version 3.5/3.6 ASCII format. Doc. ACE-SOC 0030, https://databace.scisat.ca/level2/ace_v3.5_v3.6/ACE-SOC-0030-1A-ACE-FTS_ascii_data_usage_and_fileformat_for_v3.5-3.6-16Jan2017.pdf , 16 January 2017

Wang, H. J. R., Damadeo, R., Flittner, D., Kramarova, N., Taha, G., Davis, S., et al.: Validation of SAGE III/ISS Solar Occultation Ozone Products with Correlative Satellite and Ground Based Measurements. J. Geophys. Res.: Atmospheres, 125, https://doi.org/10.1029/2020JD032430, 2020.

Wang, P., P. Stammes, R. van der A, G. Pinardi, M. van Roozendael, FRESCO+: an improved O2 A-band cloud retrieval algorithm for tropospheric trace gas retrievals, Atmospheric Chemistry and Physics, 8, 6565-6576, 2008.

Wiegner, M. and Geiß, A.: Aerosol profiling with the Jenoptik ceilometer CHM15kx, Atmos. Meas. Tech., 5, 1953–1964, doi:10.5194/amt-5-1953-2012, 2012.

Witte, J. C., Thompson, A. M., Smit, H. G. J., Vömel, H., Posny, F., & Stübi, R. : First reprocessing of Southern Hemisphere ADditional OZonesondes profile records: 3. Uncertainty in ozone profile and total column. Journal of Geophysical Research: Atmospheres, 123, 3243–3268. https://doi.org/10.1002/2017JD027791, 2018.

Wittrock, F., A. Richter, H. Oetjen, J. P. Burrows, M. Kanakidou, S. Myriokefalitakis, R. Volkamer, S. Beirle, U. Platt, and T. Wagner, Simultaneous global observations of glyoxal and formaldehyde from space, Geophys. Res. Lett., 33, L16804, doi:10.1029/2006GL026310, 2006.

WMO (2010), Guidelines for the Measurement of Atmospheric Carbon Monoxide, GAW Report No. 192, World Meteorological Organization, Geneva, Switzerland, 2010.

WMO (2013), Guidelines for the Continuous Measurements of Ozone in the Troposphere, GAW Report No. 209, World Meteorological Organization, Geneva, Switzerland, 2013.

WMO/GAW (2013), 17th WMO/IAEA Meeting on Carbon Dioxide, Other Greenhouse Gases and Related Tracers Measurement Techniques, Beijing, China, GAW Report No. 213, 2013.

Wunch, D., Toon, G. C., Wennberg, P. O., Wofsy, S. C., Stephens, B. B., Fischer, M. L., Uchino, O., Abshire, J. B., Bernath, P., Biraud, S. C., Blavier, J.-F. L., Boone, C., Bowman, K. P., Browell, E. V., Campos, T., Connor, B. J., Daube, B. C., Deutscher, N. M., Diao, M., Elkins, J. W., Gerbig, C., Gottlieb, E., Griffith, D. W. T., Hurst, D. F., Jimenez, R., Keppel-Aleks, G., Kort, E. A., Macatangay, R., Machida, T., Matsueda, H., Moore, F., Morino, I., Park, S., Robinson, J., Roehl, C. M., Sawa, Y., Sherlock, V., Sweeney, C., Tanaka, T., and Zondlo, M. A.: Calibration of the Total Carbon Column Observing Network using aircraft profile data, Atmos. Meas. Tech., 3, 1351-1362, doi:10.5194/amt-3-1351-2010, 2010. Available from: http://www.atmos-meas-tech.net/3/1351/2010/.

Wunch D., G.C. Toon, J.-F.L. Blavier, R.A. Washenfelder, J. Notholt, B.J. Connor, D.W.T. Griffith, V. Sherlock, P.O. Wennberg. The Total Carbon Column Observing Network. Phil. Trans. R. Soc. A 369, doi:10.1098/rsta.2010.0240, 2011.

Xu Philippe Q., Pawan K. Bhartia , Glen R. Jaross , Matthew T. DeLand , Jack C. Larsen , Albert Fleig , Daniel Kahn , Tong Zhu , Zhong Chen , Nick Gorkavyi , Jeremy Warner , Mike Linda , Hong Chen , Mark Kowitt , Michael Haken , Peter Hall, Release 2 data products from the Ozone Mapping and Profiler Suite (OMPS) Limb

Profiler. Proc. SPIE 9242, Remote Sensing of Clouds and the Atmosphere XIX; and Optics in Atmospheric Propagation and Adaptive Systems XVII, 92420K (October 17, 2014); doi:10.1117/12.2067320.

Yang, X. Blechschmidt, A.-M. Bognar, K. McClure–Begley, Morris, S. Petropavlovskikh, I. Richter, A. Skov, H. Strong, K. Tarasick, D. Uttal, T. Vestenius, M. Zhao, X. The pan-Arctic surface ozone: modelling vs measurements. Aug. 2019, Manuscript ready for publication.

Yver-Kwok, C., O. Laurent, A. Guemri, C. Philippon, B. Wastine, C.W. Rella, C. Vuillemin, F. Truong, M. Delmotte, V. Kazan, M. Darding, B. Lebègue, C. Kaiser, I. Xueref-Remy, and M. Ramonet: Comprehensive laboratory and field testing of cavity ring-down spectroscopy analyzers measuring H2O, CO2, CH4 and CO, Atmos. Meas. Tech., 8, 3867-3892, 2015.

Zhang, Y., & Cao, F., Fine particulate matter (PM2.5) in China at a city level. Scientific Reports, 5(1), 14884. https://doi.org/10.1038/srep14884 (2015).

18 Annex: Regions

Figure A2.1 shows the regions used for spatial data-stratification as adopted for CO total and NO_2 tropospheric column evaluation (left) as well as H_2CO tropospheric column evaluation (right). The number of regions is limited to eight, including industrially polluted regions, (tropical) biomass burning region and a polar region. The following regions are defined: Europe (15W–35E, 35N–70N), Fires-Alaska (150W–105W, 55N–70N), Fires-Siberia (100E–140E, 40N–65N), North Africa (15W–45E, 0N–20N), South Africa (15E–45E, 20S–0S), South Asia (50E–95E, 5N–35N), East Asia (100E–142E, 20N–45N), United States (120W–65W, 30N–45N). Figure A2.2 shows the aggregation of ozone sonde profiles, where all profiles within five different latitude bands are combined. Stratospheric evaluations are also aggregated within these five latitude bands.

The rationale behind the use of various regions is dictated by the emissions and chemistry at stake, in combination with available observations. Major anthropogenic and biomass burning emission hotspots emitting CO, NO_2, H_2CO are well visible from the various satellite instruments, while for O_3 this aggregation is constrained by the availability of sounding observations distributed over the globe. In the stratosphere horizontal gradients are generally more smooth.

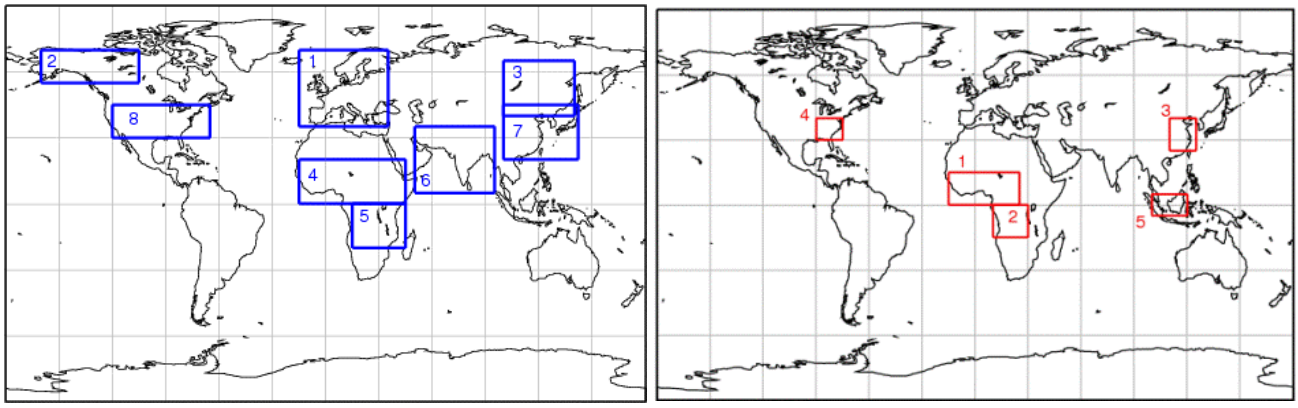

Figure A2.1. (left) Recommended regions for spatial aggregation. (right) Chosen data stratification for HCHO analysis.

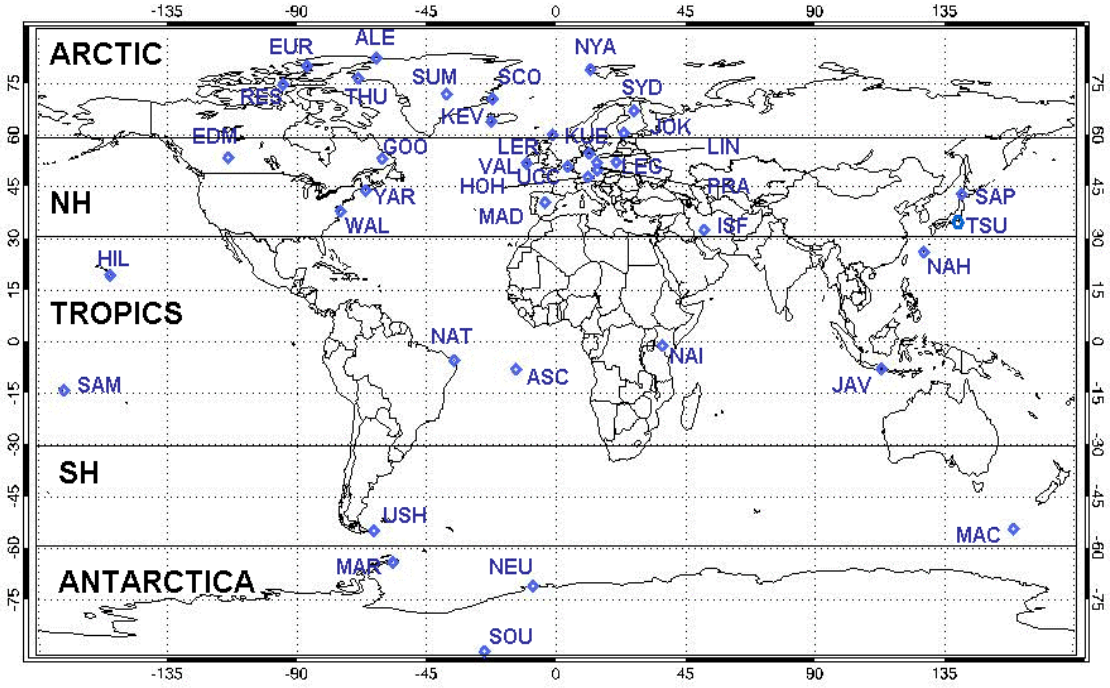

Figure A2.2: Location of the ozone sounding stations and their attribution to the different stratospheric regions

Copernicus Atmosphere Monitoring Service

ECMWF - Shinfield Park, Reading RG2 9AX, UK

Contact: info@copernicus-atmosphere.eu